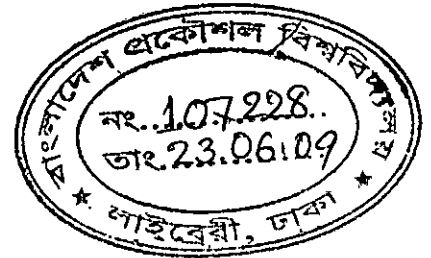


Study of Carbon Nanotubes with Defects under Tensile and Compressive Loads using Molecular Dynamics Simulation.

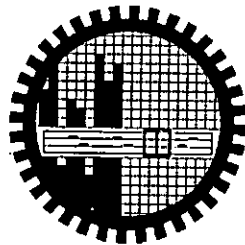


by

Shekh Nisar Hossain Rubaiyat

MASTER OF SCIENCE IN MECHANICAL ENGINEERING

Department of Mechanical Engineering



BANGLADESH UNIVERSITY OF ENGINEERING AND TECHNOLOGY

Dhaka-1000, Bangladesh.

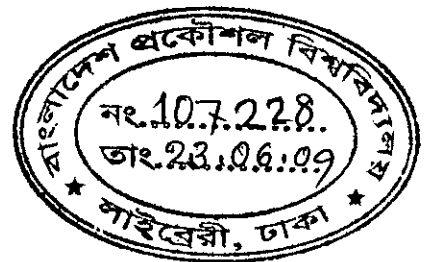


#107228#

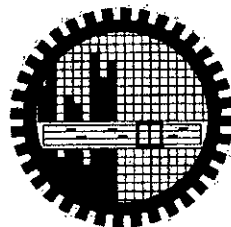
March 2009

Study of Carbon Nanotubes with Defects under Tensile and Compressive Loads using Molecular Dynamics Simulation.

A thesis submitted to the Department of Mechanical Engineering
Bangladesh University of Engineering and Technology (BUET)
In partial fulfillment for the requirement of the degree of
Master of Science in Mechanical Engineering



Submitted by
Shekh Nisar Hossain Rubaiyat
Roll No: 100510010 P
Session: October 2005



BANGLADESH UNIVERSITY OF ENGINEERING AND TECHNOLOGY

Dhaka-1000, Bangladesh

March 2009

The thesis titled “Study of Carbon Nanotubes with Defects under Tensile and Compressive Loads using Molecular Dynamics Simulation.”, submitted by Shekh Nisar Hossain Rubaiyat, Roll No: 100510010 P, Session: October 2005 has been accepted as satisfactory in partial fulfillment of the requirement for the degree of MASTER OF SCIENCE IN MECHANICAL ENGINEERING on March 21, 2009.

BOARD OF EXAMINERS



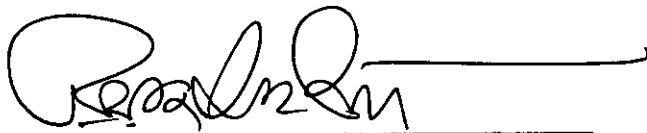
Chairman

Dr. Sanjib Chandra Chowdhury
Assistant Professor
Department of Mechanical Engineering
BUET, Dhaka, Bangladesh.



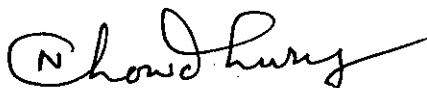
Member
(Ex-officio)

Dr. Abu Rayhan Md. Ali
Professor and Head
Department of Mechanical Engineering
BUET, Dhaka, Bangladesh.



Member

Dr. S. Reaz Ahmed
Professor
Department of Mechanical Engineering
BUET, Dhaka, Bangladesh.



Member
(External)

Dr. Md. Nurul Absar Chowdhury
Associate Professor
MCE Department,
IUT, Gazipur, Bangladesh.

Declaration

It is hereby declared that the thesis titled “**Study of Carbon Nanotubes with Defects under Tensile and Compressive Loads using Molecular Dynamics Simulation.**” is author’s original work and has not been submitted elsewhere for the award of any other degree or diploma.



Author

Shekh Nisar Hossain Rubaiyat

DEDICATIONS

This work is dedicated to my beloved parents

Mrs. Nazma Hossain

&

Mr. Shekh Tozammel Hossain

Acknowledgement

All praises to the Almighty Allah, the most merciful, the most gracious and the most cordial, who bestowed upon the author the will, the ability, the vigor and the perseverance unless which it would have been impossible for the author to complete this research work.

The author would like to take this opportunity of expressing his heartfelt gratitude and indebtedness to his supervisor Dr. Sanjib Chandra Chowdhury, Assistant Professor, Department of Mechanical Engineering, Bangladesh University of Engineering and Technology (BUET), Dhaka, Bangladesh for his cordial support and advice. His advice helped the author at every step of this work. Without his proper supervision this report could not be finished.

The author feels grateful to Dr. Abu Rayhan Md. Ali, Professor & Head, Department of Mechanical Engineering, Bangladesh University of Engineering and Technology (BUET), Dhaka, Bangladesh for his valuable co-operation from time to time.

Author's gratitude continues to The University for using Libraries, computer labs and other facilities. Without these supports this thesis could not be completed.

Finally the author thanks his colleagues, family members, friends and other relatives who shared the troubles with him.

Contents

	Page
	No.
Title page	i
Board of Examiners	ii
Declaration	iii
Dedication	iv
Acknowledgement	v
Contents	vi
Abstract	viii
List of Tables	ix
List of Figures	x
Chapter 01	INTRODUCTION
1.1.	Introduction of CNT 01
1.2.	CNT structure 02
1.3.	Types of Carbon Nanotubes 03
1.3.1.	Single walled nanotube 03
1.3.2.	Multi walled nanotube 07
1.3.3.	Other types of CNTs 08
1.4.	Mechanical Properties of CNTs 09
1.5.	Applications of CNTs 11
1.5.1.	Composite Materials 11
1.5.2.	Textiles 13
1.5.3.	Energy Storage 13
1.5.4.	Field Emitting devices 14
1.5.5.	Probes and sensors 15
1.5.6.	Transistors 17
1.6.	Synthesis and Purification 17
1.7.	CNT Defects 18
1.8.	Layout of the thesis 21
Chapter 02	LITERATURE REVIEWS
2.1	Introduction 22
2.2	Literature Reviews 22
2.3	Justification 26
2.4	Objectives 27
Chapter 03	MOLECULAR DYNAMIC SIMULATION
3.1	Introduction 28
3.2	Molecular Dynamics 28
3.3	Quantum Molecular Dynamics 28

3.4	Classical Molecular Dynamics	29
3.5	Molecular Dynamics Simulation for Nano-scale Materials	31
3.6	Fundamentals of the Simulation	32
3.6.1	Potential Functions and Parameters for CNTs	32
3.6.2	Potential Functions and Parameters for Inter-wall Interaction	34
3.6.3	Simulation Algorithm	34
3.6.4	Initialization	36
3.6.5	Relaxation	36
3.6.6	Loading	37
3.6.7	Force Calculation	37
3.6.8	Velocity Scaling for Temperature Control	39
3.7	Tensile and Compressive Test Procedure	39
3.8	Defect Formation	42
Chapter 04	RESULTS AND DISCUSSIONS	
4.1	Introduction	45
4.2	Validation of the MD Code	46
4.3	Results and discussions	48
4.3.1	Tensile Test of Pristine SWNT	48
4.3.2	Compressive Test of Pristine SWNT	52
4.3.3	Tensile Test of Defective SWNT	61
4.3.4	Compressive Test of Defective SWNT	65
4.3.5	Tensile Test of Pristine & Defective DWNT	69
4.3.6	Compressive Test of Pristine & Defective DWNT	71
Chapter 05	CONCLUSIONS AND RECOMMENDATIONS	
5.1	Introduction	74
5.2	Conclusions	75
5.3	Recommendation	76
References		77
Appendix-A		82

Abstract

After the discovery, carbon nanotubes (CNTs) have received tremendous scientific and industrial interests. This is due to their exceptional mechanical, electrical, and thermal properties. CNTs having perfect structure (i.e., structure without any defect) hold very high mechanical properties. However, CNTs suffer from defects which can appear at production stage, purification stage or be deliberately introduced by irradiation with energetic particles or by chemical treatment. In this work mechanical properties of CNTs with defects are studied under both compressive and tensile loads using molecular dynamics (MD) simulations.

In this work both single-walled and double-walled carbon nanotubes (SWNTs and DWNTs) with perfect structure, vacancy defects and Stone-Wales defects are simulated with MD. Five armchair SWNTs having indexes of (3,3), (4,4), (5,5), (6,6) and (7,7) and one armchair DWNT having index of ((3,3),(8,8)) are considered. To create Stone-Wales defect, four neighboring hexagons are converted into two pentagons and two heptagons with a 90° rotation of the horizontal bond of the hexagonal structure of the CNT whereas to create vacancy defects carbon atoms are removed from the perfect hexagonal structure of the CNTs. Molecular simulations are carried out using the classical MD method, in which the Newtonian equations of motion are solved numerically for a set of atoms. The velocity-Verlet algorithm is used for solving the Newtonian equations of motion. The Brenner potential is used for carbon-carbon interaction in the CNT and non-bonded interaction between the CNTs in DWCNTs is modeled with the Lennard-Jones potential. Temperature of the system is controlled by velocity scaling. In the simulation, tensile and compressive loads are applied by moving the end atoms of the CNTs rigidly outward and inward directions, respectively.

Simulation results show that the defects have negligible effect on the modulus of elasticity of CNTs and defect density influences the compressive and tensile strength of CNTs insignificantly. The results obtained from the compressive test by MD simulations are in well agreement with the results obtained from theoretical Euler equation.

List of Tables

	Page No.
Table 1.1 Mechanical properties of nanotubes addressed in different literatures	10
Table 4.1 SWNTs specification	48

List of Figures

	Page No.	
Figure 1.1	Classification of carbon nanotubes: (a) armchair, (b) zigzag, and (c) chiral nanotubes	4
Figure 1.2	The unrolled honeycomb lattice of a nanotube	5
Figure 1.3	(a) SWNT formation (b) an armchair (4,4) SWNT	5
Figure: 1.4	All possible structures of SWNTs	6
Figure 1.5	Multi-walled nanotube (a) side view (b) top view	7
Figure 1.6	Torus	8
Figure 1.7	Nanobud	9
Figure 1.8	CNT polymer composite	12
Figure 1.9	CNTs in Lithium ion batteries	14
Figure 1.10	A prototype field emission display (fabricated by Samsung)	15
Figure 1.11	Use of a MWNT as AFM tip	16
Figure 1.12	(a) Stone-Wales defect formation by C-C rotation in the Hexagonal lattice (b) (9,0) CNT (c) (5,5) CNT with Stone Wales defect (indicated in yellow color)	19
Figure 1.13	Helicoidal graphite with heptagons, pentagons and hexagons	20
Figure 1.14	Typical vacancy defects in SWNT	20
Figure 3.1	Typical flow chart of molecular dynamics simulation	31
Figure 3.2	Orientation of Carbon atoms in a CNT structure	33
Figure 3.3	Flow chart of relaxation	38
Figure 3.4	Flow chart of loading	40
Figure 3.5	Atomistic model for tensile test	41
Figure 3.6	Atomistic model for compressive test	41

Figure 3.7	Cross section of a SWNT	42
Figure 3.8	Structure of CNT with a) pristine structure, b) one Stone-Wales defect	43
Figure 3.9	Structure of CNT with three Stone-Wales defects	44
Figure 3.10	Structure of CNT with a) pristine structure b) one vacancy defect	44
Figure 3.11	Structure of CNT with three vacancy defects	44
Figure 4.1	Yield strength determination by offset method	46
Figure 4.2	Stress-strain behavior of a (7,7) SWNT under axial tension. (a) Comparison with literature, (b) effect of potential parameters R_1 & R_2 .	47
Figure 4.3	Tensile stress versus strain curve for (3,3) pristine SWNT	49
Figure 4.4	Tensile stress versus strain curve for (4,4) pristine SWNT	50
Figure 4.5	Tensile stress versus strain curve for (5,5) pristine SWNT	50
Figure 4.6	Tensile stress versus strain curve for (6,6) pristine SWNT	51
Figure 4.7	Tensile stress versus strain curve for (7,7) pristine SWNT	51
Figure 4.8	Snap shot of necking of a (5,5) pristine SWNT	52
Figure 4.9	Snap shot of tensile test of (5,5) pristine SWNT (a) at 0% strain, (b) at 18% strain, (c) failure at 34% strain	52
Figure 4.10	Young's modulus versus diameter curve for pristine SWNT	53
Figure 4.11	Failure stress Vs. Diameter for pristine SWNT	53
Figure 4.12	Failure strain versus diameter curve for pristine SWNT	54
Figure 4.13	Compressive stress versus strain curve for (3,3) pristine SWNT	55
Figure 4.14	Compressive stress versus strain curve for (4,4) pristine SWNT	56
Figure 4.15	Compressive stress versus strain curve for (5,5) pristine SWNT	56
Figure 4.16	Compressive stress versus strain curve for (6,6) pristine SWNT	57
Figure 4.17	Young's modulus versus diameter curve for pristine SWNT under compressive load.	57

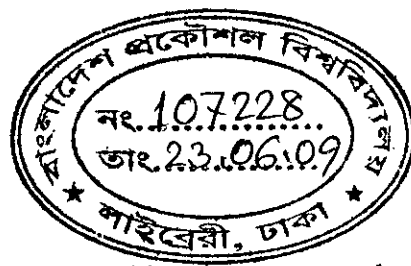
Figure 4.18	Critical stress Vs. slenderness ratio curve for (3,3) SWNT	58
Figure 4.19	Critical stress Vs. slenderness ratio curve for (4,4) SWNT	58
Figure 4.20	Critical stress Vs. slenderness ratio curve for (5,5) SWNT	59
Figure 4.21	Critical stress Vs. slenderness ratio curve for (6,6) SWNT	59
Figure 4.22	Snapshot of (5,5) SWNT with $l/k=10.13$ under compressive load a) undeformed, b) crushing (or kinking)	60
Figure 4.23	Snapshot of (3,3) SWNT with $l/k=43.57$ under compressive load a) undeformed, b) buckling	60
Figure 4.24	Comparison of stress-strain curves of pristine and defective (with vacancy defect) (3,3) SWNT under tensile load	62
Figure 4.25	Comparison of stress-strain curves of pristine and defective (with Stone-Wales defect) (3,3) SWNT under tensile load	62
Figure 4.26	Comparison of failure strength of different defective and pristine SWNTs of different diameters under tensile load	63
Figure 4.27	Snap shot of tensile test of (3,3) defective SWNT with one vacancy defect (a) at 0% strain, (b) at 10% strain, (c) failure at 20% strain	63
Figure 4.28	Snap shot of tensile test of (3,3) defective SWNT with three vacancy defects (a) at 0% strain, (b) at 10% strain, (c) failure at 23% strain	64
Figure 4.29	Snap shot of tensile test of (3,3) defective SWNT with one Stone-Wales defect (a) at 0% strain, (b) at 20% strain, (c) failure at 30% strain	64
Figure 4.30	Snap shot of tensile test of (4,4) defective SWNT with three Stone-Wales defect (a) at 0% strain, (b) at 20% strain, (c) failure at 33% strain	65
Figure 4.31	Comparison of failure strength of pristine and vacancy defect SWNT of different diameter ($l/d \approx 8$) under compressive load	66
Figure 4.32	Snap shot of compressive test of (4,4) defective SWNT with one vacancy defect, (a) at 0% strain (b) at 2% strain, (c) failure at 5% strain	66



Figure 4.33	Snap shot of compressive test of (3,3) defective SWNT with three vacancy defects (a) at 0% strain (b) at 1% strain (c) failure at 5% strain	67
Figure 4.34	Comparison of failure strength of pristine and Stone-Wales defect SWNT of different diameter under compressive load	68
Figure 4.35	Snap shot of compressive test of (3,3) defective SWNT with one Stone-Wales defect (a) at 0% strain, (b) at 1% strain, (c) failure at 5% strain	68
Figure 4.36	Snap shot of compressive test of (3,3) defective SWNT with three Stone-Wales defect (a) at 0% strain, (b) at 1% strain, (c) failure at 3% strain	69
Figure 4.37	Comparison of failure stress of pristine and defective DWNT under tensile test	70
Figure 4.38	Snap shot of tensile test of ((3,3),(8,8)) defective DWNT (a) at 0% strain, (b) at 8% strain, (c) failure at 19% strain	71
Figure 4.39	Comparison of failure stress of defective DWNT and pristine DWNT under compressive test	72
Figure 4.40	Snap shot of compressive test of ((3,3),(8,8)) defective DWCNT (a) at 0% strain, (b) at 4% strain, (c) failure at 7% strain	73
Figure A-1	Experimental set-up of an arc discharge apparatus	82
Figure A-2	Schematic drawings of a laser ablation apparatus	85

CHAPTER 01

INTRODUCTION



1.1 Introduction of CNT

Carbon nanotubes (CNTs) are an allotrope of carbon with a nanostructure that can have a length-to-diameter ratio up to 28,000,000:1[1]. They take the form of cylindrical carbon molecules and have novel properties that make them potentially useful in a wide variety of applications in nanotechnology, electronics, optics and other fields of materials science. They exhibit extraordinary strength and unique electrical properties, and are efficient conductors of heat. Inorganic nanotubes have also been synthesized.

Nanotubes are members of the fullerene structural family. Their name is derived from their size, since the diameter of a nanotube is on the order of a few nanometers (approximately 50,000 times smaller than the width of a human hair), while they can be up to several millimeters in length.

Manufacturing a nanotube is dependent on applied quantum chemistry, specifically, orbital hybridization. Nanotubes are composed entirely of sp^2 bonds, similar to those of graphite. This bonding structure, which is stronger than the sp^3 bonds found in diamonds, provides the molecules with their unique strength. Nanotubes are either wrapped into multiple layers like a parchment scroll or constructed of multiple annulus cylinders which are held together by van der Waals forces form multi-walled CNTs. Under high pressure, nanotubes can merge together, trading some sp^2 bonds for sp^3 bonds, giving the possibility for producing strong, unlimited-length wires through high-pressure nanotube linking.

The discovery of nanotubes remains a contentious issue, especially because several scientists involved in the research could be likely candidates for the Nobel Prize. Many believe that Iijima's [2] report in 1991 is of particular importance because it brought carbon nanotubes into the awareness of the scientific community as a whole. Iijima's discovery of CNTs in the insoluble material of arc-burned graphite rods created the buzz that is now associated with CNTs. Nanotube research accelerated greatly following the independent discoveries by Bethune at IBM and Iijima at NEC of single-walled carbon nanotubes and methods to specifically

produce them by adding transition-metal catalysts to the carbon in an arc discharge. The arc discharge technique was well-known to produce the famed Buckminster fullerene on a preparative scale, and these results appeared to extend the run of accidental discoveries relating to fullerenes. The original observation of fullerenes in mass spectrometry was not anticipated and the first mass-production technique by Krätschmer and Huffman was used for several years before realizing that it produced fullerenes.

1.2 CNT Structure

Many exotic structures exist: regular spheres, cones, tubes, and also more complicated and strange shapes. Here some of the most important and best-known structures are described. Single Walled Nanotubes (SWNT) can be considered as long wrapped graphene sheets. As stated before, nanotubes generally have a length to diameter ratio of about 28,000,000 so they can be considered as nearly one-dimensional structures.

More detailed, a SWNT consists of two separate regions with physical and chemical properties. The first is the end cap of the tube and the second is the sidewall of the tube. The end cap structure is similar to or derived from a smaller fullerene, such as C_{60} . C-atoms placed in hexagons and pentagons form at the end cap structures. It can be easily derived from Euler's theorem that twelve pentagons are needed in order to obtain a closed case structure which consists of only pentagons and hexagons. The combination of a pentagon and five surrounding hexagons results in the desired curvature to enclose a volume. A second rule is the isolated pentagon rule which states that the distance between pentagons on the fullerene shell is maximized in order to obtain a minimal local curvature and surface stress, resulting in a more stable structure. The smallest stable structure that can be made this way is C_{60} , the one just larger is C_{70} and so on. Another property is that all fullerenes are composed of an even number of C-atoms because adding one hexagon to an existing structure means adding two C-atoms.

The second region, sidewall structure of the tube, is a cylindrical structure which composes a SWNT. It is generated when a graphene sheet of a certain size that is wrapped in a certain direction. As the result is symmetric cylinder, it can only be rolled in a discrete set of directions in order to form a closed cylinder. Two atoms in the graphene sheet are chosen, one of which serves the role as origin. The sheet is rolled until the two atoms coincide. The vector pointing from the first atom towards the other is called the chiral vector and its length is equal to the circumference of the nanotube. The direction of the nanotube axis is perpendicular to the chiral vector. SWNT with different chiral vectors have dissimilar properties such as optical activity, mechanical strength and electrical conductivity.

1.3 Types of Carbon Nanotubes

Several types of nanotubes exist, but they can be divided in two main categories: single-walled nanotube (SWNT) and multi-walled nanotube (MWNT). Other special types like torus and nanobud are also available.

1.3.1 Single-Walled Nanotube

SWNTs have a diameter close to 1 nanometer, with a tube length that can be many thousands of times longer. The structure of a SWNT can be conceptualized by wrapping a one-atom-thick layer of graphite called graphene into a seamless cylinder. The way the graphene sheet is wrapped is represented by a pair of indices (n,m) called the chiral vector.

The integers n and m denote the number of unit vectors along two directions in the honeycomb crystal lattice of graphene. If $m=0$, the nanotubes are called "zigzag". If $n=m$, the nanotubes are called "armchair". Otherwise, they are called "chiral" (figure 1.1). Vector \vec{AA}' is called the chiral vector (Figure 1.2). It can be defined

by the vector $\vec{C}_h = m\vec{a}_1 + n\vec{a}_2$ and the chiral angle-with the zigzag axis. Vectors \vec{a}_1 and \vec{a}_2 are the lattice vectors. $A\vec{A}'$ and $A\vec{B}$ define the chiral vector \vec{C}_h and the transitional vector T of the nanotube. The chiral angle, θ is defined as the angle between the vector \vec{C}_h and \vec{a}_1 . The rectangle $AA'B'B$ defines the unit cell for the nanotube. The figure 1.2 corresponds to $\vec{C}_h=(5,3)$.

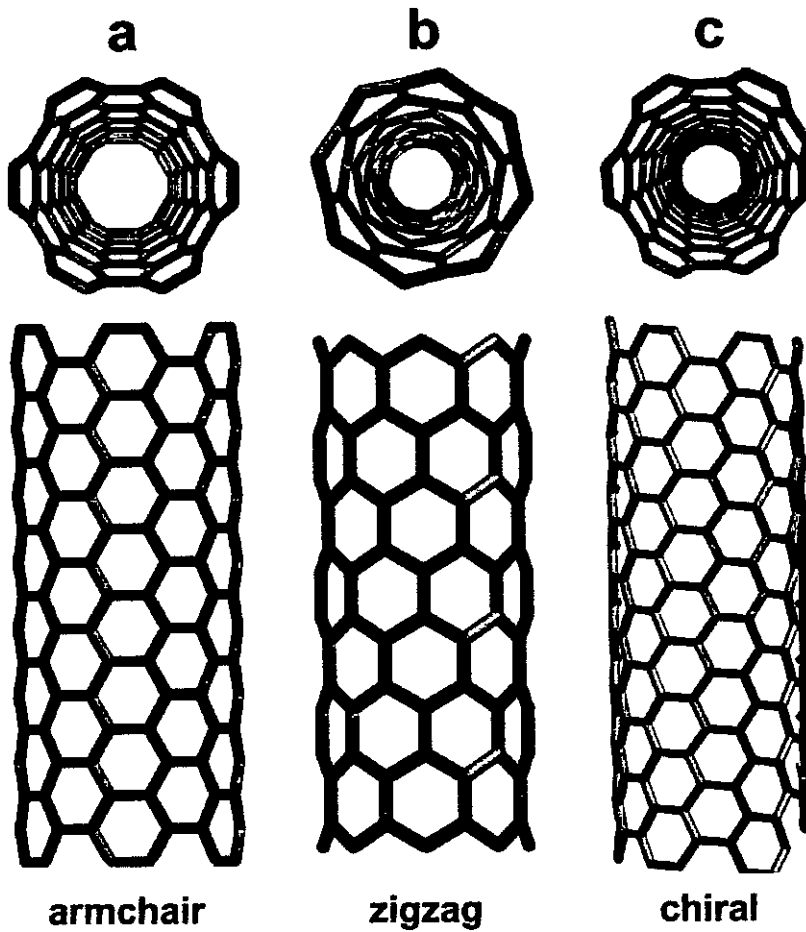


Figure 1.1 Different types of carbon nanotubes: (a) armchair, (b) zigzag, and (c) chiral nanotubes.

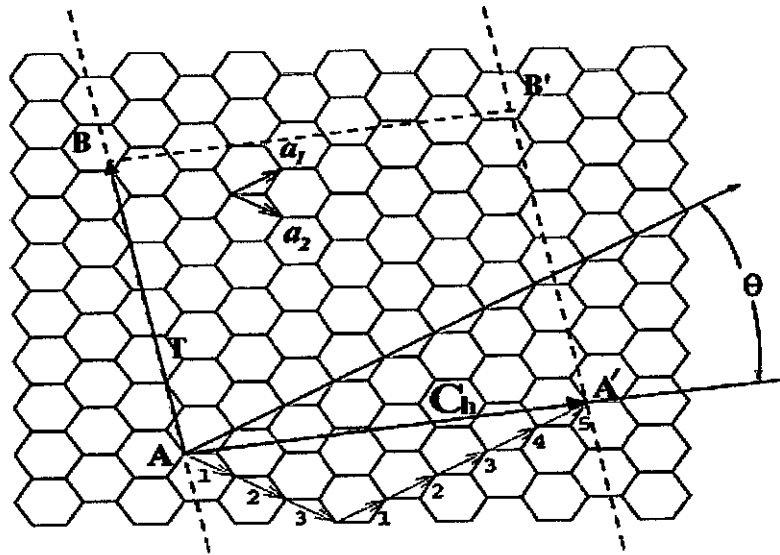


Figure 1.2 The unrolled honeycomb lattice of a nanotube.

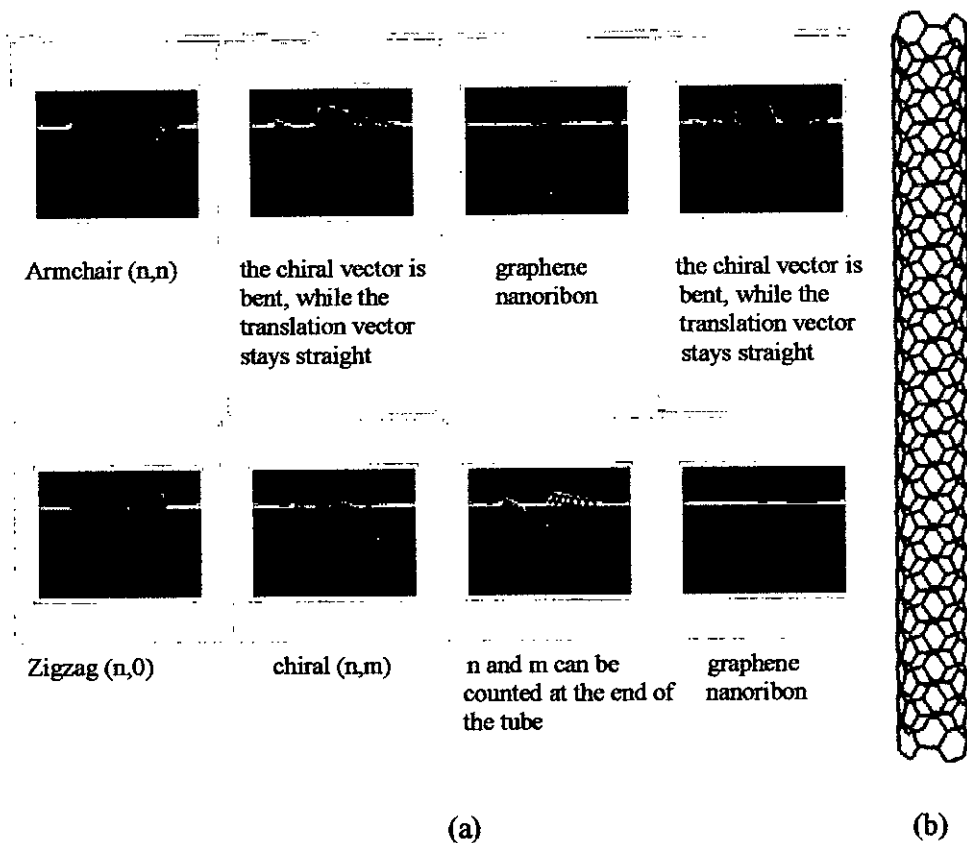


Figure 1.3 (a) SWNT formation (b) an armchair (4,4) SWNT.

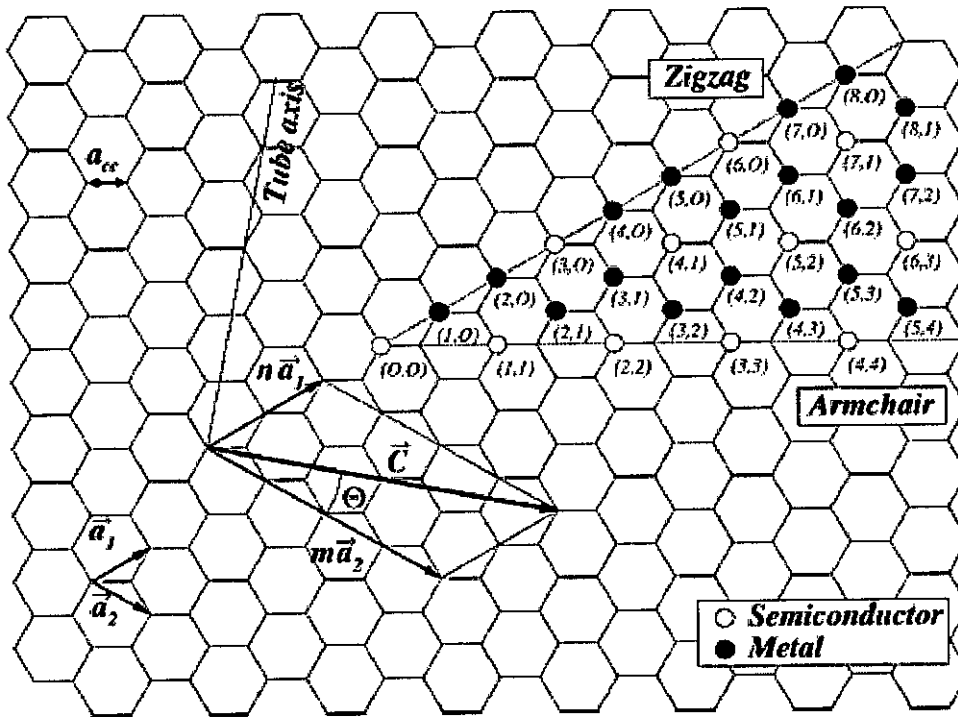


Figure 1.4 All possible structures of SWNTs.

SWNTs can be formed from chiral vectors lying in the range given by the figure 1.4. where n, m are integers, $0 \leq |m| \leq n$ and $0 \leq |\theta| \leq 30^\circ$. Particularly $\theta=0^\circ$ for zigzag and $\theta=30^\circ$ for armchair structure.

CNTs are still very expensive to produce and the development of more affordable synthesis techniques is vital to the future of carbon nanotechnology. If cheaper means of synthesis cannot be discovered, it would make it financially impossible to use CNTs to commercial-scale applications.

1.3.2 Multi-Walled Nanotube

Multi-walled nanotubes (MWNT) consist of multiple layers of graphite rolled in to form a tube shape as shown in figure 1.5. There are two models which can be used to describe the structures of MWNTs. In the Russian Doll model, sheets of graphite are arranged in concentric cylinders, for example, a (0,8) SWNT within a larger (0,10) SWNT. In the Parchment model, a single sheet of graphite is rolled in around itself, resembling a scroll of parchment or a rolled up newspaper. The interlayer distance in multi-walled nanotubes is close to the distance between graphene layers in graphite, approximately 0.34 nm.

The special place of double-walled carbon nanotubes (DWNT) must be emphasized here because they combine very similar morphology and properties as compared to SWNT, while improving significantly their resistance to chemicals. This is especially important when functionalization is required (this means grafting of chemical functions at the surface of the nanotubes) to add new properties to the CNT. In the case of SWNT, covalent fictionalization will break some C=C double bonds, leaving "holes" in the structure on the nanotube and thus modifying both its mechanical and electrical properties. In the case of DWNT, only the outer wall is modified. DWNT synthesis on the gram-scale was first proposed in 2003 by the CCVD technique, from the selective reduction of oxides solid solutions in methane and hydrogen.

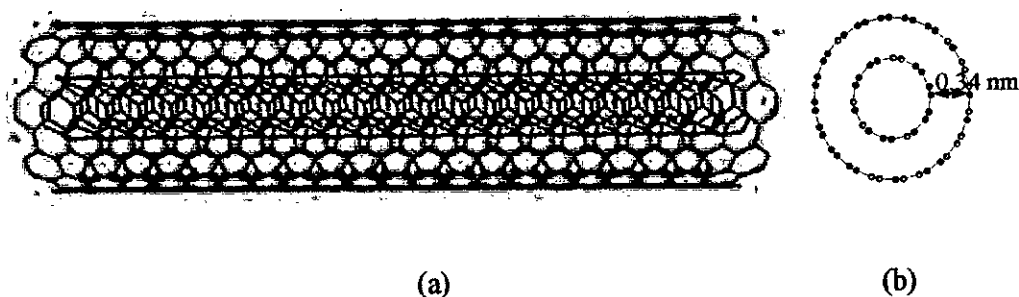


Figure 1.5 Multi-walled nanotube; (a) side view, (b) end view.

1.3.3 Other Types of CNT

Torus

A nanotorus (see figure 1.6) is a theoretically described carbon nanotube bent into a torus (doughnut shape). Nanotori have many unique properties, such as magnetic moments 1000 times larger than previously expected for certain specific radii. Properties such as magnetic moment, thermal stability, etc. vary widely depending on radius of the torus and radius of the tube.

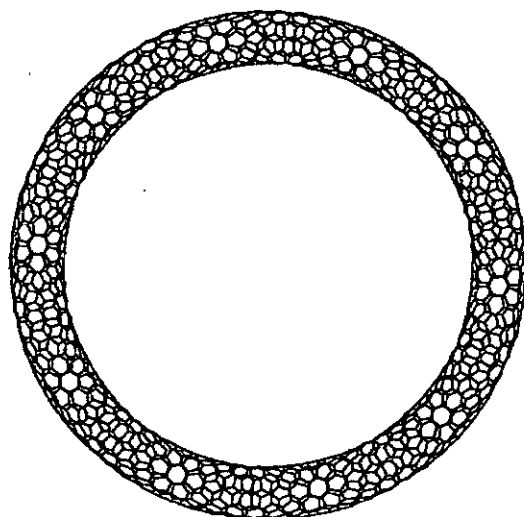


Figure 1.6 Torus.

Nanobud

Carbon nanobuds (see figure 1.7) are a newly discovered material combining two previously discovered allotropes of carbon: carbon nanotubes and fullerenes. In this new material fullerene-like “buds” are covalently bonded to the outer sidewalls of the underlying carbon nanotube. This hybrid material has useful properties of both fullerenes and carbon nanotubes. In particular, they have been found to be exceptionally good field emitters. In composite materials, the attached fullerene molecules may function as molecular anchors preventing slipping of the nanotubes, thus improving the composite’s mechanical properties.

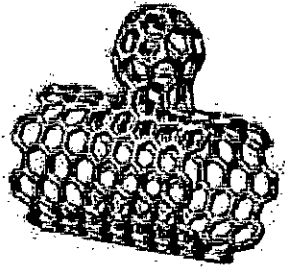


Figure 1.7 Nanobud

1.4 Mechanical Properties of CNTs

CNT has been well recognized as one of the ultra-strong materials in the World, which has been proven by both simulations and experimental measurements [3]. The extreme small size makes it suitable to be embedded into any type of light weight and soft materials as reinforcements to form strong and light nano-composites. Numerous researches have been started focusing on the feasibility of using these nano-structural materials to strengthen polymer-based composites. However, the true mechanical properties of nanotubes such as their Young's modulus, yield strength, ultimate strength, elastic properties and even fracture behavior are still uncertain to date. This actually induces many arguments in whether the nanotubes are suitable to be used as nano-reinforcements for the nano-composites or not.

Experiments conducted previously showed that the Young's moduli of nanotubes range from 270 to 950 GPa. Such a large discrepancy is due to the different sizes, lengths and numbers of wall layers used in different tests. However, the scatterings of measured results have been found in different literatures. An earlier report on the elastic modulus of pristine nanotubes has been calculated in a straight forward way by using the property of graphite which was approximately 1060 GPa [4,5]. Rouff and Lorents [6] have estimated the tensile strength of nanotubes with a wall thickness and diameter of 0.34 nm and 1 nm, respectively, which was about 20

GPa. The average macroscopic elastic modulus and Poisson's ratio of a SWNT were estimated to be about 1.347 TPa and 0.261, respectively [7]. It is also found that the Poisson's ratio of the SWNTs decreases with increasing diameter. In Table 1.1, a summary of the mechanical properties obtained from experimental measurements, molecular dynamic (MD) simulations and theoretical modeling is given.

Molecular mechanics (MM) simulations predicted that the failure strain and stress of a zigzag nanotube were between 10–15%, and 65–93 GPa, respectively [8]. Brittle failures of the nanotubes were also found in the simulation and the results agreed with the experimental measurements. However, another research using a continuum theory of fracture nucleation demonstrated that the failure strain of a single-walled nanotube was about 55%, in which the fracture nucleation was assumed to be the bifurcation instability of a homogeneously deformed nanotube at this strain level [9]. Tersoff and Rouff [10] found that nanotubes with a diameter less than 1 nm show high rigidity. Any nanotubes with a diameter beyond 2.5 nm appeared radial deformation 'flatten' due to the van der Waals attraction.

Yu et al. [11] has demonstrated the use of Atomic Force Microscopy (AFM) to measure the mechanical properties of MWNTs in the Scanning Electron Microscope (SEM). They measured that the tensile strength and modulus of the nanotubes were ranging from 11 to 63 GPa and 270 to 950 GPa, respectively. It was found that an outer layer of the nanotubes was initially failed during the test. The maximum failure strain was found about 12%.

Table 1.1: Mechanical properties of nanotubes addressed in different literatures

Author	E (TPa)	ν	Year	Method	Reference
Yakoson	5.5	0.19	1996	MD	[12]
Zhou et al.	0.77	0.32	2001	Theoretical	[13]
Chnag and Gao	1.33	0.26	2003	MD	[14]
Lau et al.	0.44	-	2004	MD	[15]
Li et al.	0.8	-	2005	Experimental	[16]

CNTs have lower strength under compressive load compared to tensile load. Because of their hollow structure and high aspect ratio, they tend to undergo buckling when placed under compressive, torsional or bending stress.

1.5 Applications of CNTs

The potential applications of carbon nanotubes have wide range of variety. Carbon nanotubes, a type of fullerene, have potential in fields such as nanotechnology, electronics, optics, materials science, and architecture. Over the years new discoveries have led to new applications, often taking advantage of their unique electrical properties, extraordinary strength, and efficiency in heat conduction.

1.5.1 Composite Materials

CNTs are used as reinforcement in high strength, low weight, and high performance composites. In concrete, they increase the tensile strength, and halt crack propagation. Theoretically, SWNTs could have a Young's Modulus of approximately 1 TPa [13]. MWNTs are weaker because the individual cylinders slide with respect to each other. Ropes of SWNTs are less strong. The individual tubes can pull out by shearing and at last the whole rope will break. This happens at stresses far below the tensile strength of individual nanotubes. Nanotubes also sustain large strains in tension without showing signs of fracture. In other direction, nanotubes are highly flexible. One of the most important applications of nanotubes based on their properties is reinforcement in composite materials. However, there have not been many successful experiments that show that nanotubes are better fillers than the traditionally used carbon fibers. The main problem is to create a good interface between nanotubes and the polymer matrix, as nanotubes are very smooth and have smaller diameter. Limiting factors for good load transfer could be sliding of cylinders in MWNTs and shearing of tubes in SWNT ropes. To solve this problem the aggregates need to be broken up dispersed

or cross-linked to prevent slippage. A main advantage of using nanotubes for structural polymer composites is that nanotube reinforcements will increase the toughness of the composites by absorbing energy during their highly flexible elastic behavior. Other advantage is the low density of the nanotubes, an increased electrical conduction and better performance during compressive load.

Another application, which is an example of a non-structural application, is filling of photoactive polymers with nanotubes. PVV (poly- p-phenylene vinylene) filled with MWNTs and SWNTs is a composite, which has been used for several experiments. These composites (see figure 1.8 [17]) show a large increase in conductivity with only a little loss in photoluminescence and electro-luminescence yields. Another benefit is that the CNT based polymer composite is more robust than the pure polymer.



Figure 1.8 CNT polymer composite [17]

Another use of nanotube composites is as antistatic shielding, on airplane wings and fuselages, for example. This is a realistic application. Another application of conducting composites is as a transparent conductor. Transparent electronic

conductors such as Indium Tin oxide (ITO) is used in displays. In this field, there is a drive towards flexible displays on plastic substrates. ITO is less good for this situation as it is brittle and has poor adhesion to plastic. Conducting composites of SWNTs can be transparent if thin enough. They have the huge advantage of being truly flexible and compatible with polymer substrates.

1.5.2 Textiles

The mechanical properties, such as stiffness, toughness, and strength lead to a wealth of applications exploiting CNTs, including advanced tear resistant textile. Fibers spun of pure CNTs have recently been demonstrated [18] and are undergoing rapid development, along with CNT composite fibers. Such super strong fibers will have many applications including body and vehicle armor, transmission line cables, woven fabrics and textiles. CNTs are also being used to make textiles stain resistant.

1.5.3 Energy Storage

CNTs have the intrinsic characteristics desired in material used as electrodes in batteries and capacitors, two technologies of rapidly increasing importance. CNTs have a tremendously high surface area ($\sim 1000 \text{ m}^2/\text{g}$), good electrical conductivity, and very importantly, their linear geometry makes their surface highly accessible to the electrolyte.

Research has shown that CNTs have the highest reversible capacity of any carbon material for use in lithium-ion batteries as shown in figure 1.9 [19]. In addition, CNTs are outstanding materials for super capacitor electrodes [20] and are now being marketed for this application.

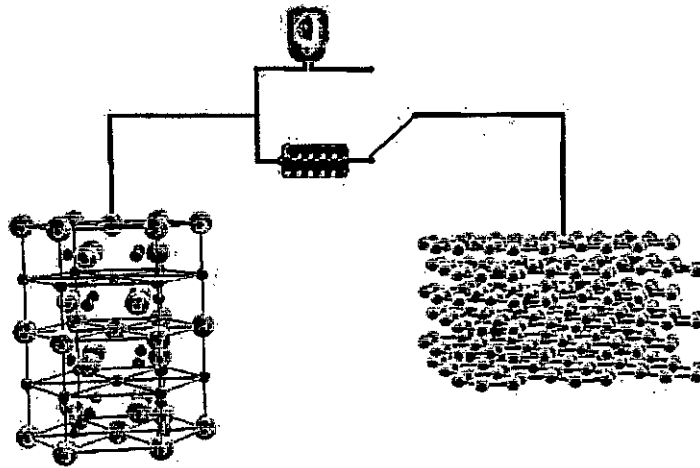


Figure 1.9 CNTs in Lithium ion batteries [19].

CNTs also have applications in a variety of fuel cell components. They have a number of properties, including high surface area and thermal conductivity, which make them useful as electrode catalyst supports in Polymer Electrolyte Membrane (PEM) fuel cells. They are also used in gas diffusion layers, as well as current collectors, because of their high electrical conductivity. CNTs' high strength and toughness-to-weight characteristics may also prove valuable as part of composite components in fuel cells that are deployed in transport applications, where durability is extremely important.

1.5.4 Field Emitting Devices

If a solid is subjected to sufficiently high electric field, electrons near the Fermi level can be extracted from the solid but funneling through the surface potential barrier. This emission current depends on the strength of the local electric field at the emission surface and its work function (which denotes the energy necessary to exact an electron from its highest bounded state into the vacuum level). The

applied electric field must be very high in order to extract an electron. This condition is fulfilled for CNTs, because their elongated shape ensures a very large field amplification. For technological applications, the emissive material should have low threshold emission field and large stability at high current density. Furthermore, an ideal emitter is required to have a nanometer size, a structural integrity, a high electrical conductivity, a small energy spread and a large chemical stability. CNTs possess all these properties. However, a bottleneck in the use of nanotubes for applications is the dependence of the conductivity and emission stability of the nanotubes on the fabrication process and synthesis conditions. Examples of potential applications for nanotubes as field emitting devices are flat panel displays (see figure 1.10), gas discharge tubes in telecom networks, electron guns for electron microscopes, AFM tips and microwave amplifiers.

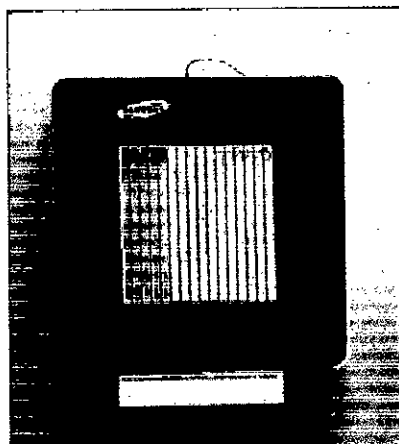


Figure 1.10 A prototype field emission display (fabricated by Samsung)

1.5.5 Probes and Sensors

Because of their flexibility [8], nanotubes can also be used in scanning probe instruments. Since MWNT tips are conducting, they can also be used in Scanning Tunneling Microscope (STM) and Atomic Force Microscope (AFM) instruments

[21]. A schematic of an AFM tip is shown in figure 1.11 [21]. The advantage is the improved resolution in comparison with conventional Si or metal tips and tips do not suffer from crashes with the surfaces because of their high elasticity. However, nanotube vibration, due to their large length, will remain an important issue until shorter nanotubes can be grown controllably.

Nanotube tips can be modified chemically by attachment of functional groups. Because of this, nanotubes can be used as molecular probes, with potential applications in chemistry and biology.

Other applications are the following:

- ▶ A pair of nanotubes can be used as tweezers to move nanoscale structures on surfaces
- ▶ sheets of SWNTs can be used as electromechanical actuators, mimicking the actuator mechanism present in natural muscles.
- ▶ SWNTs may be used as miniaturized chemical sensors. On exposure to environments, which contain NO_2 , NH_3 or O_2 , the electrical resistance changes.

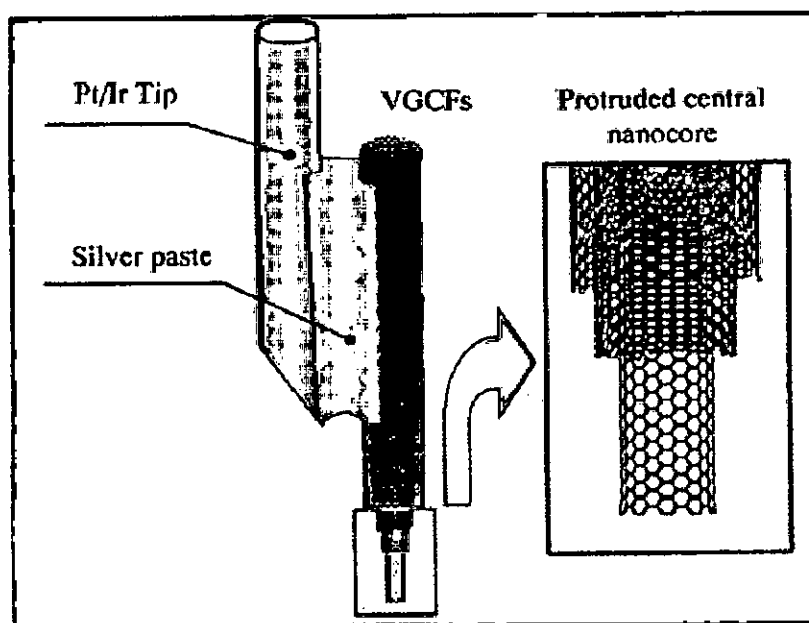


Figure 1.11 Use of a MWNT as AFM tip [21].

1.5.6 Transistors

SWNTs are a very important variety of carbon nanotube because they exhibit important electric properties that are not shared by the MWNT variants. Single-walled nanotubes are the most likely candidate for miniaturizing electronics beyond the micro electromechanical scale that is currently the basis of modern electronics. The most basic building block of these systems is the electric wire, and SWNTs can be excellent conductors [22]. Nanotube based transistors have been made that operate at room temperature and that are capable of digital switching using a single electron [23]. One useful application of SWNTs is in the development of the first intra-molecular field effect transistors (FETs). The production of the first intra-molecular logic gate using SWNT FETs has recently become possible as well [24]. To create a logic gate, both a p-FET and an n-FET are required. Because SWNTs are p-FETs when exposed to oxygen and n-FETs when unexposed to oxygen, it is possible to protect half of a SWNT from oxygen exposure, while exposing the other half to oxygen. This results in a single SWNT that acts as a NOT logic gate with both p and n-type FETs within the same molecule.

1.6 Synthesis and Purification

Techniques have been developed to produce nanotubes in sizeable quantities, including arc discharge, laser ablation, high pressure carbon monoxide (HiPCO), and chemical vapor deposition (CVD). Most of these processes take place in vacuum or with process gases. CVD growth of CNTs can take place in vacuum or at atmospheric pressure. Large quantities of nanotubes can be synthesized by these methods; advances in catalysis and continuous growth processes are making CNTs more commercially viable. The details of these technique are stated in appendix A.

Along with large scale synthesis of CNTs, another problem is the purification of CNTs. CNT soot contains a lot of impurities. The main impurities in the soot are

graphite (wrapped up) sheets, amorphous carbon, metal catalyst and the smaller fullerenes. These impurities will interfere with most of the desired properties of the CNTs. Also in the fundamental research, it is preferred to obtain CNTs as pure as possible. In order to understand the measurements better, the CNT samples also have to be as homogeneous as possible. The common industrial techniques use strong oxidation and acid refluxing techniques, which have an effect on the structure of the tubes. The purification of CNTs are also discussed in appendix A.

1.7 CNT Defects

After ideal structures without flaws, we discuss the possible or undesirable defects. The defects can appear at the stage of CNT growth and purification or later on during device or composite production. Moreover, defects in CNTs can deliberately be created by chemical treatment or by irradiation to achieve the desired functionality.

There are two types of defects, geometric defects and atomistic defects. The most important atomistic defect “Stone-Wales” defect is a combination of two pentagons and two heptagons (5-7-7-5 defect). This kind of defect causes little change to the diameter and chirality and the deformation effect is rather local. And this transformation effectively elongates the tube in the strain direction, releasing the excess strain energy. This defect can be incorporated in a normal tube by 90° rotation of carbon – carbon bond between two hexagons. This rotation changes four neighboring hexagons into two pentagons and two heptagons as shown in figure 1.12.

Another atomistic defect is vacancy defects. The removal of carbon atoms from the hexagonal network of the CNT creates a number of carbon atoms with unsaturated valence orbital. The excess energy arising from the unsaturated valence orbital promotes reconstructions local to the vacancy, forming energetically more stable configurations. For the one and two-atom vacancies, each has two possible

reconstructed configurations, symmetric or asymmetric with respect to the axial direction of the CNT. These reconstructions lead to dimensional changes local to the defects. This defect affects the dimensions of the CNT only locally.

Geometric defects, such as bends and nanotube junctions, are introduced by replacing a hexagon with a heptagon or pentagon (see figure 1.13[25]). Deformations can be inward or outward and, among others, electrical properties are seriously changed by these deformations.

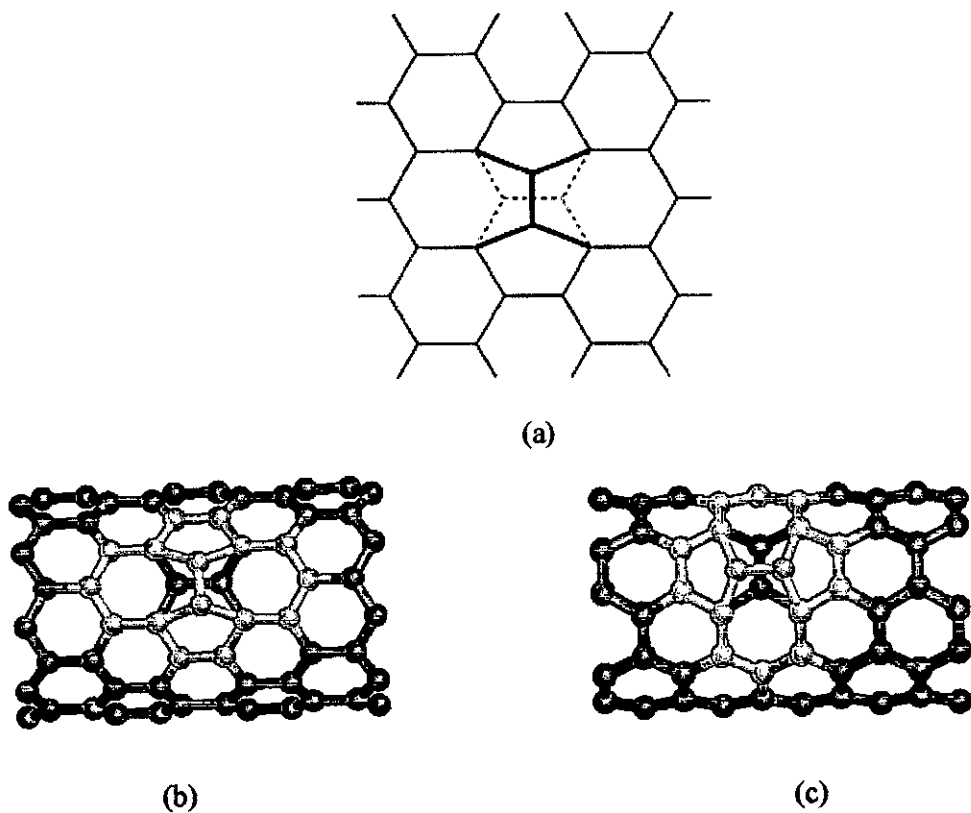


Figure 1.12 (a) Stone-Wales defect formation by C-C rotation in the hexagonal lattice (b) (9,0) CNT (c) (5,5) CNT with Stone Wales defect (indicated in yellow color).

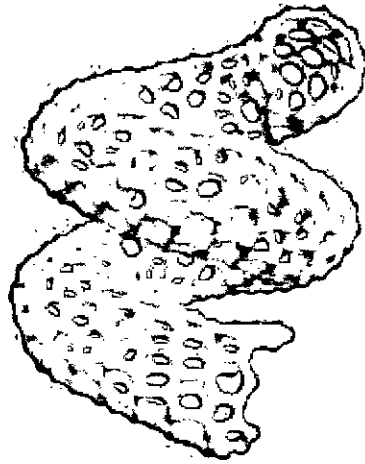


Figure 1.13 Helicoidal graphite with heptagons, pentagons and hexagons [25].

Another class of defects is caused by impurities that are built in during or after the nanotube growth process. Compounds that can be incorporated into the structure are, for example, catalyst particles. The configurations of CNTs with vacancy defects are presented in figure 1.14.

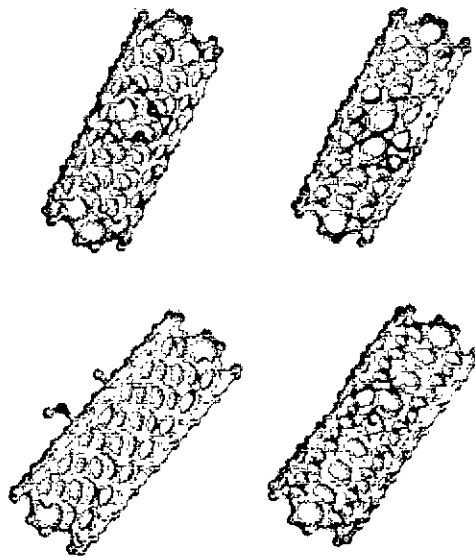


Figure 1.14 Typical vacancy defects in SWNT.

1.8 Layout of the Thesis

For the convenience of presentation, the contents of this thesis are divided into five chapters. Chapter-1 contains introduction about CNTs, potential applications of CNTs and CNT defects. Chapter-2 contains the brief discussion on the available literature related to the present investigation, justification of the present work and objectives of this work. Chapter-3 contains a brief discussion on the MD, potential functions and parameters for CNTs, simulation procedure and defect formation. Chapter-4 consists of results and discussions of present investigation. Conclusion and recommendations are presented in Chapter-5.

CHAPTER 02

LITERATURE REVIEWS

2.1 Introduction

Since the discovery of carbon nanotubes (CNTs) by Iijima [2] in 1991, they have received tremendous scientific and industrial interests. This is due to their exceptional mechanical, electrical, and thermal properties. CNTs can be seen as dream materials whose Young's modulus and tensile strength are in the order of 1000 GPa and 200 GPa, respectively [26] whereas they are much lighter than conventional materials. Due to high strength and stiffness, CNTs are ideal candidate for reinforcement of various materials specially polymers. Having high strength and stiffness along with better thermal and electric properties, CNTs are used in making nano-devices/nanostructure like nano-probe for nano-scale metrology, micro- and nano-electronics, sensors, actuators, field emitters etc.

2.2 Literature Review

Depending on the production process, CNTs are of different structures. They may be single-walled nanotubes (SWNTs) or multi-walled nanotubes (MWNTs), straight or curved tubes and zigzag or armchair nanotubes [26]. Outstanding mechanical properties hold for nearly perfect graphite structure of CNTs. Both stiffness and strength of pristine CNT have been assessed experimentally [27, 28]. Most of the employed methods are classical mechanical tests scaled down to the nanometer scale; this scaling being in most cases a rather difficult task. There is also effort on the evaluation of Young's modulus of carbon nanotubes by micro-Raman spectroscopy [29]. Tensile tests on macroscopic ropes have also given an estimate of Young's modulus of CNTs [30].

The vibrational methods [31, 32] are the best experimental methods for determination of the elastic constants of materials. In case of CNTs, most experiments were interpreted in the framework of the Euler beam theory, which gives access to the Young's modulus considering only the first mode of vibration [32]. Nearly all types

of nanotube structures have been measured by the vibration technique. Vibrating methods are surely the most precise ones for measuring stiffness, but they cannot be used for strength determination. Another set of experiments utilized an atomic force microscope (AFM) to measure elastic modulus and strength of individual nanotubes of various kinds [11, 33-36]. All these methods suffer from a lack of precision due to the difficulty of calibrating the AFM lever on one hand, and measuring the geometry of the tested nanotubes on the other.

The SWNT is supposed to be formed by rolling a graphene sheet and has a Young's modulus of about 1 TPa [37]. Another work also reported the Young's modulus of 4.7 TPa [38]. However, some computational studies found that the true moduli of the nanotubes were far below the estimated values obtained from the graphene sheet. Molecular dynamics (MD) simulation is one of the useful tools to estimate the physical, mechanical and thermal properties of the nanotubes, because it is able to reproduce the realistic nanotube structures. Several kinds of local defects, such as Stone-Waals defect and dislocation of carbon atoms may influence the properties of the nanotubes, which have been discussed in some computational work [39, 40]. Unfortunately, the accuracy of the calculation is highly dependent on the initial boundary condition applied to the simulated models and the sizes of the systems. Also, the weak van der Waals interaction between layers of MWNTs causes the reduction of the mechanical strength subject to a uniaxial tensile load in nanocomposites. Besides, many theoretical works using the continuum mechanics approach have been done to comprehensively investigate all the parameters that influence the properties of nano-materials and to anticipate their macro-scale properties. However, this method is somehow inaccurate and has to be combined with the MD simulation. The time required for MD simulation is typically long and the investment on facilities is also huge [41].

Although CNTs can now be readily produced, it is quite difficult to produce CNTs with completely perfect structure. Usually there are various types of defects present in the actual CNTs [37]. The defects can appear at the stage of CNT growth, purification and latter on during devices and composite production. Moreover, defects in CNTs can deliberately be incorporated during chemical treatment, irradiation to achieve the

desired functionality. As an example of this, defects are expected to increase CNT adhesion to a polymer matrix,[42,43] which should result in improvements of the composite mechanical characteristics. Likewise, defects may enhance the overall characteristics of bundles of SWNTs and MWNTs. In these structures the interactions between intact nanotubes are governed by weak van der Waals forces, so that the axial mechanical load is carried only by the SWNTs at the rope perimeter [33] or by the outermost shell in MWNTs. Thus, creating strong defect mediated covalent bonds between SWNTs in bundles[44-49] or between shells of MWNTs [50] by, for example, irradiation should provide load transfer to the inner tubes (shells). On the other hand, irradiation will create not only covalent bonds between the tubes but also defects in the atomic network. Very recent experiment [49] on electron irradiation of carbon nanotube bundles followed by mechanical testing of the bundle bending modulus (which is proportional to the Young's modulus) indicate that small dose irradiation gives rise to a very large improvement in the mechanical properties of irradiated bundles. This result was understood in terms of irradiation-induced inter-tube links which provided load transfer and correspondingly enhanced the shear modulus inside the bundle. However, high-dose irradiation resulted in deterioration of mechanical characteristics due to accumulation of the irradiation-induced damage, and specifically vacancies, in the nanotube atomic network.

The most common types of defects are Stone-Waals defect and missing atoms (vacancy) defect. These defects may influence the mechanical properties of CNTs to some extent. Therefore, it is necessary to have a deep understanding about the effect of defects on the mechanical properties of CNTs. There are few research works regarding the mechanical properties characterization of defective CNTs. It should be mentioned here that due to the small size of CNTs, their experimental investigation is quite challenging. Sammalkorpi [51] has calculated the Young's modulus, tensile strength, and critical strain of SWNTs with single vacancy defect of different sizes under tensile loading using molecular dynamics (MD) simulation. They have found that the nanotube Young's modulus depends weakly on the vacancy concentration, a relatively high defect density of one vacancy per 5 nm gives rise to a small decrease in the Young's modulus, about 3% only. Double and triple vacancies have a stronger effect on the modulus. However, vacancy reconstructions by saturating dangling

bonds diminish the degradation for the majority of the tubes. They have further shown that vacancies have a much stronger effect on the tensile strength of nanotubes and can degrade to 60% of the strength of intact tube. For the critical strain the effect can be even more deleterious. The critical strain of the defective SWNT can be half of the intact tube value. Similar to the nanotube Young's modulus, the degradation of tensile characteristics is partly alleviated by the ability of the nanotube carbon network to heal the vacancy damage by saturating the dangling bonds. However, even reconstructed defects decrease the tensile characteristics by 5–10% for the zig-zag tubes and 10–15% (tensile strength) and 25–30% (critical strain) for the armchair tubes. These results indicate that the Young's modulus of nanotubes with defects will essentially be the same unless the vacancy concentration is extremely high. On the other hand, the tensile strength will substantially drop due to the quasideimensional atomic structure of SWNTs if already a single vacancy is present—the tensile strength of a SWNT is governed by the 'weakest' segment of the tube. Given that a small number of defects are always present in nanotubes; this may explain why the theoretically predicted Young's modulus agrees well with the experimentally measured values, while the tensile characteristics are much worse.

Zhang [52] have studied the effects of single vacancy defects on the fracture strength of SWNTs using molecular and Continuum Mechanics (CM). They have used numerical simulation, Molecular Mechanics (MM) and a coupled MM/CM (Continuum Mechanics) method, to study the fracture of CNTs under tensile load. They have showed that MM calculations agrees with quantum mechanical (QM) benchmarks, and indicated that one- and two-atom vacancies reduce the fracture strength of CNTs by 20%–33% (whereas the QM calculations predict 14%–27%), but these fracture strengths are still much higher than the experimental data. This experimental and theoretical discrepancy can be attributed to the presence of large-scale defects, such as those that may arise from oxidative purification processes. Simulations on MWNTs and tubes twisted prior to tensile loading show negligible effects on the fracture strength, which indicates that these are not the causes of low experimental values. The effects of chirality and tube diameter on fracture strengths are also investigated in their research.

The effect of two neighboring defects (vacancy or Stone-Wales type) on the mechanical properties of SWNTs under tensile loading has been investigated by Tunvir et al. [53]. Their simulation was performed using classical molecular dynamics at the atomic scale. It was found that two neighboring vacancy defects reduces the failure strength as much as 46% and the failure strain as much as 80% in comparison with those of pristine SWNTs, while two neighboring Stone-Wales defects reduce them as much as 34% and 70% respectively.

Elastic properties and tensile strength of defective SWNTs have been investigated by Xia et al. [54]. They have considered both vacancy and Stone-Wales defects and examined axial and transverse Young's modulus under different hydrostatic pressure using MD and *ab initio* electronic structure calculation. They have determined both the axial and the radial Young's moduli and found that axial Young's modulus is significantly larger than the radial one at the same strain level. The elastic moduli are changed with the strain level in a graded manner. The SWNTs are softened under large tensile strains. SWNT's are somewhat softer at 0.1 K than at room temperature. The local strain induced by the defects lowers the tensile strength of the SWNT's although the elastic moduli are not affected significantly by these defects. The strain at failure for the SWNT's under the hydrostatic stress is estimated to be about 17%. The local bond breakage appears most likely around the defects.

Buckling behavior of double-walled nanotubes (DWNTs) with vacancy defects under combined axial and radial load is studied by Shen et al. [55] using CM.

2.3 Justification

Understanding the role of defects is importance for at least three reasons:

(1) CNTs produced by CVD methods can contain a large quantity of defects and impurities, which are expected to lower their mechanical strength.

(2) A controlled introduction of defects can be used to tailor mechanical behavior.

(3) Chemical purification and functionalisation treatments of CNTs, which are recognized as necessary steps in the fabrication of various composites, inevitably produce point defects.

Therefore, it is necessary to have better knowledge about the effects of defect and defect density on the mechanical behavior of SWNT and MWNT under tensile and compressive loads.

2.4 Objectives

The specific objectives of the present study are as follows:

- a. To simulate perfect and defective SWNTs and DWNTs of different diameter and different slenderness ratio using MD simulation approach.
- b. To investigate the effect of defect density (i.e., number of defects) on the tensile strength and strain of SWNTs of different diameter.
- c. To investigate the effect of defect density (i.e., number of defects) on the compressive strength and strain of SWNTs of different diameter with constant slenderness ratio.
- d. To investigate the effect of defect density (i.e., number of defects) on the tensile strength and strain of DWNT.
- e. To investigate the effect of defect density (i.e., number of defects) on the compressive strength and strain of DWNT.
- f. To compare the present MD simulation results with available results in the literature.

CHAPTER 03

**MOLECULAR DYNAMICS
SIMULATION**

3.1 Introduction

Molecular dynamics (MD) method is used to investigate the mechanical behavior of pristine and defective SWNTs and DWNTs of different diameters in the current work. In this chapter MD technique, potential functions, simulation algorithm, simulation procedure, force and strain calculation procedures will be briefly discussed. The book of Frenkel [56] and references cited therein are referred for a detailed description of the background of this method.

3.2 Molecular Dynamics

MD simulation is a technique to compute the equilibrium and transport properties of a classical many-body system. The time evolution of the system is needed to be compute from some initial state using the fundamental laws of physics, i.e. the microscopic evolution equations of the system. MD simulations are in many respects very similar to real experiments. It represents an interface between laboratory experiments and theory, and can be understood as a 'virtual experiment'. MD is a form of computer simulation in which atoms and molecules are allowed to interact for a period of time by approximations of known physics, giving a view of the motion of the atoms. Because molecular systems generally consist of a vast number of particles, it is impossible to find the properties of such complex systems analytically; MD simulation circumvents this problem by using numerical methods.

3.3 Quantum Molecular Dynamics

The true evolution of the system will be described by the laws of quantum mechanics. This means that, in order to compute the evolution of the system, we would need to solve the time-dependent Schrödinger equation,

$$i\hbar \frac{\partial}{\partial t} \Psi(r,t) = \hat{H}\Psi(r,t). \quad (3.1)$$

Where, i is the imaginary unit, $\Psi(r,t)$ is the wave function, \hbar is reduced Plank's constant ($h/2\pi$), r is the position of the particle and \hat{H} is the Hamiltonian operator.

For the N -particle, time-dependent wave function is $\Psi(r_1, r_2, \dots, r_N, t)$. However, the task of finding the wave function of the system for N more than 4 or 5, is extraordinarily difficult. To represent an n -dimensional function on a grid with M points in each dimension requires M^n points. For $n=3N+1$ and if N is larger than 4 or 5 the number of points become exponentially large, beyond the storage capacity of modern-day computers, for example.

3.4 Classical Molecular Dynamics

The classical MD method is based on Newton's second law or the equation of motion, $F=ma$, where F is the force exerted on the particle, m is its mass and a is its acceleration. From knowledge of the force on each atom, it is possible to determine the acceleration of each atom in the system. Integration of the equations of motion then yields a trajectory that describes the positions, velocities and accelerations of the particles as they vary with time. From this trajectory, the average values of properties can be determined. The method is deterministic; once the positions and velocities of each atom are known, the state of the system can be predicted at any time in the future or the past. MD simulations can be time consuming and computationally expensive. However, computers are getting faster and cheaper. Newton's equation of motion for a particular particle is given by

$$F_i = m_i a_i, \quad (3.2)$$

where F_i is the force exerted on particle i , m_i is the mass of particle i and a_i is the acceleration of particle i . The force can also be expressed as the gradient of the potential energy,

$$F_i = -\nabla_i E. \quad (3.3)$$

Combining these two equations yields

$$-\frac{dE}{dr_i} = m_i \frac{d^2 r_i}{dt^2}, \quad (3.4)$$

where E is the potential energy of the system and r_i is the position vector of particle i . Newton's equation of motion can then relate the derivative of the potential energy to the changes in position as a function of time.

The acceleration is given as the derivative of the potential energy with respect to the position as

$$a = -\frac{1}{m} \frac{dE}{dr}. \quad (3.5)$$

Therefore, to calculate a trajectory, one only needs the initial positions of the atoms, an initial distribution of velocities and the acceleration, which is determined by the gradient of the potential energy function. The equations of motion are deterministic, e.g., the positions and the velocities at time zero determine the positions and velocities at all other times, t . The initial positions of the atom should be chosen compatible with the structure that is aiming to simulate. The initial distribution of velocities are usually determined from a random distribution with the magnitudes conforming to the required temperature and corrected so there is no overall momentum, i.e.,

$$P = \sum_{i=1}^N m_i v_i = 0 \quad (3.6)$$

The velocities, v_i , are often chosen randomly from a Maxwell-Boltzmann distribution [56] at a given temperature, which gives the probability that an atom i has a velocity v_x in the x direction at a temperature T . The equation (3.7) shows the form of the Maxwell-Boltzmann distribution.

$$p(v_{ix}) = \left(\frac{m_i}{2\pi k_B T} \right)^{1/2} e^{\left[-\frac{1}{2} \frac{m_i v_{ix}^2}{k_B T} \right]} \quad (3.7)$$

The temperature can be calculated from the velocities [56] using the relation

$$T(t) = \sum_{i=1}^N \frac{m_i v_i^2(t)}{k_B N_f}, \quad (3.8)$$

where N = number of atoms in the system.

k_B = Boltzmann constant

N_f = number of degrees of freedom = $3N-3$

3.5 Molecular Dynamics Simulation for Nano-Scale Materials

Molecular dynamics is a well established simulation technique to study the properties of nano-materials. There are different types of molecular dynamics. In classical molecular dynamics, atomic positions are determined by solving Newton's equation of motion, $F = Ma$, where F is the force on an atom, M is the mass of the atom, and a is the acceleration of the atom. The force on an atom can be calculated from the change in energy between its current position and its later position a small distance away. This can be recognized as the derivative of the energy with respect to the change in the atom's position. Energy is expressed by the inter-atomic potential, which varies from material to material. The procedure for a classical molecular-dynamics simulation is laid out in figure 3.1.

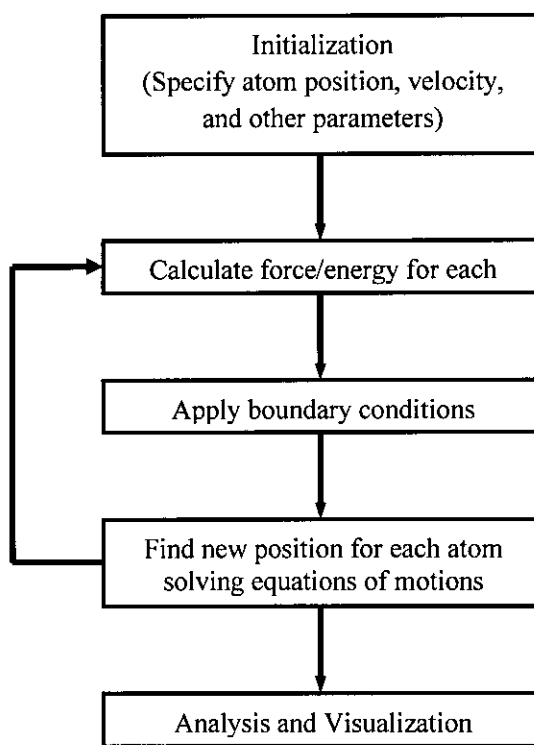


Figure 3.1 Typical flow chart of molecular dynamics simulation.

3.6 Fundamentals of the Simulation

In this work, simulations are performed to investigate the mechanical behavior of pristine and defective SWNTs and DWNTs. At first, SWNT or DWNT structure is generated with known coordinate of each atom. Then molecular simulation is carried out using the classical MD method [57], in which the Newtonian equations of motion are solved numerically for a set of atoms. The velocity-Verlet algorithm [56] is used for solving the Newtonian equations of motion. To control the temperature velocity scaling is used. The Brenner potential [58] is used for carbon-carbon interaction in the CNT and non-bonded interaction between the CNTs in case of DWNTs is modeled with the Lennard-Jones potential [57]. Atoms of two rings of both ends of the nanotube are moved rigidly with incremental displacement in outward and inward direction for tension and compression, respectively. Applied force is calculated by calculating the inter-atomic force of the atoms of the two rings of any end.

Effects of defects on the mechanical behavior of CNTs under tensile and compressive loads are studied using MD simulation. Two types of defects – Stone Wales and vacancy defects are considered here. To create Stone Wales defect, four neighboring hexagons are converted into two pentagons and two heptagons with a 90° rotation of the horizontal bond of the hexagonal structure whereas to create vacancy defects carbon atoms are removed from the perfect hexagonal structure of the CNTs.

3.6.1 Potential Functions and Parameters for CNTs

The Brenner potential function [58], which is used for carbon-carbon interaction in the CNT, is given as

$$E_{tot} = \sum_i \sum_{j(<i)} \{V_R(r_{ij}) - B^*_{ij} V_A(r_{ij})\}. \quad (3.9)$$

Where E_{tot} is the total potential energy and r_{ij} is the length of the bond between atom i and atom j (see figure 3.2). Here $V_R(r_{ij})$ and $V_A(r_{ij})$ are pair-additive repulsive and

attractive interactions, and B^*_{ij} represents a many body coupling between the bond from atom i to atom j and the local environment of atom i , given as

$$V_R(r) = f(r) \frac{D_e}{S-1} \exp\left\{-\beta\sqrt{2S}(r-R_e)\right\} \quad (3.10)$$

$$V_A(r) = f(r) \frac{D_e S}{S-1} \exp\left\{-\beta\sqrt{\frac{2}{S}}(r-R_e)\right\} \quad (3.11)$$

$$B^*_{ij} = \frac{B_{ij} + B_{ji}}{2}, \quad B_{ij} = \left[1 + \sum_{k \neq i,j} \{G_c(\theta_{ijk}) f(r_{ik})\}\right]^{-\delta} \quad (3.12)$$

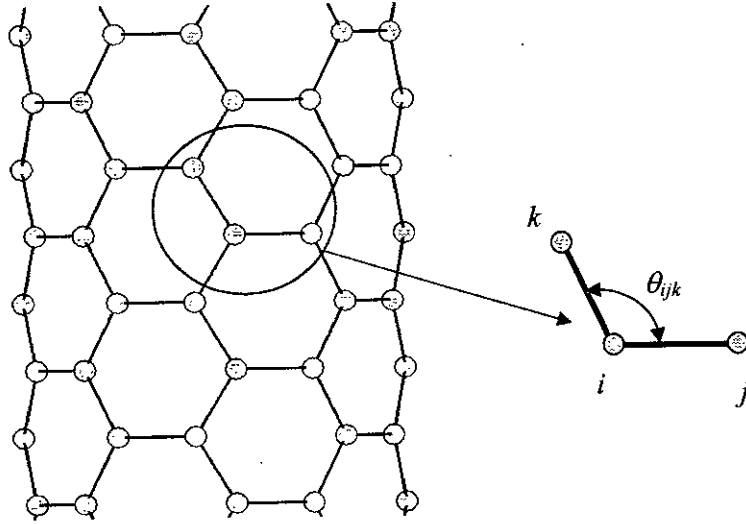


Figure 3.2 Orientation of Carbon atoms in a CNT structure.

In this equation, $G_c(\theta_{ijk})$ is a function of the angle between bonds $i-j$ and $i-k$, given by

$$G_c(\theta_{ijk}) = a_0 \left(1 + \frac{c_0^2}{d_0^2} - \frac{c_0^2}{d_0^2 + (1 + \cos \theta_{ijk})^2}\right) \quad (3.13)$$

Here $f(r)$ is cut-off function whose value is as follows

$$f(r) = \begin{cases} 1 & r < R_1 \\ \frac{1}{2} + \frac{1}{2} \cos \left\{ \frac{\pi(r - R_1)}{(R_2 - R_1)} \right\} & R_1 < r < R_2 \\ 0 & r > R_2 \end{cases} \quad (3.14)$$

Brenner [58] has proposed two sets of potential parameters. The first set of parameters which are adapted here is shown below. It should be mentioned that the first set of parameter can adequately represents the C-C interaction [58].

$$\begin{aligned} D_e &= 6.325 \text{ eV} & S &= 1.29 & \beta &= 1.5 \text{ \AA}^{-1} & R_e &= 1.315 \text{ \AA}, \\ a_0 &= 0.11304 & c_0 &= 19 & d_0 &= 2.5 & R_1 &= 1.95 \text{ \AA}, \\ R_2 &= 2.0 \text{ \AA}. \end{aligned}$$

3.6.2 Potential Functions and Parameters for Inter-Wall Interactions

The nonbonded interfacial interaction between the CNTs and of DWNTs is modeled with 12-6 Lennard-Jones potential [58], given by

$$E_{\text{int}} = 4\varepsilon \left\{ \left(\frac{\sigma}{r} \right)^{12} - \left(\frac{\sigma}{r} \right)^6 \right\}, \quad (3.15)$$

where E_{int} is the potential energy between a pair of atoms, r is the distance between the pair of atoms, ε is the potential well depth, and σ is the van der Waals separation distance. We adopt $\varepsilon = 0.276$ kJ/mol and $\sigma = 0.3468$ nm [59] in the simulation.

3.6.3 Simulation Algorithm

The simulation proceeds iteratively by alternatively calculating forces and solving the equations of motion based on the accelerations obtained from the new forces. In practice, almost all MD codes use much more complicated versions of the algorithm,

including two steps (predictor and corrector) in solving the equations of motion and many additional steps, for example, temperature and pressure control, analysis and output. In MD, the most commonly used time integration algorithm is the Verlet algorithm. Verlet algorithm is a method used to integrate Newton's equations of motion. It is frequently used to calculate trajectories of particles in MD simulations. The Verlet algorithm offers greater stability, time-reversibility and area preserving properties of physical system than the much simpler Euler method [58]. This algorithm is not only one of the simplest, but also usually the best.

The Verlet algorithm reduces the level of errors introduced into the integration by calculating the position at the next time step from the positions at the previous and current time steps, without using the velocity. It is derived by writing two Taylor expansions of the position vector $\vec{r}(t)$ in different time directions

$$r(t + \Delta t) = r(t) + v(t)\Delta t + \frac{f(t)}{2m} \Delta t^2 + \frac{\Delta t^3}{3!} \ddot{r} + O(\Delta t^4), \quad (3.16)$$

here, $f(t)$ is force.

Similarly,

$$r(t - \Delta t) = r(t) - v(t)\Delta t + \frac{f(t)}{2m} \Delta t^2 - \frac{\Delta t^3}{3!} \ddot{r} + O(\Delta t^4) \quad (3.17)$$

Summing the equations (3.15) and (3.16),

$$\begin{aligned} r(t + \Delta t) + r(t - \Delta t) &= 2r(t) + \frac{f(t)}{m} \Delta t^2 + O(\Delta t^4) \\ \Rightarrow r(t + \Delta t) &\approx 2r(t) - r(t - \Delta t) + \frac{f(t)}{m} \Delta t^2 \end{aligned} \quad (3.18)$$

The estimate of the new position contains an error that is of order Δt^4 , where Δt is the time step in MD scheme. However, it is possible to obtain more accurate estimates of the velocity and thereby of the kinetic energy using velocity Verlet algorithm. The velocity Verlet algorithm is the form of Verlet algorithm that uses positions and velocities computed at equal times. This algorithm looks like a Taylor expansion for the coordinates:

$$r(t + \Delta t) = r(t) + v(t)\Delta t + \frac{f(t)}{2m} \Delta t^2 + O(\Delta t^3) \quad (3.19)$$

For the velocity:

$$v(t + \Delta t) = v(t) + \frac{f(t)}{m} \Delta t + \frac{f'(t)}{2m} \Delta t^2 \quad (3.20)$$

For force:

$$\begin{aligned} f(t + \Delta t) &= f(t) + f'(t) \Delta t \\ \Rightarrow f'(t) \Delta t &= f(t + \Delta t) - f(t) \end{aligned} \quad (3.21)$$

Putting the value of equation (3.21) in equation (3.20), the expression for updated velocity becomes:

$$v(t + \Delta t) = v(t) + \frac{f(t + \Delta t) + f(t)}{2m} \Delta t \quad (3.22)$$

3.6.4 Initialization

To begin a MD simulation, first of all, an initial configuration of the system is chosen and $t=0$ is set for starting. The choice of the initial configuration must be done carefully as this can influence the quality of the simulation. It is often good to choose a configuration close to the state that is going to be simulated. The particles should not be positioned at positions that result in an appreciable overlap of the atomic or molecular cores.

3.6.5 Relaxation

Prior to starting a molecular dynamics simulation, it is advisable to do an energy minimization of the structure. Relaxation is the energy minimization without applying loading. In this simulation, relaxation is done by the conjugate energy minimization method and 100 MD steps for equilibration of the system. During the relaxation, the atoms in both ends are kept fixed in their position. When the energy variation with two successive steps is less than 0.01% the relaxation is stopped. Relaxation flow chart is shown in the figure 3.3. For simplicity, only x-component of force, x-component of velocity and x-component of position are shown in the flow chart.

3.6.6 Loading

Loading can be done by two ways: 1) by displacing 2) by force. This simulation is done by displacement method. The atoms of two extreme layers of both ends of the CNT are displaced to a fixed amount (0.0005 nm) in z-direction in every iteration followed by conjugate energy minimization and 100 MD steps for equilibration of the system and strain, force and stress are calculated. In fact, programming procedures in case of relaxation and loading condition are nearly same. The only difference is in the position calculation. In relaxation, atoms of two extreme end rings are fixed in their position. But in case of loading, atoms of two extreme end rings are moved axially outward or inward. The flow chart for loading is shown in the figure 3.4. For simplicity, only x-component of force, x-component of velocity and x-component of position are shown in the flow chart.

3.6.7 Force Calculation

The most time consuming part of the molecular dynamics simulation is the calculation of the force acting on every particle. If a model system with pair wise additive interactions is considered, the contribution to the force on particle i due to all its neighbors should also be considered. When interactions between a particle and the nearest image of another particle is considered only, $N(N-1)/2$ pair distances must be evaluated for a system of N particle.

If a given pair of particles is close enough to interact, the force between these particles can be calculated by differentiating the potential energy between these two atoms. For example, x-component of the force acting on a particle is

$$f_x(r) = -\frac{\partial E(r)}{\partial x} = -\left(\frac{x}{r}\right)\left(\frac{\partial E(r)}{\partial r}\right) \quad (3.23)$$

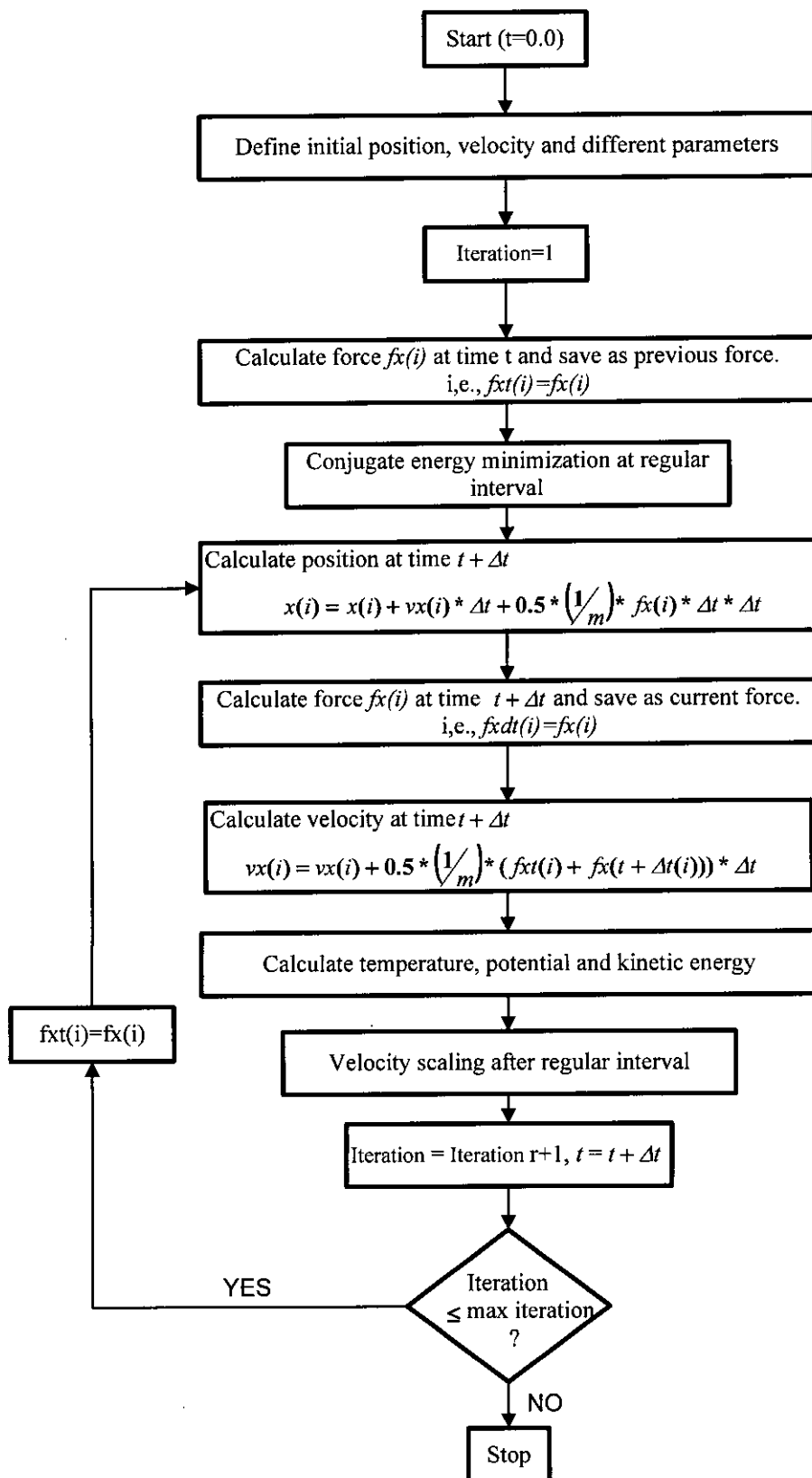


Figure 3.3 Flow chart of relaxation.

3.6.8 Velocity Scaling for Temperature Control

To keep the temperature constant during the simulation, velocity scaling is performed after every few steps according to the following way:

$$T = \frac{v^2 m}{3k_B} \quad (3.24)$$

Here,

T = current temperature

v = velocity

m = mass

k_B = Boltzmann constant

The velocity of every atom in x , y & z direction is scaled by the following equation

$$v = v \sqrt{\frac{T_{ini}}{T}} \quad \text{where, } T_{ini} = \text{initial temperature.}$$

3.7 Tensile and Compressive Test Procedure

To examine the effects of defects on the mechanical properties of nanotube, tensile and compressive tests are conducted using molecular dynamics simulations for both armchair SWNTs and DWNTs. Both pristine CNTs (i.e., CNTs without defects) and defective CNTs are considered in the simulations. In the MD simulation, the atoms of two rings of both ends of the nanotube are moved with incremental displacement of 0.0005 nm. Each incremental displacement of the CNT is followed by the conjugate energy minimization method and 100 molecular dynamics steps for equilibration of the system. In molecular dynamics simulations, equations of motion are solved using the velocity-Verlet algorithm with time step of 0.1 fs. The temperature of the system is kept constant at 300 K and controlled by velocity scaling. During the equilibration period, ends atoms are kept fixed in plane.

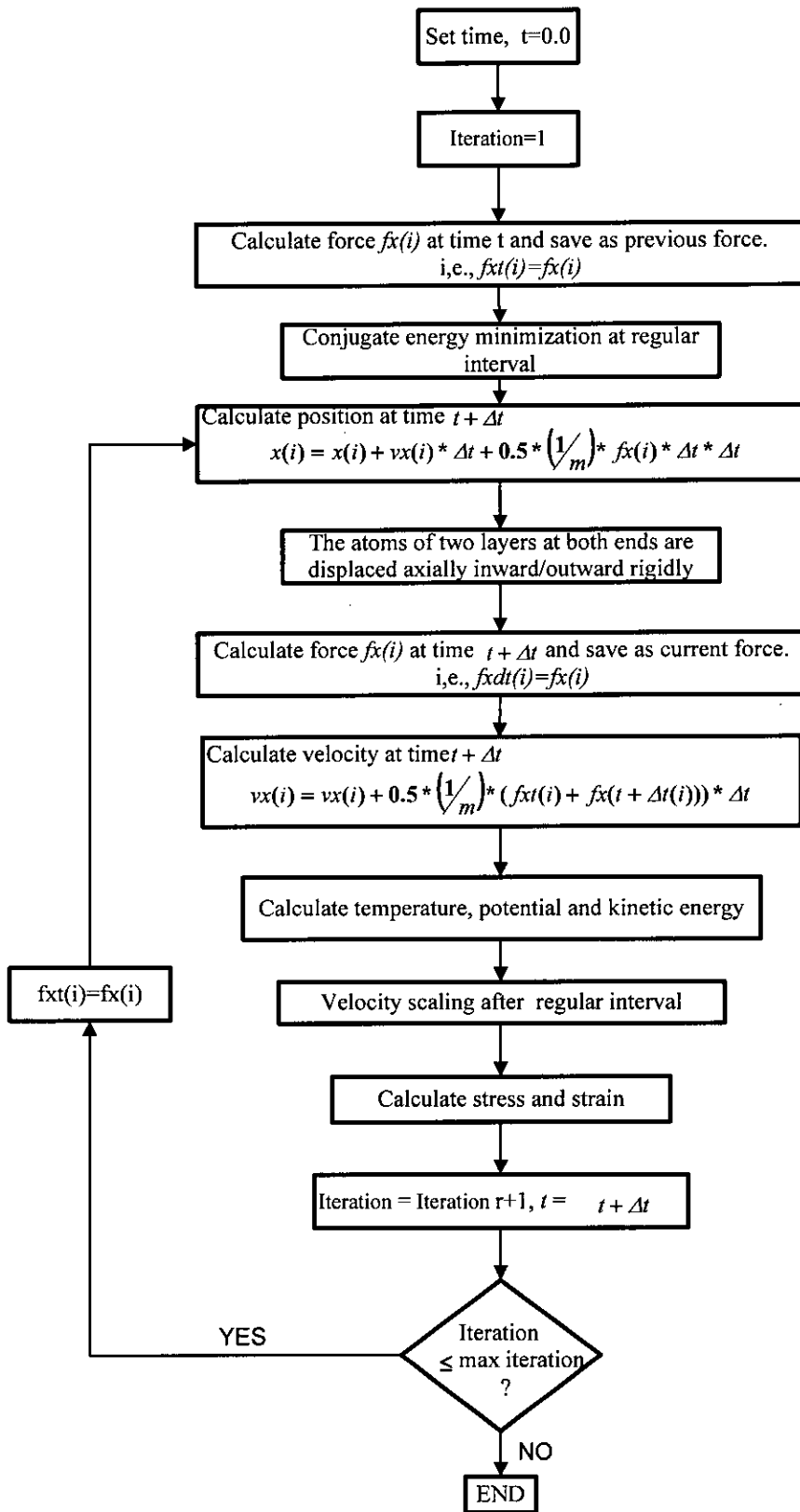


Figure 3.4 Flow chart of loading.

Atomistic model of the tensile test of SWNT is shown in the figure 3.5. Here tensile load is applied by displacing rigidly two rings of each ends axially outward. Atomistic model of the compressive test of SWNT is shown in the figure 3.6. Here compressive load is applied by displacing rigidly two rings of each ends axially inward.

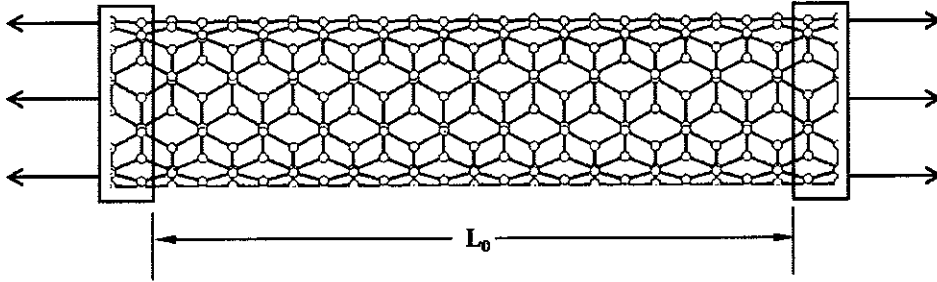


Figure 3.5 Atomistic model for tensile test.

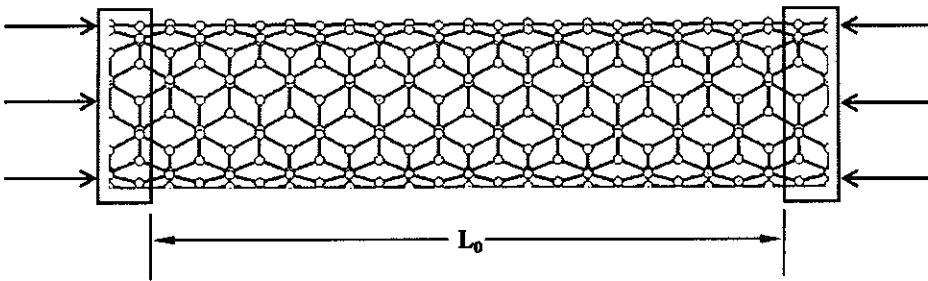


Figure 3.6 Atomistic model for compressive test.

Stress Calculation

Stress is calculated using the following formula:

$$\sigma = \frac{F}{S} \quad (3.24)$$

The axial force $F = F_1 - F_0$, where, F_1 = the total inter atomic force at the corresponding strain, and F_0 = the total inter atomic force at zero strain. Cross-sectional area $S = \pi dh$, where d is the diameter of the CNT and h is the thickness of the CNT (see figure. 3.7) and $h = 0.34$ nm is used.

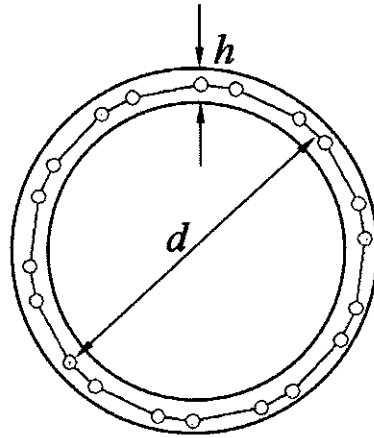


Figure 3.7 Cross section of a SWNT.

Strain Calculation

Strain is calculated according to the following formula:

$$\varepsilon = \frac{L_1 - L_0}{L_1} \quad (3.25)$$

Where, ε = axial strain , L_0 =initial length of the CNT , and L_1 = current length of the CNT.

3.8 Defect Formation

Effects of defects and defect density on the mechanical behavior of CNTs under tensile and compressive loads are studied using MD simulation in this work. Two types of defects – Stone-Wales and vacancy defects with different defect density are considered here.

To create Stone-Wales defect, four neighboring hexagons are converted into two pentagons and two heptagons with a 90° rotation of the horizontal bond of the

hexagonal structure as shown in the figure 3.8. In case of single Stone-Wales defect the defect is placed at the middle ring of the CNT structure whereas in case of three Stone-Wales defects the other two defects are placed in equal distance from the defect at the middle as shown in figure 3.9 . The orientations of all three defects are in the same vertical line.

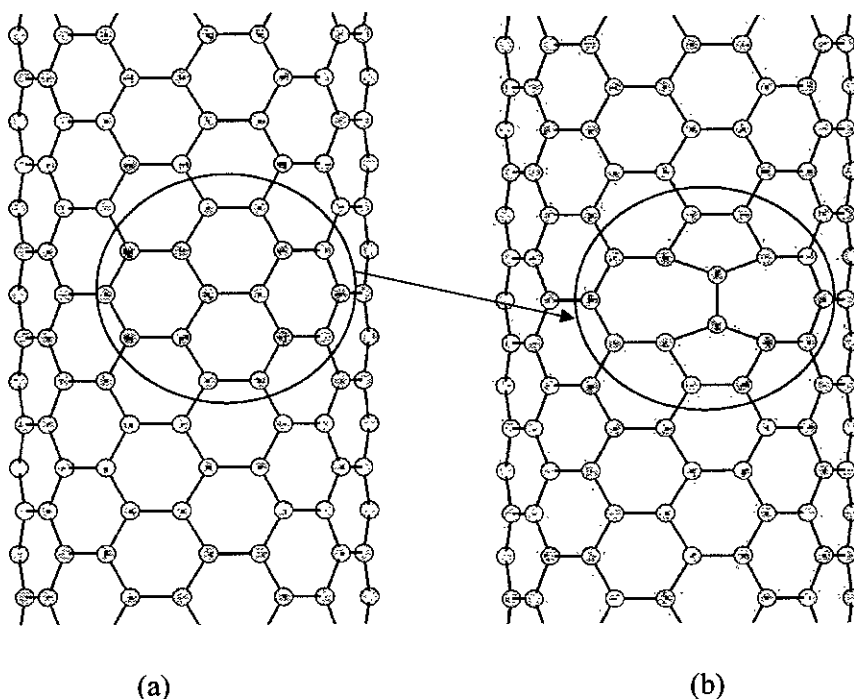


Figure 3.8 Structure of CNT with a) pristine structure, b) one Stone-Wales defect.

To create vacancy defects, carbon atoms are removed from the perfect hexagonal structure of the CNTs creating a vacancy at the place of missing atom. This is shown in the figure 3.10. In case of single vacancy defect the defect is placed at the middle ring of the CNT structure whereas in case of three vacancy defects the other two defects are placed in equal distance from the defect at the middle as shown in the figure 3.11. The orientations of all three defects are in the same vertical line.

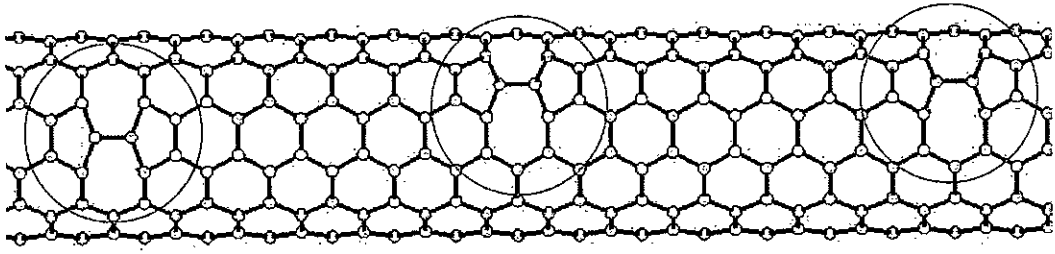


Figure 3.9 Structure of CNT with three Stone-Wales defects.

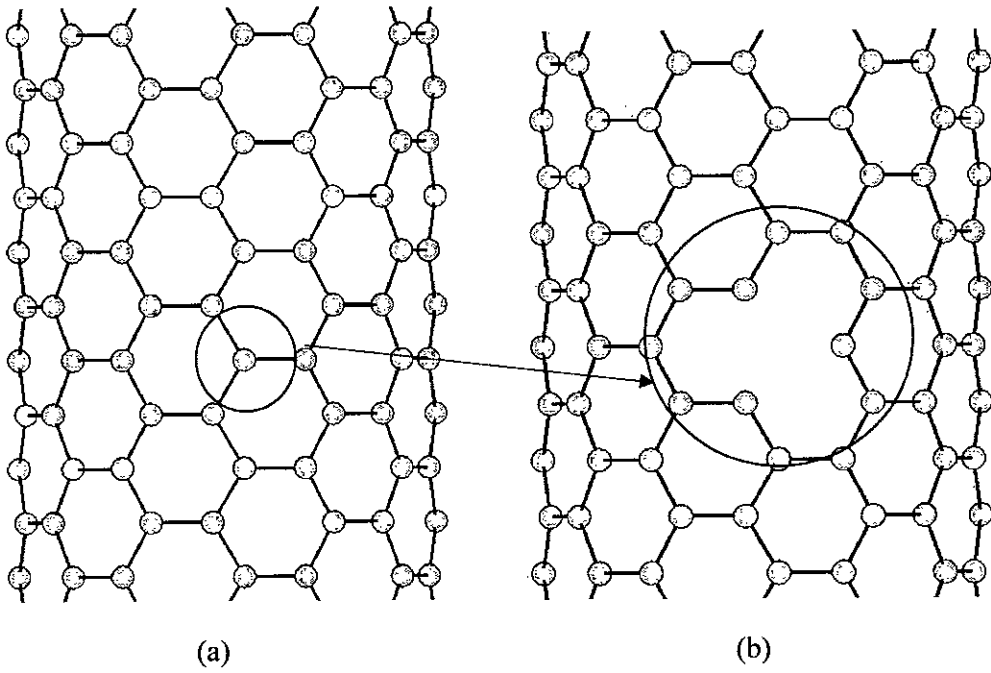


Figure 3.10 Structure of CNT with a) pristine structure, b) one vacancy defect.

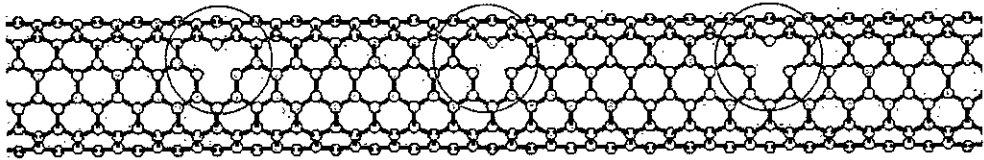


Figure 3.11 Structure of CNT with three vacancy defects.

CHAPTER 04

RESULTS & DISCUSSIONS

4.1 Introduction

The strength of a material refers to the material's ability to withstand the developed stress without failure. Stress is the ratio of developed internal load to the cross-sectional area of an element. Compressive (or compression) stress is the stress state caused by an applied load that acts to reduce the length of the material (compression member) in the axis of the applied load. Tensile stress is the stress state caused by an applied load that tends to elongate the material in the axis of the applied load. The tensile strength or compressive strength of a material is the maximum amount of tensile or compressive stress that it can sustain before failure or buckling. The definition of failure can vary according to material type and design methodology. This is an important concept in engineering, especially in the field of material science, mechanical engineering and structural engineering. Strain is the unit deformation of the geometry of an element. Stress-strain diagram shows the stress-strain response and many important mechanical properties for a material. These properties depend greatly on the material's chemical composition and several other factors of fabrication and service conditions. Since stress is proportional to load and strain is proportional to deformation, this implies that stress is proportional to strain. Hooke's law is the statement of that proportionality and this limit is known as proportional limit. Stress-strain curve remain straight line up to this proportional limit. The proportional constant, E , is the modulus of elasticity, Young's modulus or the tensile modulus is the material's stiffness. Elasticity is the ability of a material to return to its previous shape after stress is released. Elastic limit is the stress beyond which the material will not return to its original shape when unloaded. Other concepts developed from the stress-strain curve are yield point, yield strength, ultimate strength, rupture strength etc. Yield point is the point at which there is an appreciable elongation or yielding of the material without any corresponding increase of load. The corresponding stress is called yield stress. Yield strength is closely related with yield point. All materials do not have well defined yield point. For this reason yield strength is often defined by offset method. This consists of drawing a line parallel to initial tangent of stress-strain curve at 0.2 or 0.5% strain. As shown in figure 4.1, the intersection of this line with the stress-strain curve is called the yield strength. The ultimate stress or ultimate

strength is the highest ordinate on the stress-strain curve. The rapture strength is the stress at failure and corresponding strain is known as failure strain.

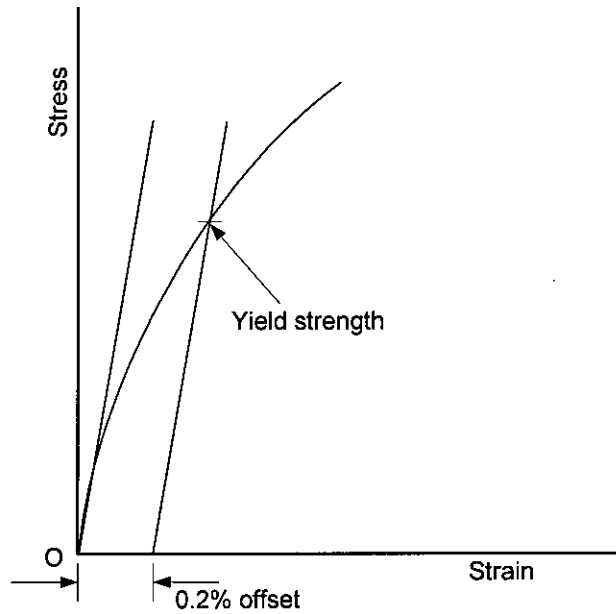


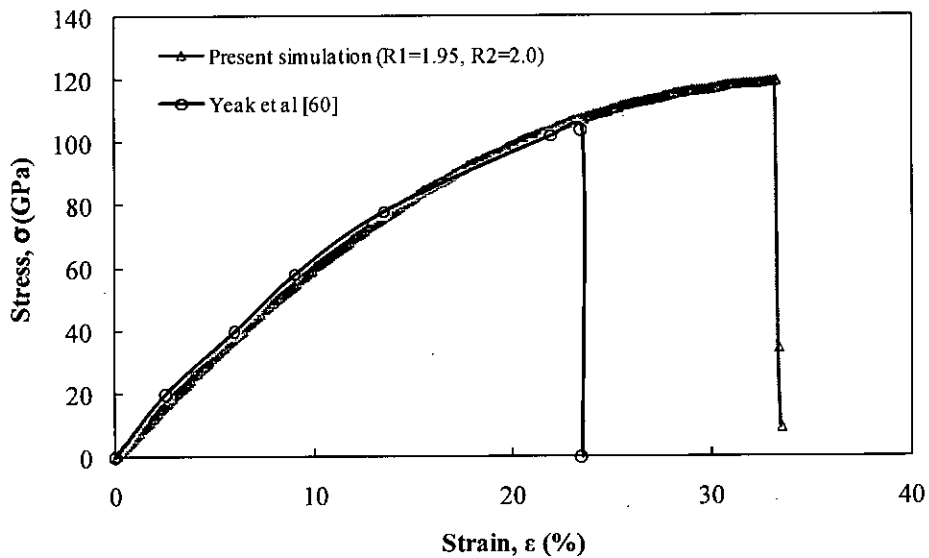
Figure 4.1 Yield strength determination by offset method.

Single-walled and double-walled carbon nanotubes (SWNTs and DWNTs) with perfect structure, vacancy defects and Stone-Wales defects are simulated with Molecular Dynamics (MD) in this work. The mechanical behavior of defective nanotubes under tensile and compressive load are studied and compared with those of pristine nanotubes (i.e. nanotubes without defects).

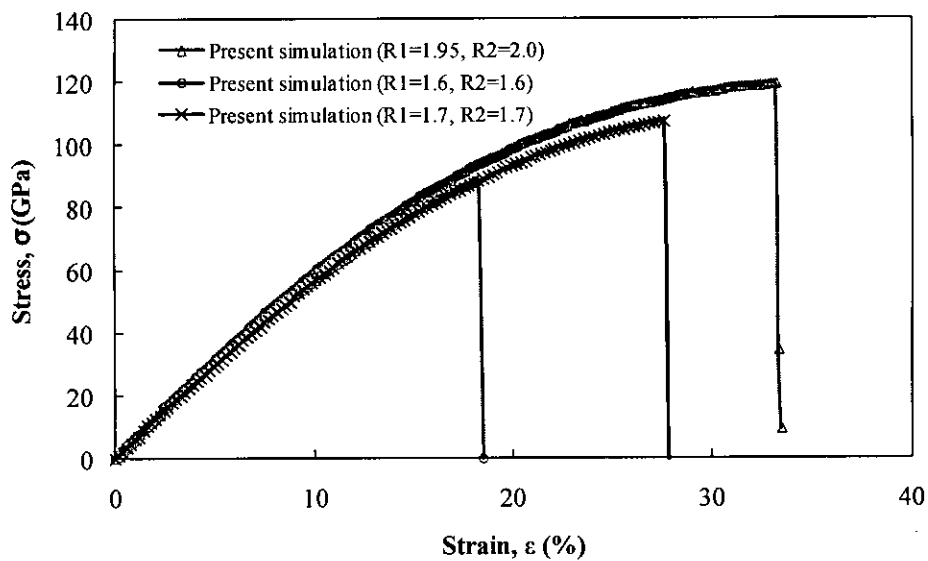
4.2 Validation of the MD Code

In order to validate the present MD simulation code, the stress-strain response is simulated for a (7,7) SWNT with a length-to-diameter ratio $L/D=8$. The results of the current simulation is compared with the results of Yeak et al. [60] as depicted in figure 4.2 (a). It is observed that the present simulation stress-strain results deviate

slightly from the results of Yeak et al. The present simulation results yield a slightly higher failure strain and failure stress because of the different values of potential parameters used in the simulations. It is seen that if the values of Brenner parameter, R_1 and R_2 [58] change the failure stress and strain also change (Figure 4.2(b)). Since we are concerned about the Young's modulus and failure behavior of the CNTs, we consider the maximum values of R_1 and R_2 [61].



(a)



(b)

Figure 4.2 Stress-strain behavior of a (7,7) SWNT under axial tension. (a) Comparison with literature, (b) effect of potential parameters R_1 & R_2 .

4.3 Results and Discussions

To examine the effects of defects on the mechanical properties of nanotube, tensile and compressive tests of (3,3), (4,4), (5,5), (6,6), (7,7) armchair SWNT and ((3,3),(8,8)) DWNT are conducted using molecular dynamics simulations. Perfect structure, vacancy defects, and Stone Wales defects with different density are considered for simulation. The physical specification of the SWNT are listed in the table 4.1. Failure strength, failure strain and modulus of elasticity for tensile and compressive load are calculated. Failure behaviors of nanotubes under tensile and compressive loads are also examined.

Table 4.1 SWNTs specification

CNT index	Diameter (nm)	Length (nm)	Aspect Ratio (l/d)	Number of Atoms		
				Pristine CNT	CNT with one vacancy defect	CNT with three vacancy defects
(3,3) armchair	4.13×10^{-1}	3.49	8.46	174	173	171
(4,4) armchair	5.50×10^{-1}	4.49	8.16	296	295	293
(5,5) armchair	6.87×10^{-1}	5.74	8.34	470	469	467
(6,6) armchair	8.25×10^{-1}	6.73	8.16	660	659	657
(7,7) armchair	9.63×10^{-1}	7.73	8.03	882	881	879

4.3.1 Tensile Test of Pristine SWNT

The stress-strain curve of (3,3), (4,4), (5,5), (6,6) and (7,7) pristine SWNT are presented in the figures 4.3 to 4.7. It is found from the figures that the SWNT do not have a well defined yield point. Since there is no well defined yield point, therefore yield strength is calculated by offset method (see figure 4.1). The yield strength is calculated at 0.2% strain. The average yield strength found for different diameter

SWNT is about 103 GPa. When SWNT is loaded above the yield strength, it begins to 'neck' (see figure 4.8) as the cross sectional area of the nanotube decreases due to plastic flow. The snap shot of SWNT for tensile test at different strains are shown in figure 4.9. When necking become substantial, it may causes reversal of the engineering stress-strain curve, where decreasing stress correlates to increasing strain because of geometric effect. From the stress-strain curves of SWNT, it is seen that the ultimate strength and failure strength are the same. This is the character of typical brittle materials.

The Young's modulus of elasticity is calculated from the slope of the stress-strain curve. It is found that the Young's modulus varies significantly with diameter. The variation of Young's modulus with diameter is presented in the figure 4.10. It is found from the figure that Young's modulus increases as the diameter increases.

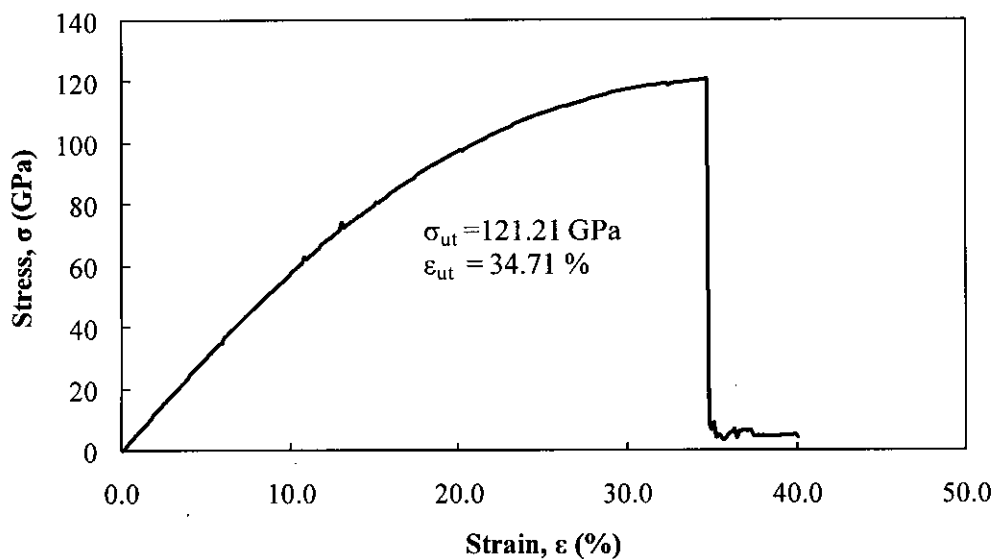


Figure 4.3 Tensile stress versus strain curve for (3,3) pristine SWNT.

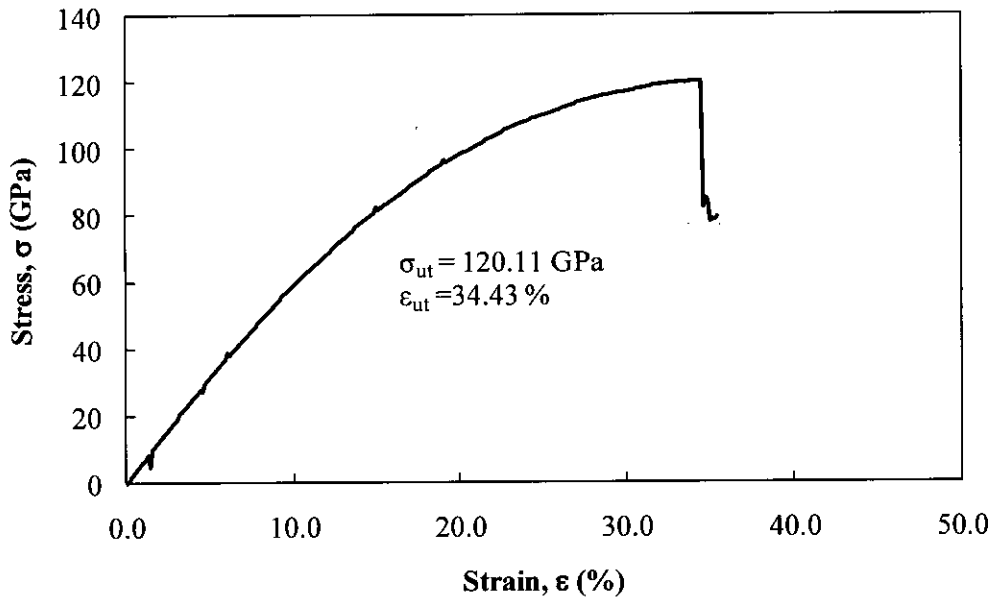


Figure 4.4 Tensile stress versus strain curve for (4,4) pristine SWNT.

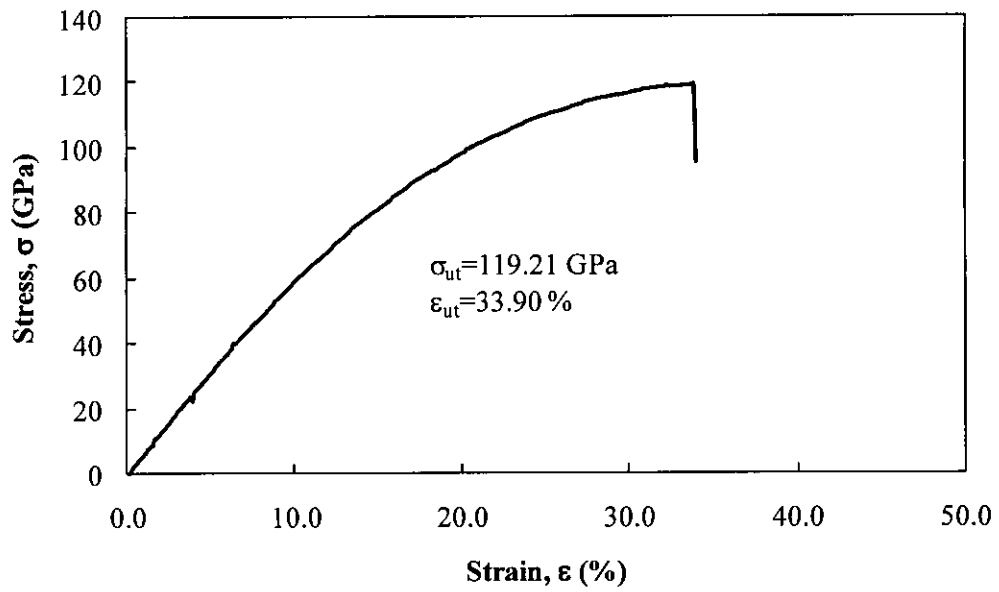


Figure 4.5 Tensile stress versus strain curve for (5,5) pristine SWNT.

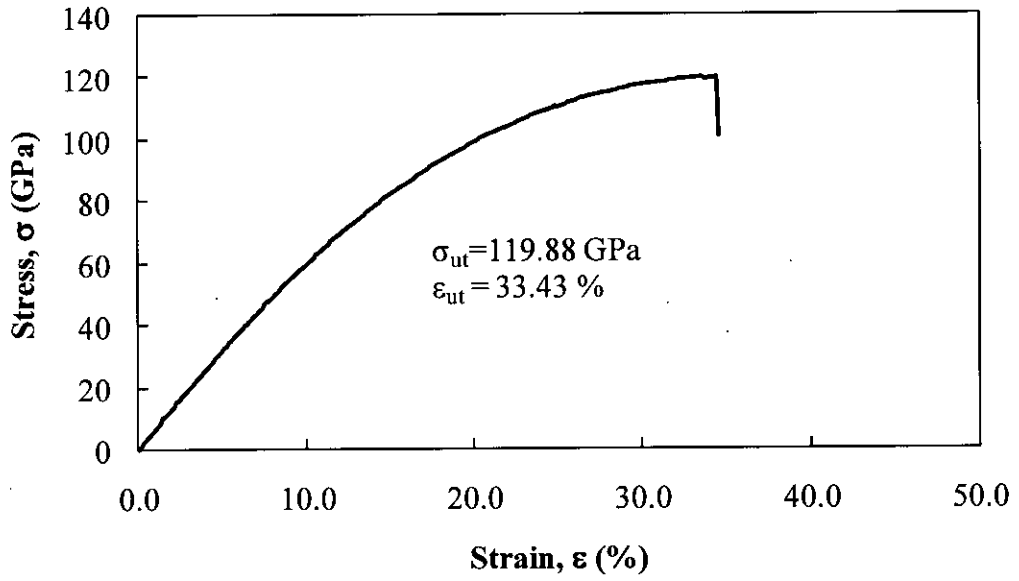


Figure 4.6 Tensile stress versus strain curve for (6,6) pristine SWNT.

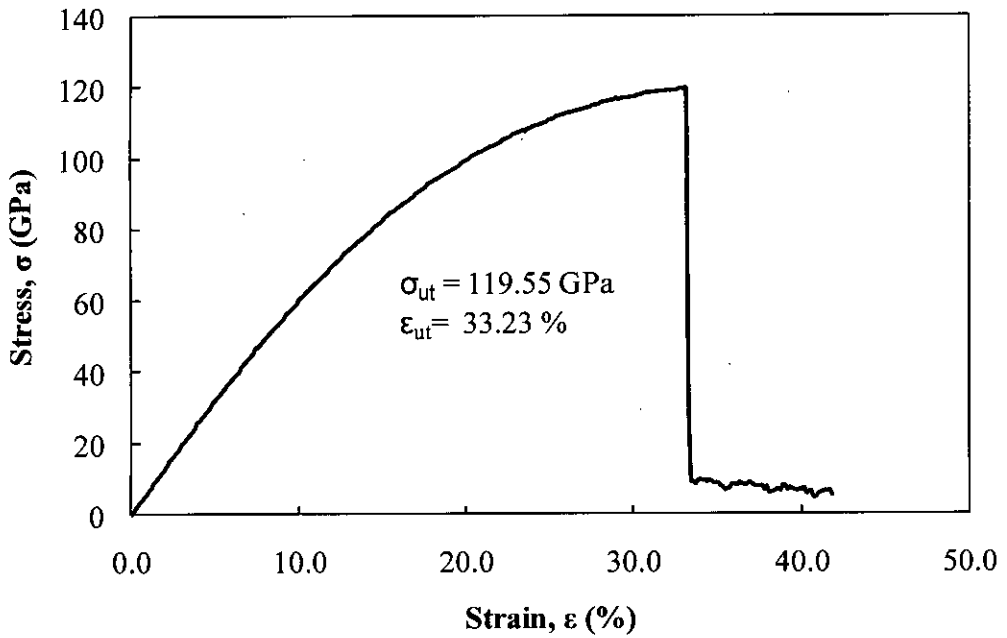
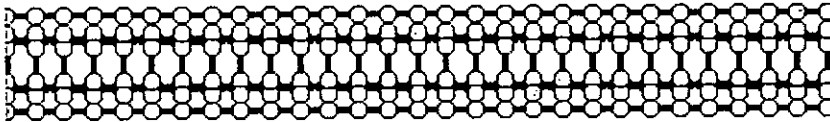


Figure 4.7 Tensile stress versus strain curve for (7,7) pristine SWNT.

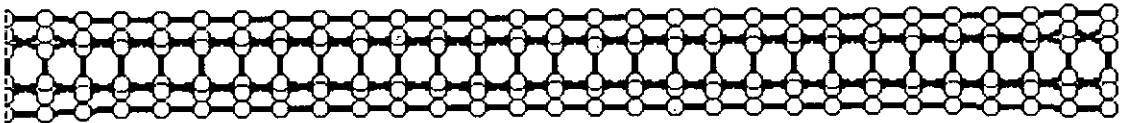


Figure 4.8 Snap shot of necking of a (5,5) pristine SWNT.

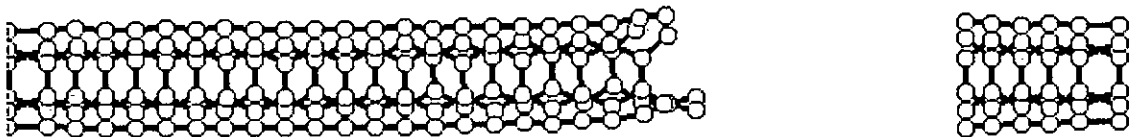
The failure stress variation with diameter is illustrated in the figure 4.11. It is seen that the variation of the failure stresses with the diameter of the SWNTs is negligible. The failure stress decreases only by 1.3% with the increase of diameter by 233%. The failure strain versus diameter curve is presented in the figure 4.12. It is found that the variation of failure strains with the diameter of SWNT is also negligible. Failure strain decreases by 4.23% for the increase of diameter by 233%.



(a)



(b)



(c)

Figure 4.9 Snap shot of tensile test of (5,5) pristine SWNT (a) at 0% strain, (b) at 18% strain, (c) failure at 34% strain.

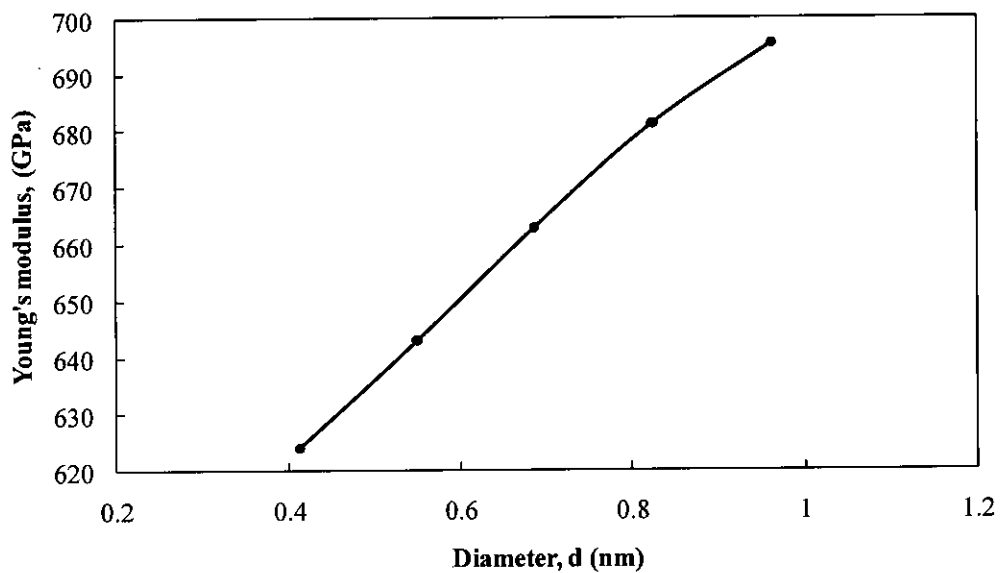


Figure 4.10 Young's modulus versus diameter curve for pristine SWNT under tensile load.

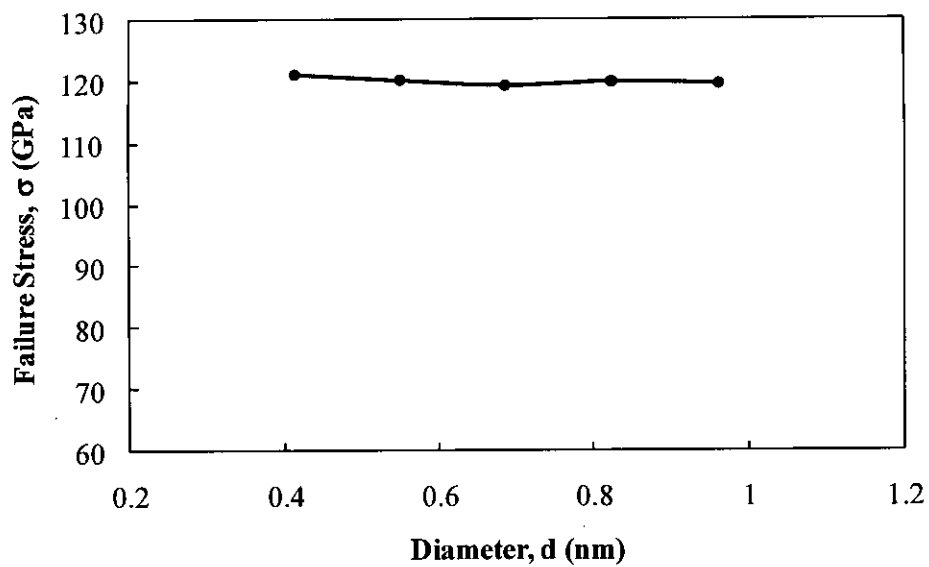


Figure 4.11 Failure stress versus diameter for pristine SWNT.

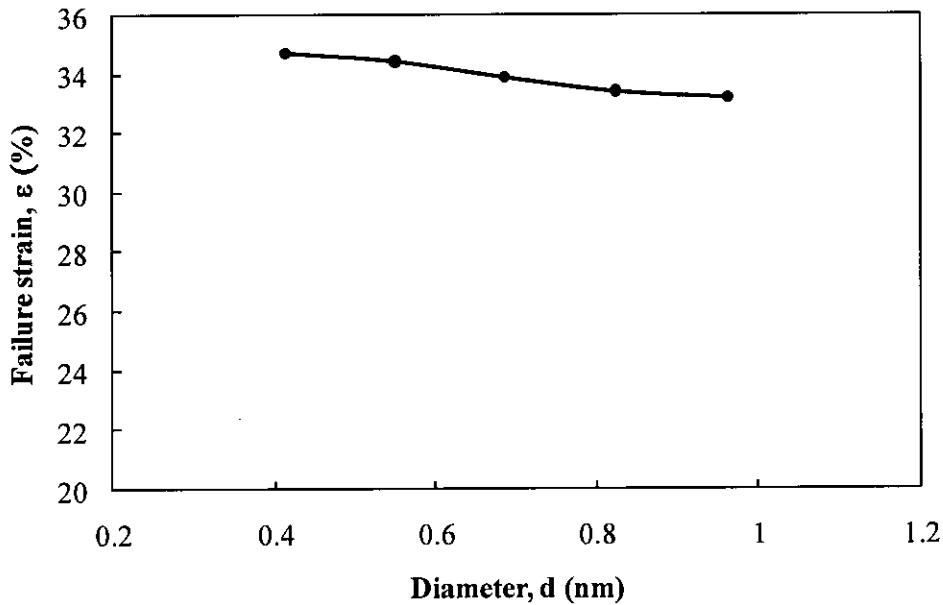


Figure 4.12 Failure strain versus diameter curve for pristine SWNT.

4.3.2 Compressive Test of Pristine SWNT

Like tensile tests, compressive tests are also performed for SWNTs with various diameters. Again, for each diameter, different slenderness ratio is taken under consideration. The end condition of the CNTs for the simulation used is fixed-fixed. The buckling behavior of the SWNT as column is observed for larger slenderness ratio. The stress-strain curve of (3,3), (4,4), (5,5) and (6,6) pristine SWNT under compressive loads are presented in the figures 4.13 to 4.16. The nature of the stress-strain curve of SWNT under compressive load is almost similar to that of stress-strain curve under tensile load. The Young's modulus is calculated from the slope of the stress-strain curve under compressive load. For CNT with specific diameter, Young's modulus in compressive test is found almost the same as that found in the tensile test. The variation of Young's modulus with diameter is presented in the figure 4.17. It is seen from the figure that Young's modulus increases as the diameter increases.

The critical stress (i.e. failure stress) versus slenderness ratio curve is presented in figures 4.18 to 4.21. The results obtained from MD simulations are compared with results obtained from theoretical parabolic and Euler equation. The comparisons are also presented in these figures. Critical slenderness ratio of particular CNT is calculated at half of the corresponding yield strength using the Euler equation [61]. Based on the critical slenderness ratio, the columns are divided as short column and long column. From the figures it is clear that MD simulation results are well agreed with those of theoretical parabolic equation for long columns and theoretical Euler equation for short columns.

During the compressive tests deformation pattern of SWNTs with different slenderness ratios are observed. Two types of deformations namely crushing (or kinking) and buckling are found for different slenderness ratios of SWNT and these are shown in figures 4.22 and 4.23. It is observed that crushing occurs at lower slenderness ratio whereas buckling is found at higher slenderness ratio.

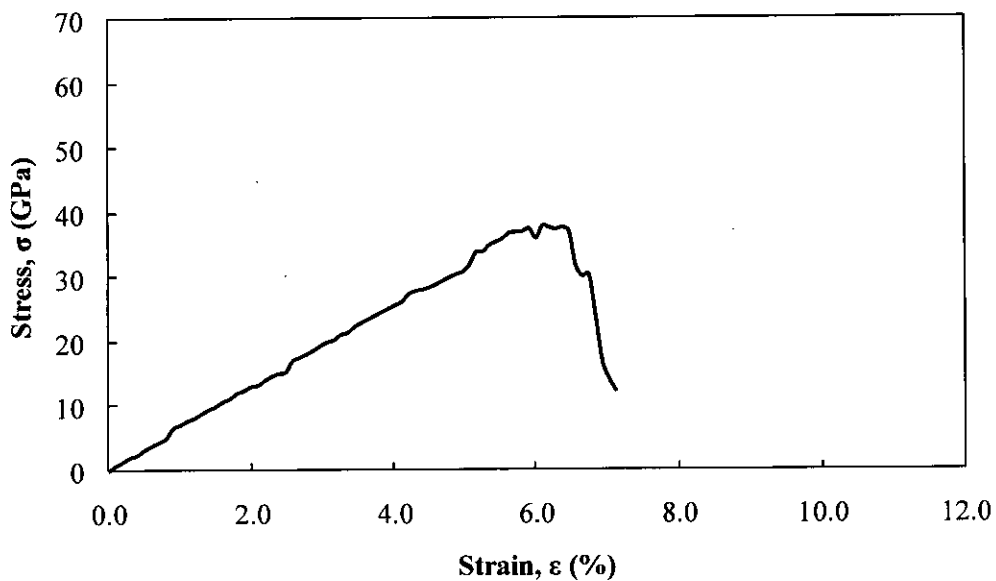


Figure 4.13 Compressive stress versus strain curve for (3,3) pristine SWNT.

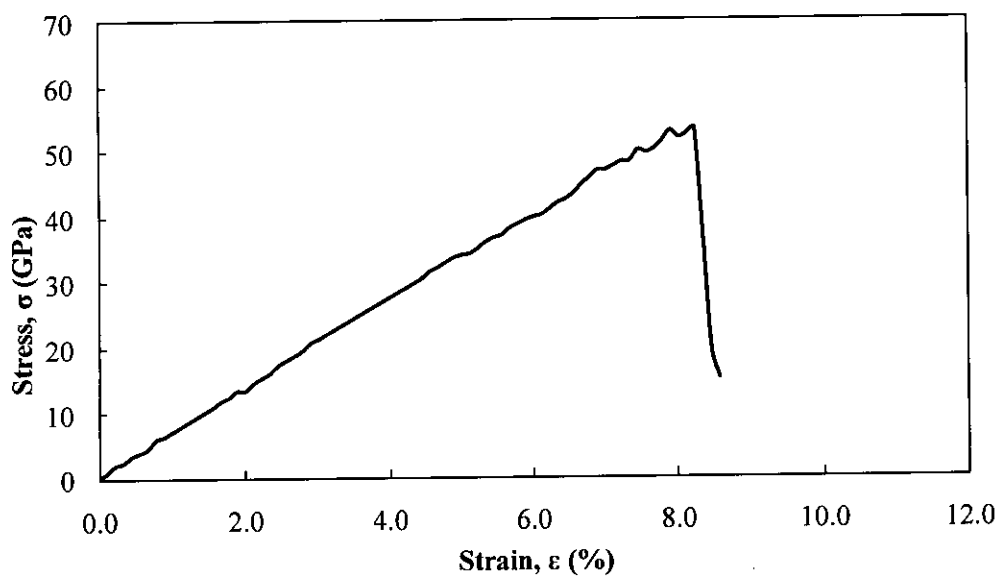


Figure 4.14 Compressive stress versus strain curve for (4,4) pristine SWNT.

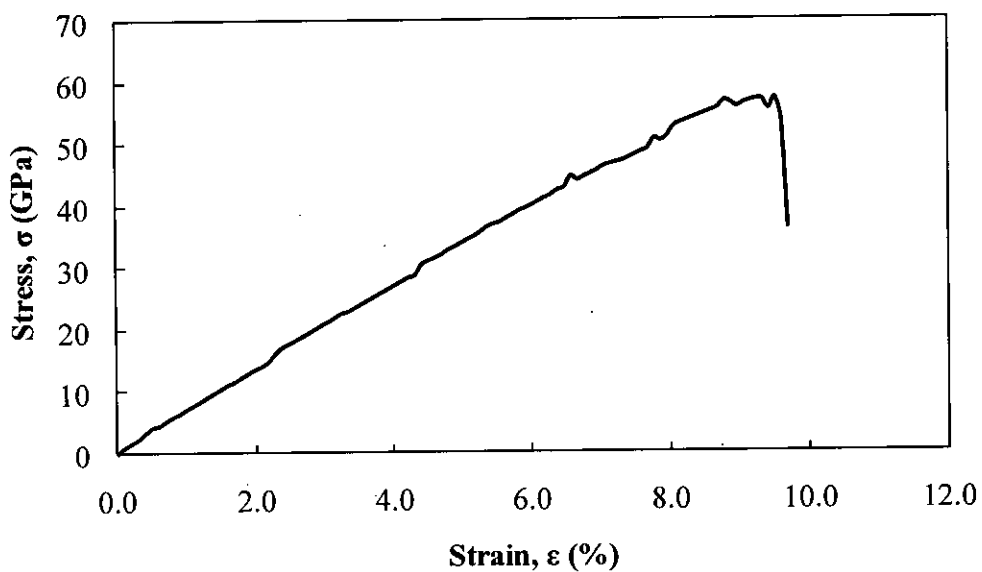


Figure 4.15 Compressive stress versus strain curve for (5,5) pristine SWNT.

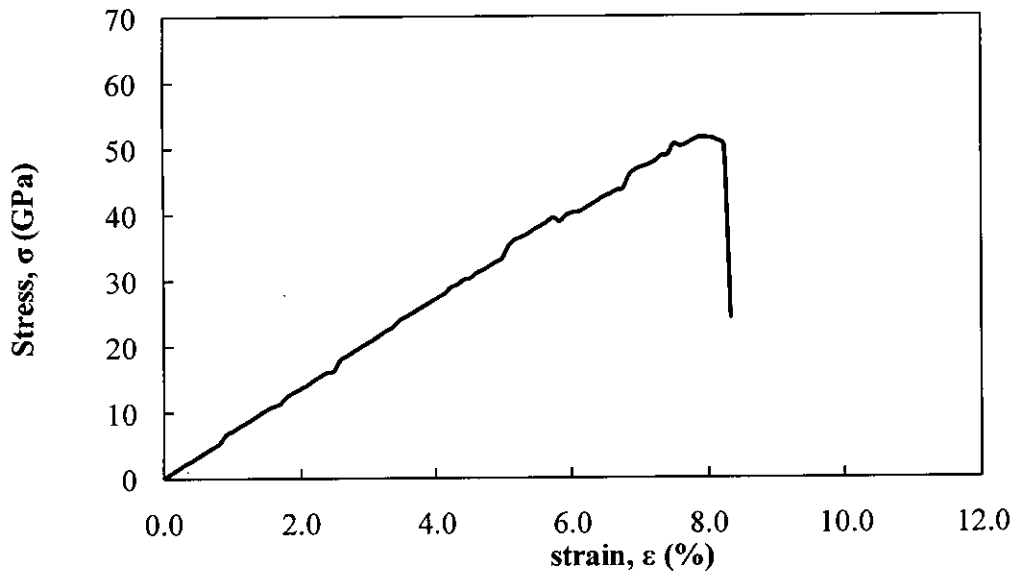


Figure 4.16 Compressive stress versus strain curve for (6,6) pristine SWNT.

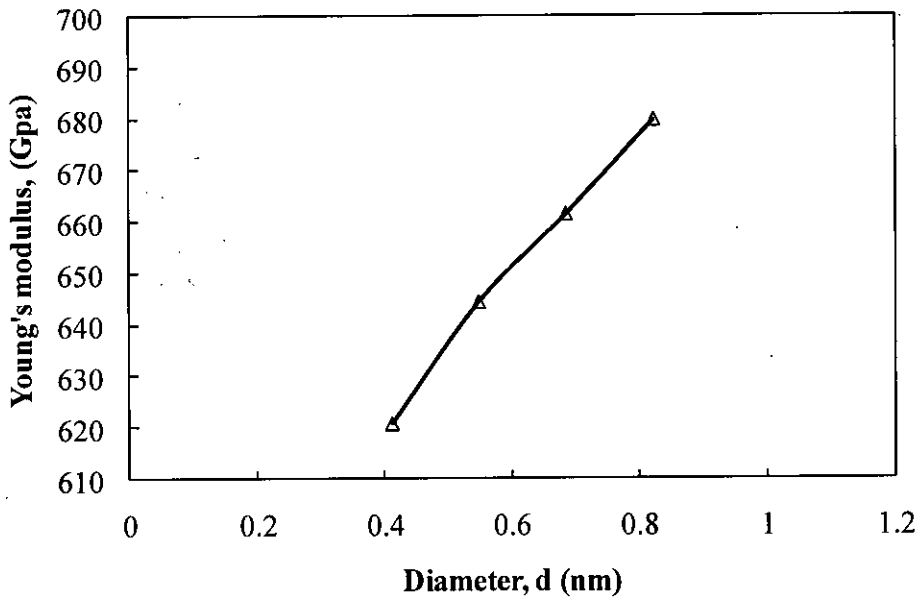


Figure 4.17 Young's modulus versus diameter curve for pristine SWNT under compressive load.

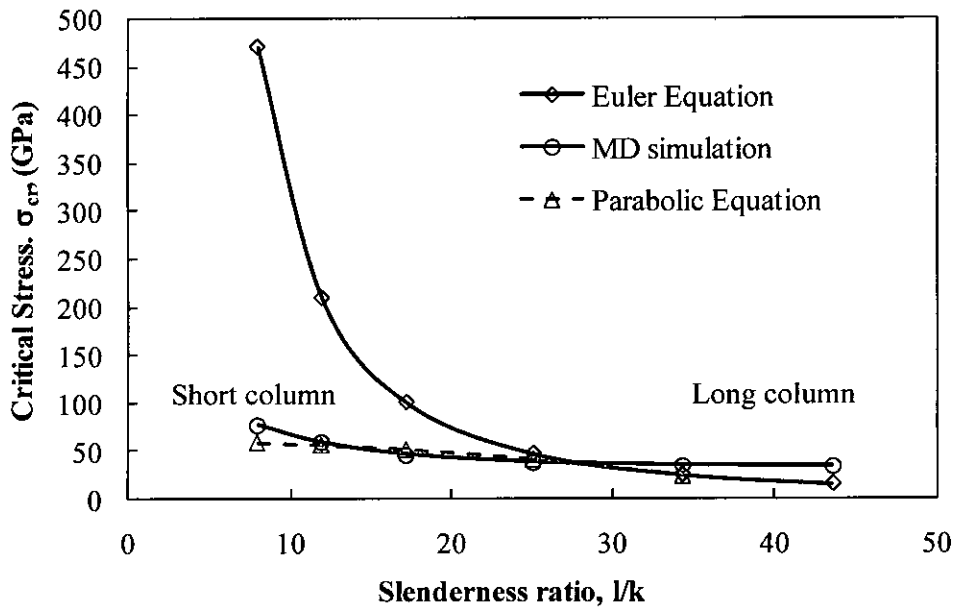


Figure 4.18 Critical stress versus slenderness ratio curve for (3,3) SWNT.

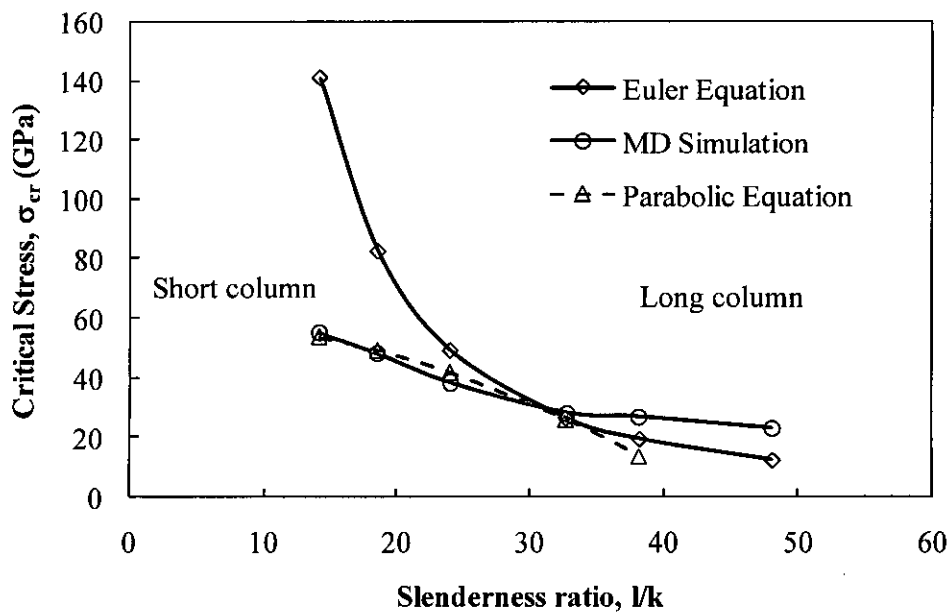


Figure 4.19 Critical stress versus slenderness ratio curve for (4,4) SWNT.

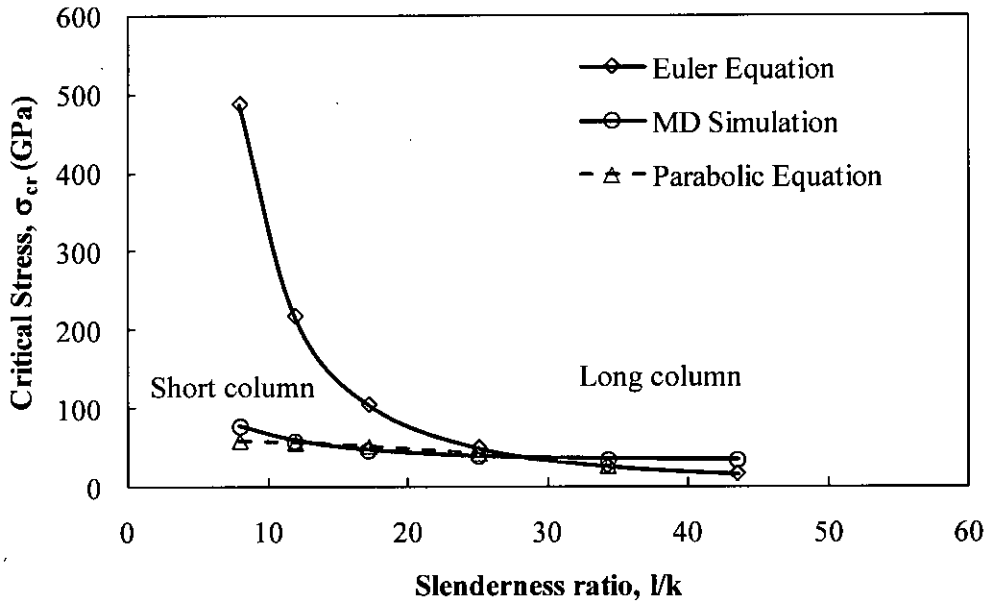


Figure 4.20 Critical stress versus slenderness ratio curve for (5,5) SWNT.

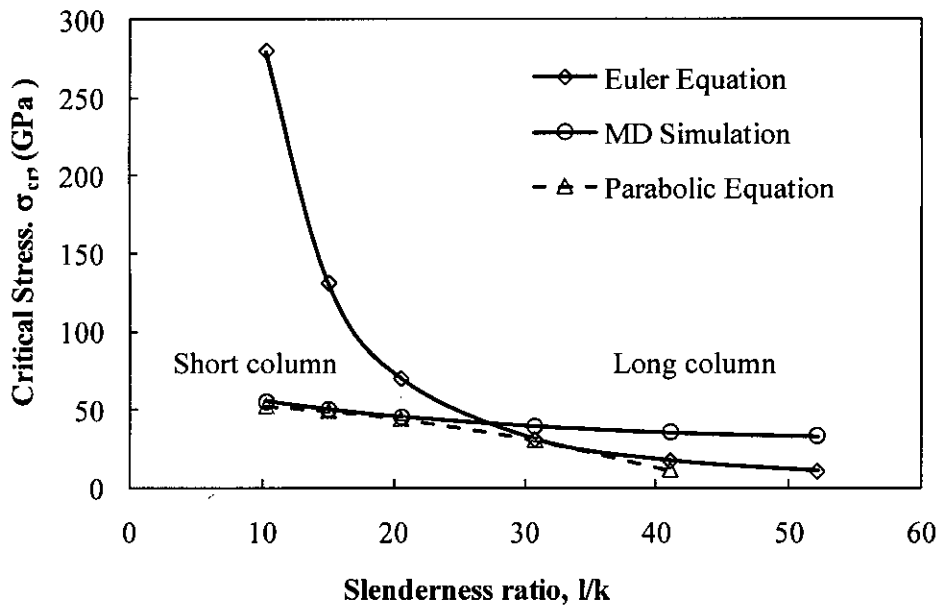


Figure 4.21 Critical stress versus slenderness ratio curve for (6,6) SWNT.

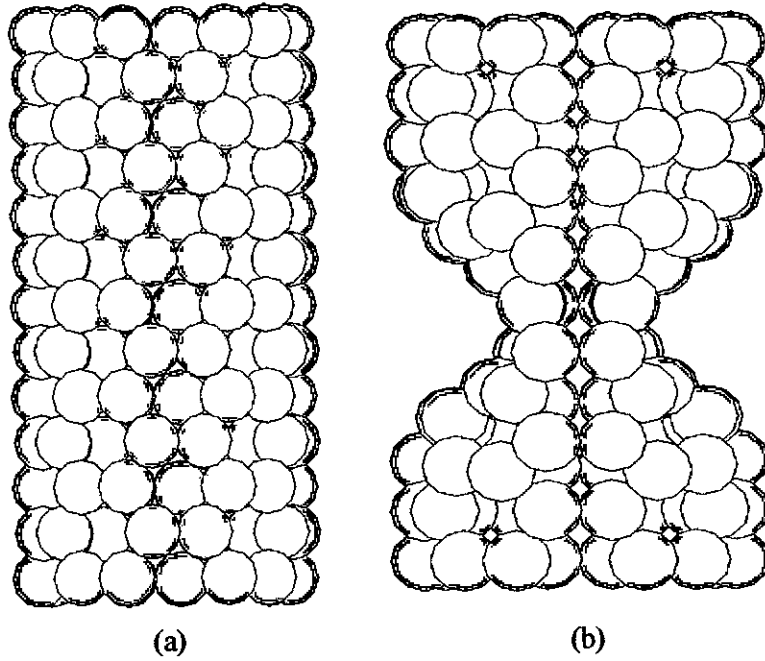


Figure 4.22 Snapshot of (5,5) SWNT with $l/k=10.13$ under compressive load
 a) undeformed, b) crushing (or kinking).

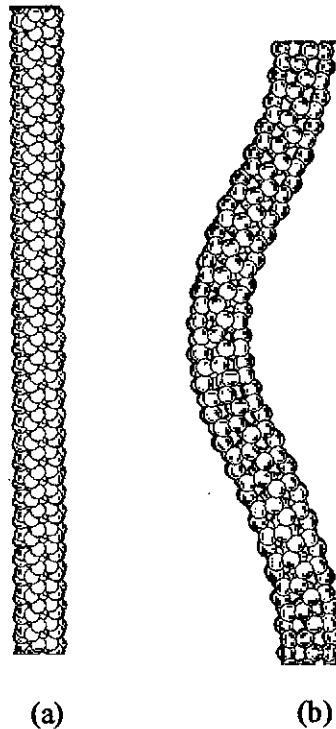


Figure 4.23 Snapshot of (3,3) SWNT with $l/k=43.57$ under compressive load
 a) undeformed, b) buckling.

4.3.3 Tensile Test of Defective SWNT

As with any other material, the issue of defects cannot be neglected when trying to analyze the properties of the nanotube or its composites. Considering only perfect nanotubes is oversimplified. The effect of presence of vacancy and Stone-Wales defect in SWNT with various defect densities are studied in this section. Here (3,3), (4,4), (5,5), (6,6) and (7,7) defective SWNT of same aspect ratio (i.e. l/d) is studied for tensile test. The tensile test procedure is exactly same as that of pristine tensile test of pristine SWNT.

The stress-strain curves of defective SWNT along with pristine SWNT are shown in figure 4.23. It is seen from the figure that the defective structure behaves similar manner as pristine structure. Looking at the stress-strain curve it is seen that Young's modulus does not change for defective SWNTs significantly. But failure strength and failure strain change due to the presence of vacancy defects in the SWNTs. Failure strength is almost same for one vacancy defect and three vacancy defect but failure strain increases with the increase of defect density (i.e. number of defects). Figures 4.24 and 4.25 also show that with the increase of vacancy defects or Stone-Wales defects slope of the stress-strain curve at higher strain decreases and behaving like softer materials which indicates lower stiffness /strain hardening at relatively larger deformation.

This is more explicitly shown in the figure 4.26. With the presence of one vacancy defect and three vacancy defects, tensile strength of the nanotube reduces by 16.19% and 16.66% on an average, respectively, for different diameter. However, in case of Stone-Wales defect this reduction in strength is only 9.58% and 9.27% for one Stone-Wales defect and three Stone-Wales defects. The figure shows that as the number of defects increases, the strength is hardly influence by the number of defects. Because, stress concentration occurs at a specific single defect site from where fracture of the nanotube starts. These can be clear from observing the snapshots in figures 4.27 to 4.30 where SWNT failure is shown for one and three vacancy and Stone-Wales defects.

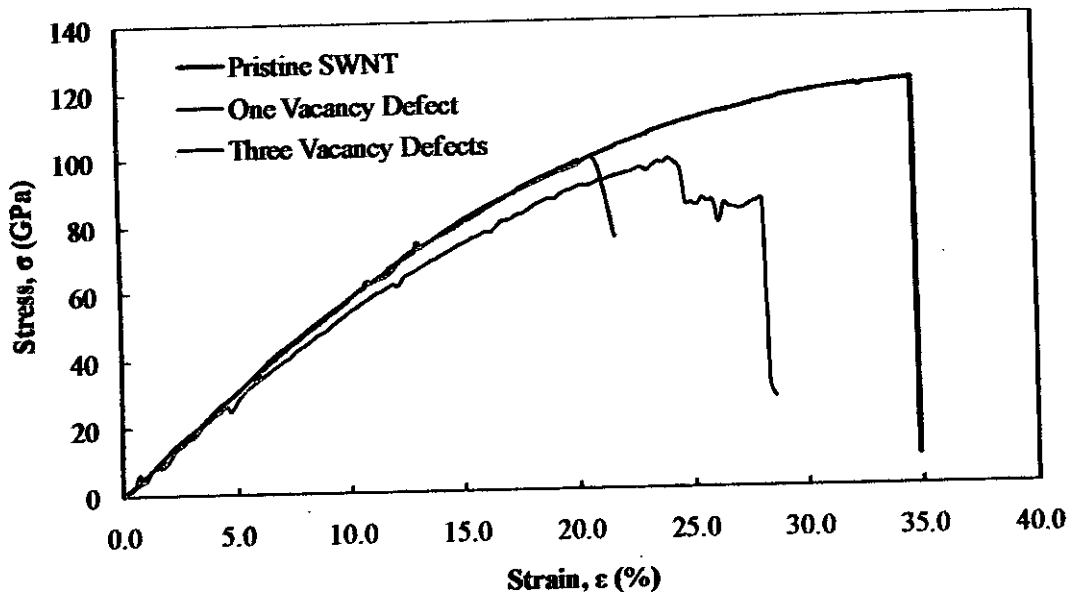


Figure 4.24 Comparison of stress-strain curves of pristine and defective (with vacancy defect) (3,3) SWNT under tensile load.

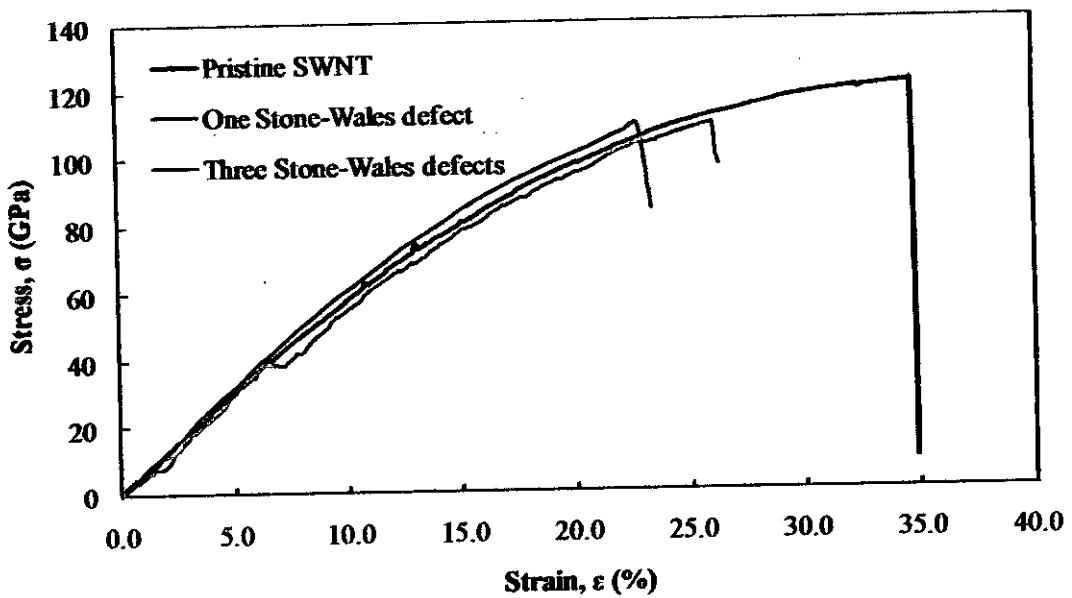


Figure 4.25 Comparison of stress-strain curves of pristine and defective (with Stone-Wales defect) (3,3) SWNT under tensile load.

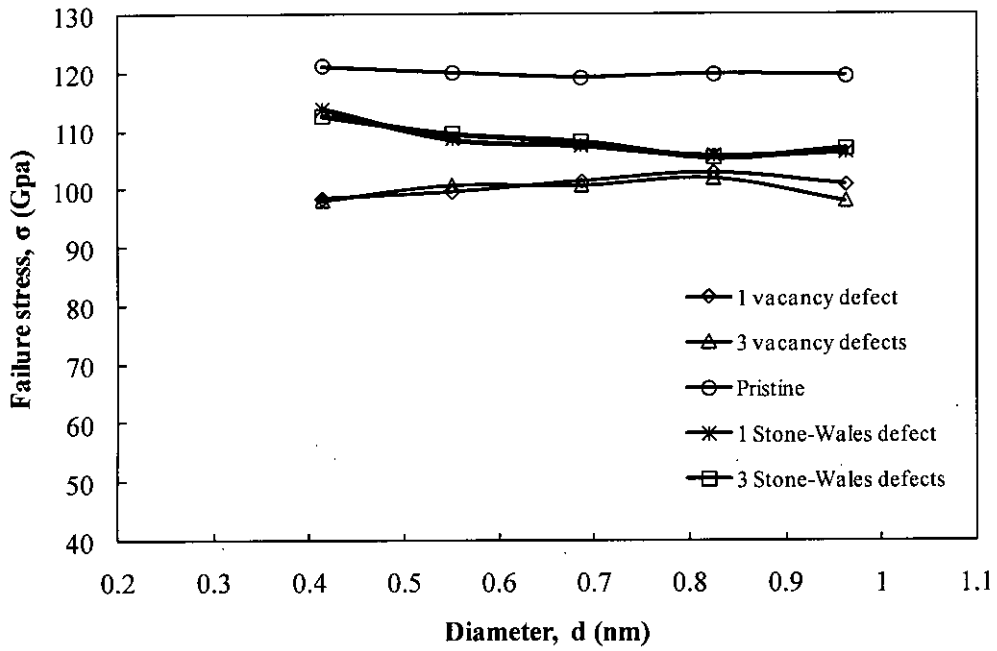


Figure 4.26 Comparison of failure strength of different defective and pristine SWNTs of different diameters under tensile load.

107228

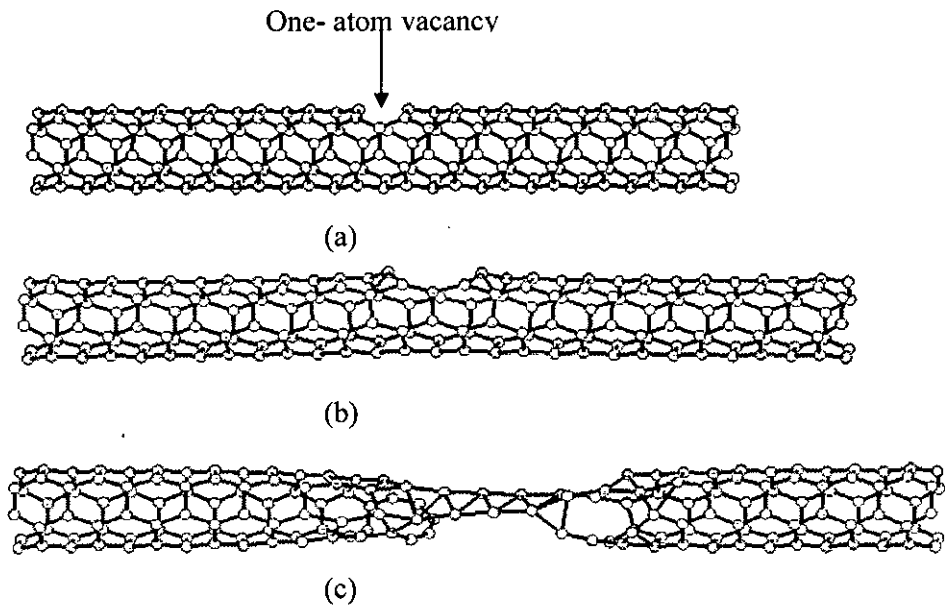


Figure 4.27 Snap shot of tensile test of (3,3) defective SWNT with one vacancy defect (a) at 0% strain, (b) at 10% strain, (c) failure at 20% strain.

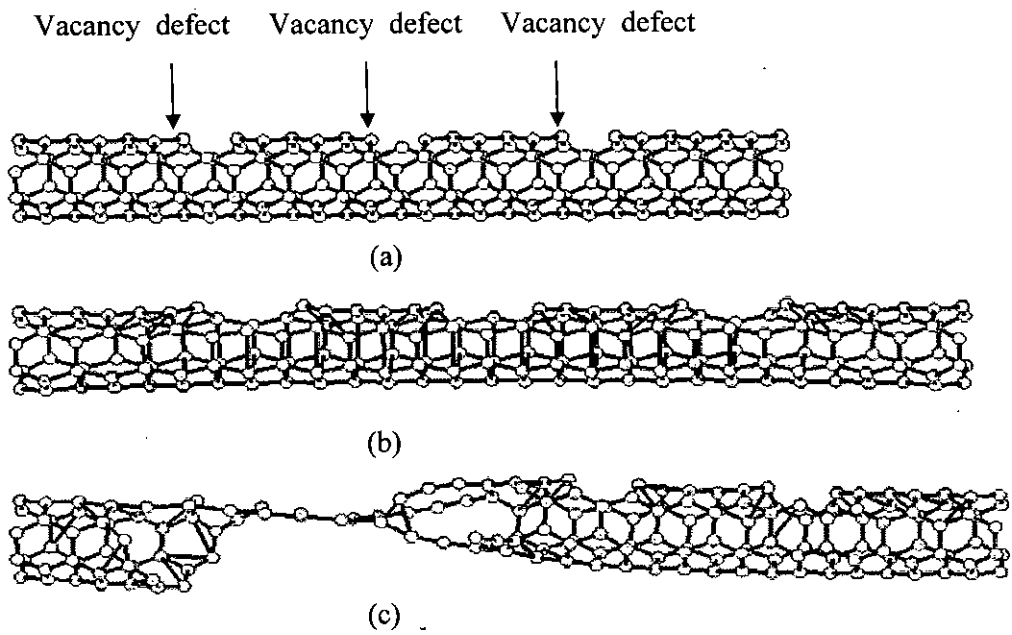


Figure 4.28 Snap shot of tensile test of (3,3) defective SWNT with three vacancy defects (a) at 0% strain, (b) at 10% strain, (c) failure at 23% strain.

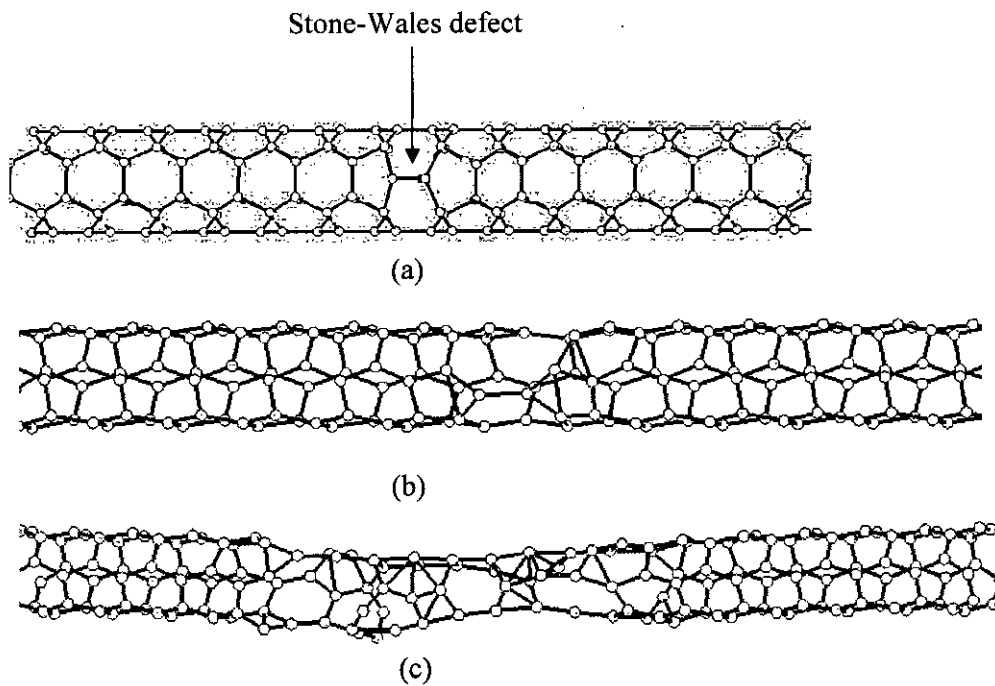


Figure 4.29 Snap shot of tensile test of (3,3) defective SWNT with one Stone-Wales defect (a) at 0% strain, (b) at 20% strain, (c) failure at 30% strain.

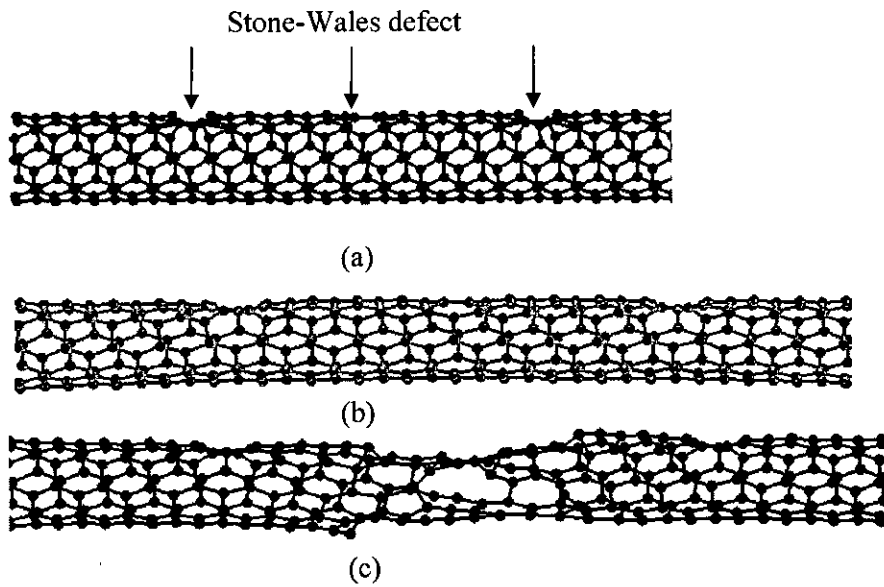


Figure 4.30 Snap shot of tensile test of (4,4) defective SWNT with three Stone-Wales defect (a) at 0% strain, (b) at 20% strain, (c) failure at 33% strain.

4.3.4 Compressive Test of Defective SWNT

The effect of presence of vacancy and Stone-Wales defects in SWNTs with various densities are studied in this section. Here (3,3), (4,4), (5,5), (6,6) and (7,7) defective SWNTs of same slenderness ratio (i.e. l/k) are considered for compressive test. The compressive test procedure is exactly the same as that of compressive test of pristine SWNTs.

Figure 4.29 shows the comparison of failure strength of pristine SWNT and SWNT with one and three vacancy defects. As seen in the figure, the presence of vacancy defects reduces the compressive strength of the nanotube about 33.97% and 34.95% for one vacancy defect and three vacancy defects, respectively. As the number of defects increases there is hardly any influence of extra defects on the compressive strength. Snap shot of compressive test of (4,4) SWNT with one and three vacancy defects are shown in figures 4.30 and 4.31.

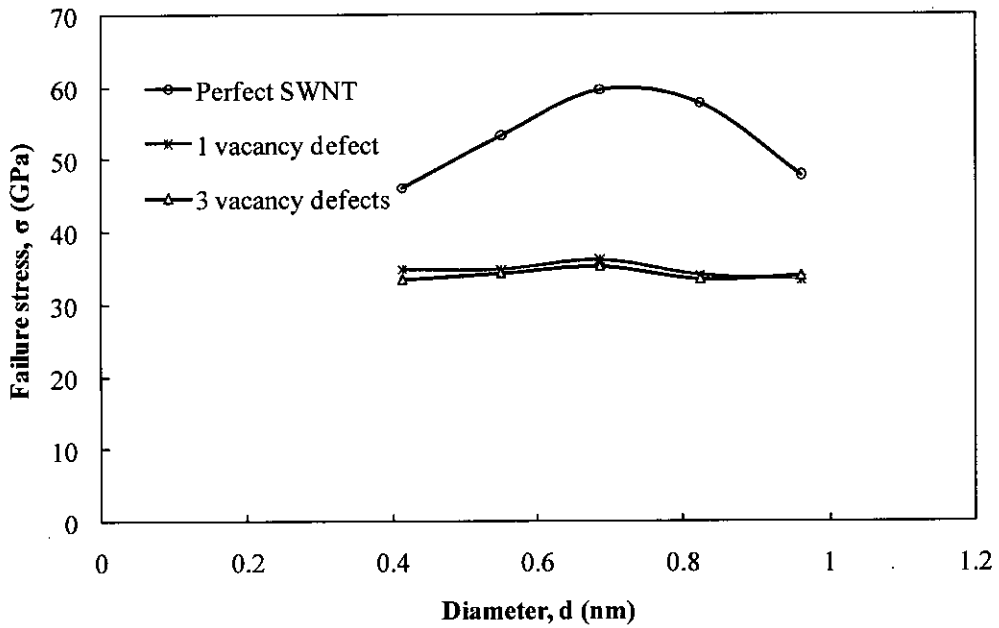


Figure 4.31 Comparison of failure strength of pristine and vacancy defect SWNT of different diameter ($l/d=8.04$) under compressive load.

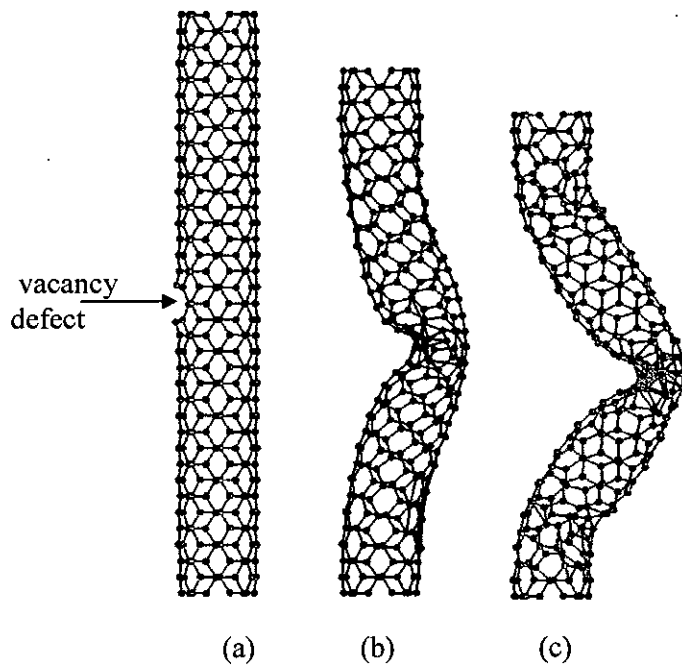


Figure 4.32 Snap shot of compressive test of defective (4,4) SWNT ($l/k=38.20$) with one vacancy defect, (a) at 0% strain, (b) at 2% strain, (c) failure at 5% strain.

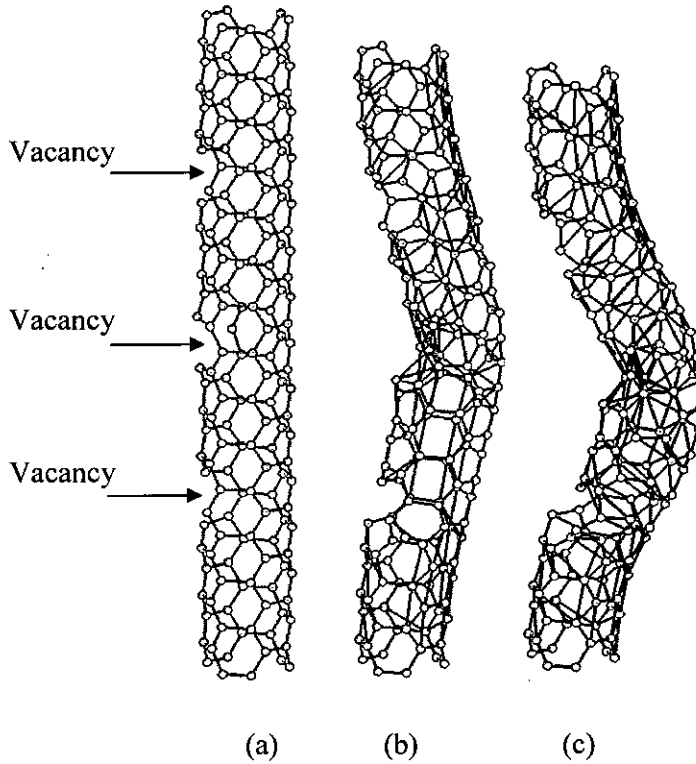


Figure 4.33 Snap shot of compressive test of defective (3,3) SWNT ($l/k=34.34$) with three vacancy defects (a) at 0% strain, (b) at 1% strain, (c) failure at 5% strain.

Figure 4.32 shows the comparison of failure strength of pristine SWNT and SWNT with one and three Stone-Wales defects. As seen in the figure, the presence of Stone-Wales defects reduce the compressive strength of the nanotube about 29.80% and 31.46% for one and three Stone-Wales defects, respectively. As the number of defects increases there is hardly any influence of extra defects on the compressive strength. Because, stress concentration occurs at a specific single defect site from where buckling of the nanotube starts. Snap shot of compressive test of (3,3) SWNT with one and three Stone-Wales defects are shown in figures 4.33 and 4.34.

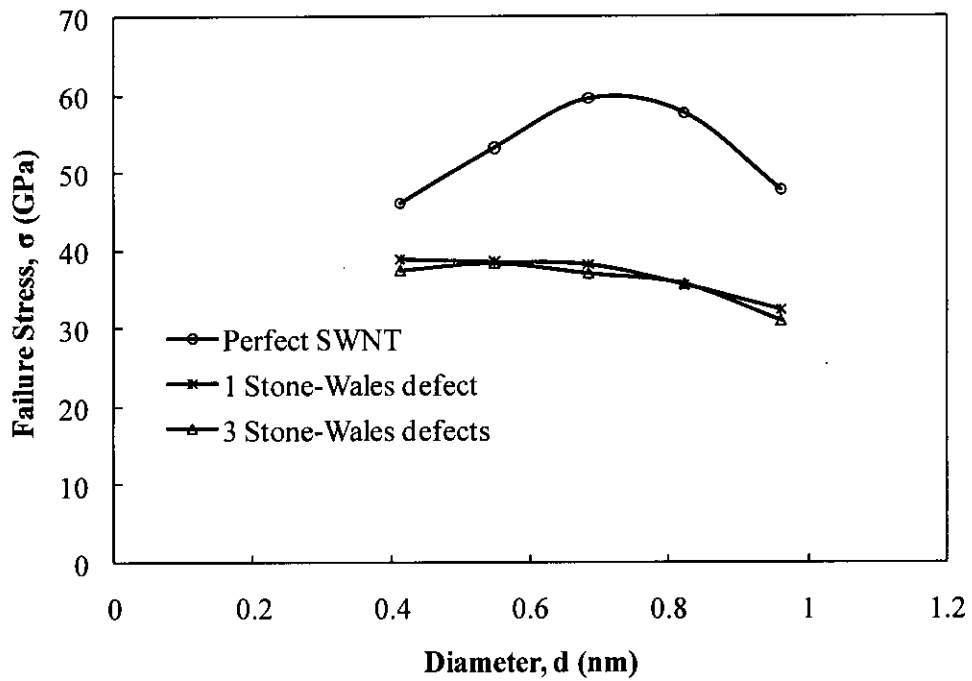


Figure 4.34 Comparison of failure strength of pristine and Stone-Wales defect SWNT of different diameter ($l/d=8.04$) under compressive load.

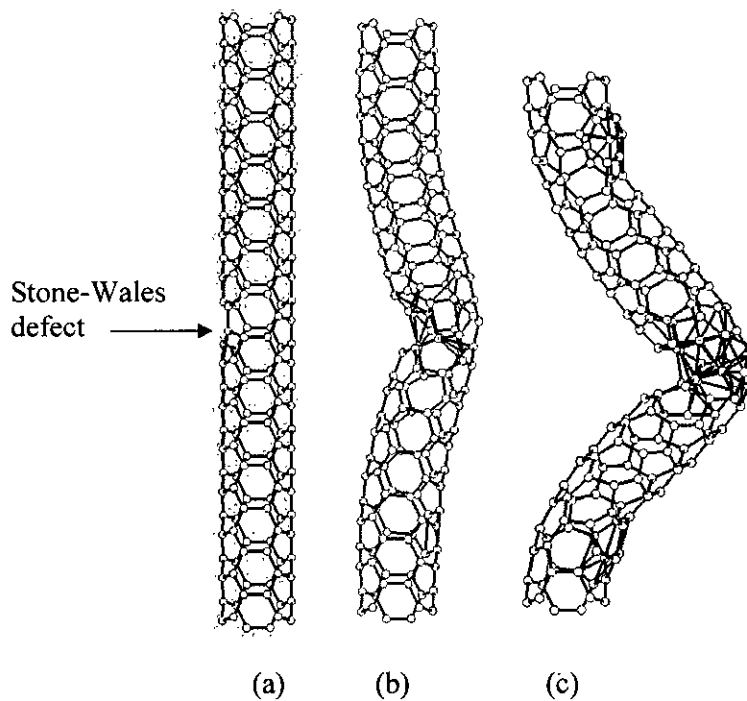


Figure 4.35 Snap shot of compressive test of defective (3,3) SWNT ($l/k=34.34$) with one Stone-Wales defect (a) at 0% strain, (b) at 1% strain, (c) failure at 5% strain.

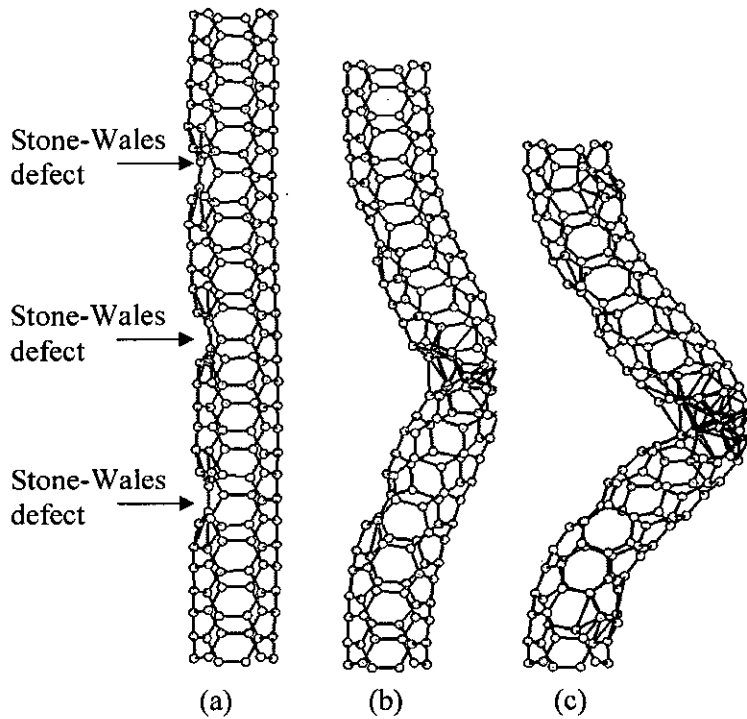


Figure 4.36 Snap shot of compressive test of defective (3,3) SWNT ($l/k=34.34$) with three Stone-Wales defect (a) at 0% strain, (b) at 1% strain, (c) failure at 3% strain.

4.3.5 Tensile Test of Pristine and Defective DWNT

The effect of presence of vacancy and Stone-Wales defects in DWNTs with various orientations is studied in this section. Here $((3, 3), (8, 8))$ pristine and defective DWNTs of same length are studied. The tensile test procedure and initial conditions is exactly the same as that of the tensile test of SWNT.

Figure 4.35 shows the failure stress of defective and pristine DWNTs. It is seen that failure stress decreases due to presence of defects. The failure strength decreases by 15% of pristine DWNT for one vacancy defect at the middle of either outer or inner tube. However, failure strength decreases by 22% of pristine DWNT for one vacancy defect at the middle of both inner and outer tube.

The failure strength decreases by 10% and 31% of pristine DWNT for one Stone-Wales defect at the middle of outer tube only and inner tube only respectively. However, failure stress decrease by 36% for one Stone-Wales defect at the middle of both inner and outer tube.

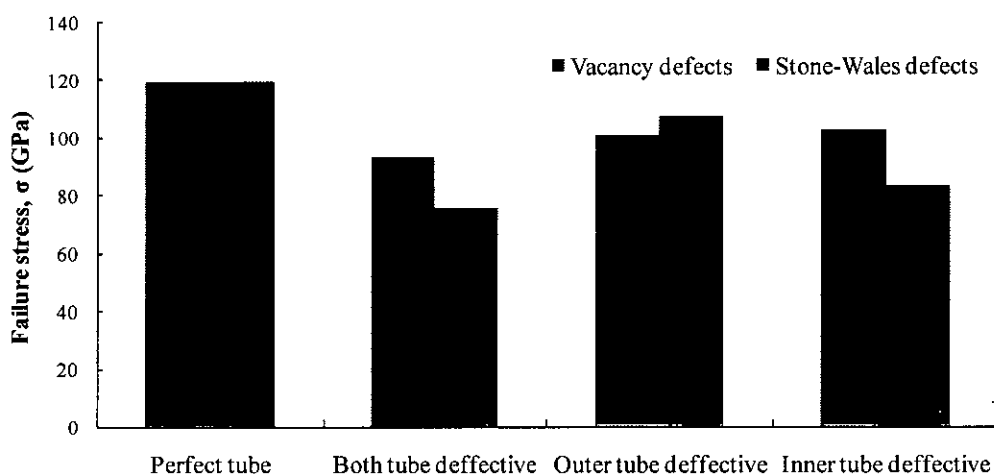


Figure 4.37 Comparison of failure stress of pristine and defective DWNT under tensile test.

Figure 4.36 represent the snap shots of tensile test of a ((3,3),(8,8)) DWNT with one vacancy defect on each tube. It is found from the figure that necking of the tube starts at 8% strain and the tube fails at the defect site. This is because stress concentration occurs at the specific defect site. The similar phenomenon is observed in case of Stone-Wales defects.

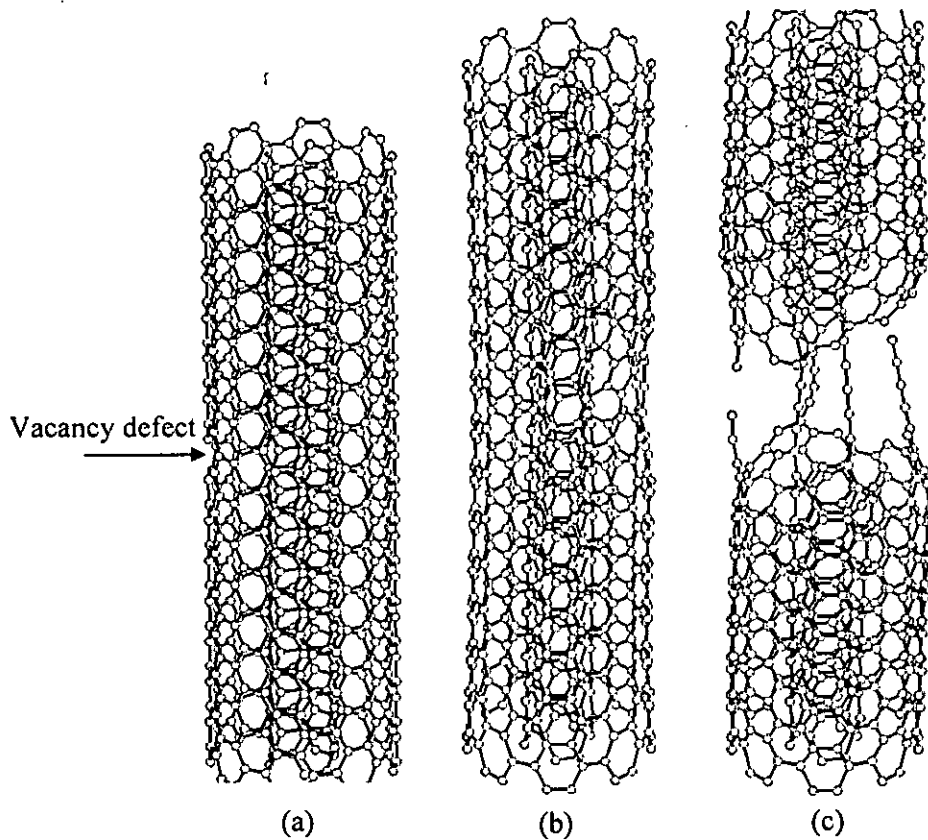


Figure 4.38 Snap shot of tensile test of $((3,3),(8,8))$ defective DWNT (a) at 0% strain, (b) at 8% strain, (c) failure at 19% strain.

4.3.6 Compressive Test of Pristine and Defective DWNT

The effect of presence of vacancy and Stone-Wales defects in DWNTs with various orientations is studied in this section. Here $((3, 3), (8, 8))$ pristine and defective DWNTs of same length are studied for compressive test. The compressive test procedure is exactly the same as that of the compressive test of SWNT.

Figure 4.37 shows the failure stress of pristine and defective and pristine DWNTs. It is clear from the figure that the failure stress decreases if there is defect in any of the tubes of DWNT. The failure strength decreases by 16% of pristine DWNT for one

vacancy defect at the middle of either outer or inner tube. However, failure strength decreases by 20% of pristine DWNT for one vacancy defect at the middle of both inner and outer tube.

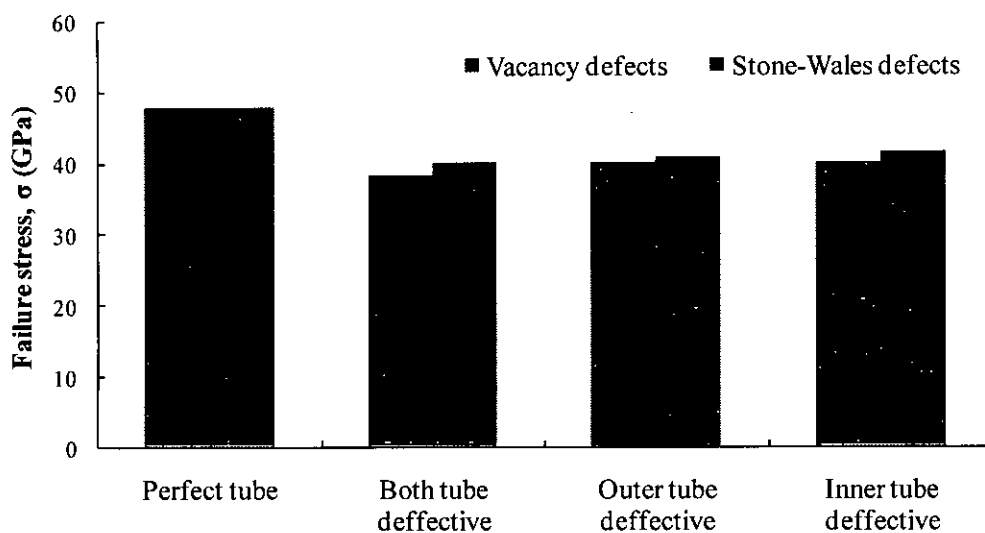


Figure 4.39 Comparison of failure stress of defective ((3,3),(8,8)) DWCNT ($l/k=15.29$) and pristine DWNT under compressive test.

The failure strength decrease by 14% of pristine DWNT in case of one Stone-Wales defect at the middle of either outer or inner tube. However, the failure strength reduces by 16% for one Stone-Wales defect at the middle of both inner and outer tube.

Figure 4.38 represent the snap shots of compressive test of a ((3,3),(8,8)) DWNT with one vacancy defect on each tube. It is found from the figure that the tube buckles at the defect site. This is because stress concentration occurs at the specific defect site.

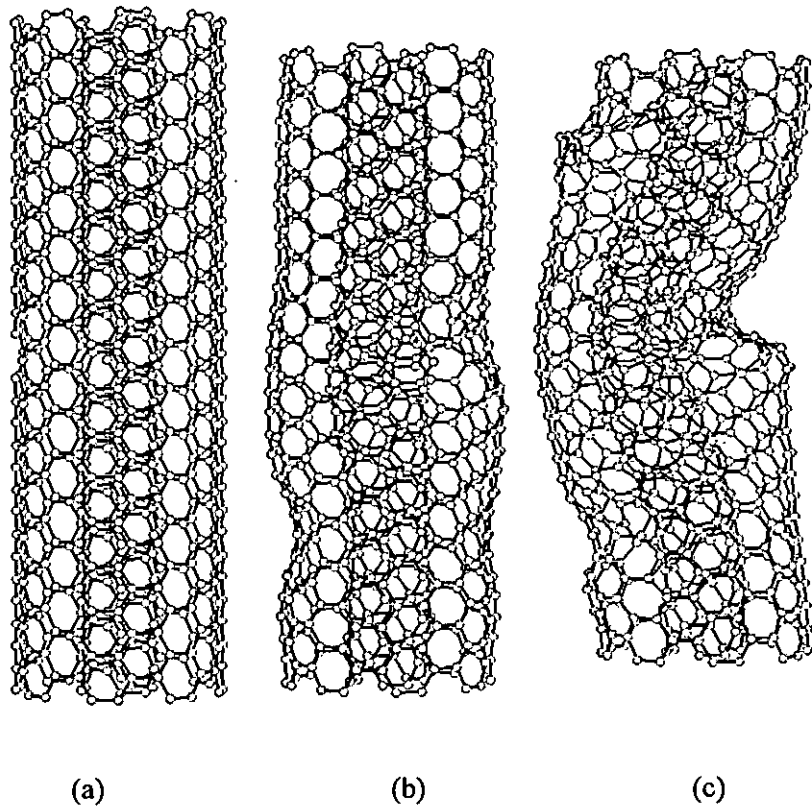


Figure 4.40 Snap shot of compressive test of defective ((3,3),(8,8)) DWCNT ($l/k=15.29$) (a) at 0% strain, (b) at 4% strain, (c) failure at 7% strain.

CHAPTER 05

CONCLUSIONS & RECOMMANDATIONS

5.1 Introduction

Carbon Nanotubes (CNTs) have exceptional mechanical, electrical, and thermal properties. CNTs having perfect structure (i.e., structure without any defect) hold very high mechanical properties. However, defects in CNTs affect their these exceptional properties. In this work mechanical properties of CNTs with defects are studied under both compressive and tensile loads using molecular dynamics (MD) simulations.

In this work both single-walled and double-walled carbon nanotubes (SWNTs and DWNTs) with perfect structure, vacancy defects and Stone-Wales defects are simulated with MD. Five armchair SWNTs having indexes of (3,3), (4,4), (5,5), (6,6) and (7,7) and one armchair DWNT having index of ((3,3),(8,8)) are considered. To create Stone-Wales defect, four neighboring hexagons are converted into two pentagons and two heptagons with a 90° rotation of the horizontal bond of the hexagonal structure of the CNT whereas to create vacancy defects carbon atoms are removed from the perfect hexagonal structure of the CNTs. Molecular simulations are carried out using the classical MD method, in which the Newtonian equations of motion are solved numerically for a set of atoms. The velocity-Verlet algorithm is used for solving the Newtonian equations of motion. The Brenner potential is used for carbon-carbon interaction in the CNT and non-bonded interaction between the CNTs in DWCNTs is modeled with the Lennard-Jones potential. Temperature of the system is controlled by velocity scaling. In the simulation, tensile and compressive loads are applied by moving the end atoms of the CNTs rigidly outward and inward directions respectively.

Results and discussions have been presented in Chapter 4. Main findings and recommendations are given in current chapter.

5.2 Conclusions

The following major conclusions can be drawn from the current investigation:

1. From the tensile test of pristine SWNTs, it is found that Young's modulus varies with CNT diameter significantly. However, failure strength and failure strain remain almost same with variation of diameter.
2. From the compressive test of pristine SWNTs, it is seen that failure strength decreases with the increase of slenderness ratio and the MD simulation results well agree with theoretical Euler's equation for long column.
3. The SWNTs with defects fail at lower tensile strength than that of pristine SWNTs. Tensile failure strain increases with increase of defect density which means that the SWNTs with higher defect density behaves as soft material. With the presence of one vacancy defect and three vacancy defects, tensile strength of the nanotube reduces by 16.19% and 16.66% on an average respectively for different diameter. However, in case of Stone-Wales defect this reduction in strength is only 9.58% and 9.27% for one Stone-Wales defect and three Stone-Wales defects.
4. The presence of vacancy defects reduces the compressive strength of the nanotube about 33.97% and 34.95% for one vacancy defect and three vacancy defects, respectively. In case of Stone-Wales defects, the compressive strength of the nanotube is reduced about 29.80% and 31.46% for one and three Stone-Wales defects, respectively.
5. From the tensile test of DWNT with vacancy defect, it is seen that the failure strength decreases by 15% of pristine DWNT for one vacancy defect at the middle of either outer or inner tube. However, failure strength decreases by 22% of pristine DWNT for one vacancy defect at the middle of both inner and outer tube. The failure strength decreases by 10% and 31% of pristine DWNT for one Stone-Wales defect at the middle of outer tube only and inner tube only respectively. However, failure stress decrease by 36% for one Stone-Wales defect at the middle of both inner and outer tube.
6. From the compressive test of DWNT with vacancy defect, the failure strength decreases by 16% of pristine DWNT for one vacancy defect at the middle of either outer or inner tube. However, failure strength decreases by 20% of pristine

DWNT for one vacancy defect at the middle of both inner and outer tube. The failure strength decrease by 14% of pristine DWNT in case of one Stone-Wales defect at the middle of either outer or inner tube. However, the failure strength reduces by 16% for one Stone-Wales defect at the middle of both inner and outer tube.

5.3 Recommendations

Following recommendations can be suggested for further improvement:

1. CNTs with larger diameter and length can be simulated for further investigation.
2. Multi-walled nanotubes (MWNTs) with three or more layers can be simulated to investigate the effect of defects.
3. Cross-link between inter wall of MWNTs can be considered for further studies.
4. The results obtained by MD technique can be compared with other methods like Quantum Mechanics (QM), Continuum Mechanics (CM) or Finite Element (FE) technique.
5. The results presented in current study are obtained from computer simulation. These results can be verified by experiment.

REFERENCES

References

- [1] L. X. Zheng et al. (2004). Ultralong Single-Wall Carbon Nanotubes. *N. Mat.* 3. pp. 673–676.
- [2] Iijima S. Helical microtubules of graphite carbon. *Nature* 1991;354: 56–8.
- [3] Li Y, Wang K, Wei JQ, Gu Z, Wang ZC, Luo JB, et al. Tensile properties of long aligned double-walled carbon nanotube strands. *Carbon* 2005;43: 31–5.
- [4] Lu JP. Elastic properties of single and multilayered nanotubes. *J PhysChem Solids* 1997;58:1649–52.
- [5] Kelly BT, editor. *Physics of graphite*. London: Applied Science, 1981.
- [6] Ruoff RS, Lorents DC, Mechanical and thermal properties of carbon nanotubes. *Carbon* 1995;33:925-30.
- [7] Chang TC, Gao HJ. Size-dependent elastic properties of a single-walled carbon nanotube via molecular mechanics model. *J Mech Phys Solids* 1997;51:1059–74.
- [8] Belytschko T, Xiao SP, Schatz GC, Ruoff. Atomistic simulations of nanotube fracture. *Phys Rev B* 2002;65:235430.
- [9] Zhang P, Huang Y, Gao H, Hwang KC. Fracture nucleation in single-wall carbon nanotubes under tension: a continuum analysis incorporating interatomic potentials. *Trans ASME* 2002;69:454–8.
- [10] Tersoff J, Ruoff RS. Structural properties of a carbon-nanotube crystal. *Phys Rev Lett.* 1994;73:676-9.
- [11] Yu MF, Lourie O, Dyer M, Molony K, Kelly TF, Ruoff RS. Strength and breaking mechanism of multi-walled carbon nanotubes under tensile load. *Science* 2000;287:637-9.
- [12] Yakobson BI, Brabec CJ, Bernhoc J. Nanomechanics of carbon tubes: instabilities beyond linear response. *Phys Rev Lett* 1996;76(14):2511–4.
- [13] Zhou G, Duan WH, Gu BL. First-principles study on morphology and mechanical properties of single-walled carbon nanotube. *Chem Phys Lett* 2001;333:344–9.
- [14] Chang TC, Gao HJ. Size-dependent elastic properties of a single-walled carbon nanotube via molecular mechanics model. *J Mech Phys Solids* 1997;51:1059–74.

- [15] Lau KT, Gu C, Gao GH, Ling HY, Reid SR. Stretching process of single and multi-walled carbon nanotubes for nanocomposite applications. *Carbon* 2004;42:423–60.
- [16] Li YJ, Wang KKL, Wei JQ, Gu ZY, Wang ZC, Luo JB, et al. Tensile properties of long aligned double-walled carbon nanotube strands. *Carbon* 2005;43:31–5.
- [17] R.H. Baughman, Putting a New Spin on Carbon Nanotubes. *Science* 290, 1310 (2000).
- [18] Ajayan PM, Stephan O, Colliex C, Trauth D. Aligned carbon nanotube arrays formed by cutting a polymer resin nanotube composite. *Science*. 265:1212-4. (1994).
- [19] B. Gao, C. Bower, J. Lorentze, L. Fleming, A. Kleinhamme, X. P. Tang, L. E. McNeil, Y. Wu, and O. Zhou, Enhanced saturation lithium composition in ball-milled single-walled carbon nanotubes *Chem. Phys. Lett.* 327, 69–75 (2000).
- [20] R.Z. Ma, et al., *Science in China Series E-Technological Sciences* 43 178 (2000).
- [21] Ajayan, P. M. and Zhou, O. Z., *Applications of Carbon Nanotubes*, *Appl. Phys.* 80, 391-425, (2001).
- [22] Dekker C., Carbon nanotubes as molecular quantum wires, *Physics Today* 52 (5): 22–28. (May 1999).
- [23] Postma H. W. Ch., Teepen T., Yao Z., Grifoni M., Dekker C. Carbon Nanotube Single-Electron Transistors at Room Temperature. *Science* 293 (5527), (2001).
- [24] Martel, R., V. Derycke, C. Lavoie, J. Appenzeller, K. K. Chan, J. Tersoff, and Ph. Avouris, Ambipolar Electrical Transport in Semiconducting Single-Wall Carbon Nanotubes. *Physical Review Letters* 87 (25), (December 2001).
- [25] Terrones H. and Terrones M. Curved nanostructured materials., *N. J. of Phys.* 5, 126.1–126.37 (2003).
- [26] Lau KT, Hui D. The revolutionary creation of new advanced materials-carbon nanotubes composites. *Compos Part B* 2002;33: 263–77.
- [27] Ruoff R. S, Liu W. K, and Qian D. C.R. Mechanical properties of carbon nanotubes: theoretical predictions and experimental measurements *Phys* 4, 993 (2003).

- [28] Srivastava D. Wei C. and Cho K. Nanomechanics of carbon nanotubes and composites *Appl. Mech. Rev.* 56, 215 (2003).
- [29] Lourie O and Wagner H. D. Evaluation of Young's modulus of carbon nanotubes by micro-Raman spectroscopy *J. Matt. Res.* 13, 2418 (1998) .
- [30] Pan Z. W, Xie S.S, Lu L, Chang B. H, Sun L. F, Zhou W. Y, Wang G and Zhang D. L Tensile tests of ropes of very long aligned multiwall carbon nanotubes. *Appl. Phys. Lett.* 74, 3152 (1999).
- [31] Treacy M. M. J, Ebbesen T. W, and Gibson J. M. Exceptionally high Young's modulus observed for individual carbon nanotubes. *Nature* 381, 678 (1996).
- [32] Poncharal P, Heer De W.A, Wang Z. L, and Ugarte D. Electrostatic Deflections and Electromechanical Resonances of Carbon Nanotubes. *Science* 283, 1513 (1999).
- [33] Salvétat J.-P, Bhattacharyya S. and Pipes R.B. Progress on Mechanics of Carbon Nanotubes and Derived Materials, *J. Nanoscience and Nanotechnology*, Vol 6, 1857-1882 (2006).
- [34] Yu M. F, Ruoff R. S, Files and Arepalli S. Tensile Loading of Ropes of SingleWall Carbon Nanotubes and their Mechanical Properties *Phys Rev. Lett.* 84, 5552(2000).
- [35] Salvétat J.-P, Briggs G. A. D, Bonard J.-M, Bacsá R. R, Kulik A. J, Stöckli T, Burnham N.A and Forró L. Elastic and Shear Moduli of Single-Walled Carbon Nanotube Ropes. *Phys Rev. Lett.* 82, 944 (1999)
- [36] Wong E. W, Sheehan P. E and Lieber C. M. Nanobeam Mechanics: Elasticity, Strength, and Toughness of Nanorods and Nanotubes *Science* 277 (5334), 1971-75(1997).
- [37] Lukie B, Seo J. W, Couteau E, Lee K, Kis A, Kulik A. J, Forro L, Gradecak S, Berkecz R, Hernadi K, Delpeux S, Cacciaguerra T, Beguin F, Fonseca A, Nagy J. B and Csányi G. Elastic modulus of multi-walled carbon nanotubes produced by catalytic chemical vapour deposition. *Appl. Phys. A-Mater*, 80, 695(2005).
- [38] Hashimoto, A., Suenaga, K., Gloter, A., Urita, K., Iijima, S., Direct evidence for atomic defects in graphene layers, *Nature* 2004; 430:870-873.
- [39] Tu ZC, Ou-yang ZC. Single-walled and multiwalled carbon nanotubes viewed as elastic tubes with effective Young's moduli dependent on layer number. *Phys Rev B* 2002;65:233-407.
- [40] Maiti A, Svizhenko A, Anantram MP. Electronic transport through carbon nanotubes: effects of structural deformation and tube chirality. *Phys Rev Lett* 2002;88(12):126905.

- [41] Lau K.-t, Gu C., Hui D. A critical review on nanotube and nanotube/nanoclay related polymer composite materials. *Composites: Part B* 37 (2006) 425–436.
- [42] Hu Y. and Sinnott S. B., Compos. Molecular dynamics simulations of polyatomic-ion beam deposition-induced chemical modification of carbon nanotube/polymer composites *J. Mater. Chem.*, 14, 2004, 719 - 729,
- [43] Cooper C. A., Cohen S. R., Barber A. H., and Wagner H. D., Detachment of nanotubes from a polymer matrix. *Appl. Phys. Lett.* 81, 3873 (2002).
- [44] Ni B. and Sinnott S. B., Chemical functionalization of carbon nanotubes through energetic radical collisions *Phys. Rev. B* 61, R16343 (2000).
- [45] Ni B., R. Andrews, D. Jacques, D. Qian, M. B. J. Wijesundara, Y. Choi, L. Hanley, and S. B. Sinnott, A Combined Computational and Experimental Study of Ion-Beam Modification of Carbon Nanotube Bundles *J. Phys. Chem. B*, 105, 12719-12725 (2001)
- [46] C. Mikó, M. Milas, J. W. Seo, E. Couteau, N. Barisæ, R. Gaál, and L. Forró, Effect of electron irradiation on the electrical properties of fibers of aligned single-walled carbon nanotubes. *Appl. Phys. Lett.* 83, 4622 (2003).
- [47] H. Stahl, J. Appenzeller, R. Martel, P. Avouris, and B. Lengeler, Intertube Coupling in Ropes of Single-Wall Carbon Nanotubes, *Phys. Rev. Lett.* 85, 5186 (2000).
- [48] E. Salonen, A. V. Krasheninnikov, and K. Nordlund, Ion-irradiation-induced defects in bundles of carbon nanotubes *Nucl. Instrum. Methods Phys. Res. B* 193, 603 (2002).
- [49] A. Kis, G. Csányi, J.-P. Salvetat, T.-N. Lee, E. Couteau, A. J. Kulik, W. Benoit, J. Brugger, and L. Forró, Reinforcement of single-walled carbon nanotube bundles by intertube bridging *Nat. Mater.* 3, 153 (2004).
- [50] M. Huhtala, A. V. Krasheninnikov, J. Aittoniemi, K. Nordlund, and K. Kaski, Improved mechanical load transfer between shells of multiwalled carbon nanotubes *Phys. Rev. B* 70, 045404 (2004).
- [51] Sammalkorpi M., Krasheninnikov A., Kuronen A., Nordlund K., and Kaski K., Mechanical properties of carbon nanotubes with vacancies and related defects, *PHYSICAL REVIEW B* 70, 245416 (2004).
- [52] Zhang S, Mielke S.L, Khare R, Troya D, Ruoff R.S, Schatz G.C and Belytschko T. Mechanics of defects in carbon nanotubes: Atomistic and multiscale simulations *Phys. Rev. B* 71, 115403 (2005).
- [53] Tunvir K., Kim A. and Nahm S. H., The effect of two neighboring defects on the mechanical properties of carbon nanotubes, *J. Nanotechnology* 19((2008).

- [54] Xia Y. Zhao M., Ma Y., Ying M., Liu X., Liu P. and Mei L., Tensile strength of single-walled carbon nanotubes with defects under hydrostatic pressure, *PHYSICAL REVIEW B*, **65**, 155415 2007.
- [55] Shen H. and Zhang C., Postbuckling of double-walled carbon nanotubes with temperature dependent properties and initial defects under combined axial and radial mechanical loads, *J. Solids and Structures* **44** (2007) 1461-1487.
- [56] Frenkel D. and Smit B. *Understanding molecular simulation from algorithms to applications*. Academic Press Inc. USA, 1996.
- [57] Allen, M. P., Tildesley, D. J., *Computer simulation of liquids*, Oxford: Clarendon Press;1987.
- [58] Brenner, D. W., Empirical potential for hydrocarbons for use in simulating the chemical vapor deposition of diamond films, *Phys. Rev. B* 1990; **42**(15): 9458-9471.
- [59] Xia Z. and Curtin W.A., Pullout forces and friction in multiwall carbon nanotubes. *Phys. Rev. B* **69**, 233408(2004).
- [60] Yeak S. H. , Ng T. Y. and Liew K. M. Multiscale modeling of carbon nanotubes under axial tension and compression, *Phys. Rev. B* **72**, 165401, (2005).
- [61] Chowdhury S.C., Okabe T., Computer simulation of carbon nanotube pull-out from polymer by the molecular dynamics method, *Composites: Part A* **38** (2007) 747–754.
- [62] Shigley J. E., *Mechanical Engineering Design*. McGraw-Hill Book company. USA. 1986.
- [63] Ebbesen, T. W. and Ajayan, P. M., Large-scale synthesis of carbon nanotubes. *Nature*, **358**, 220-222, (1992)
- [64] Journet, C. and Bernier, P., Production of carbon nanotubes. *Applied Physics A-Materials Science & Processing*, **67**, (1), 1-9, 1998.
- [65] Guo, T., Nikolaev, P., Thess, A., Colbert, D. T., and Smalley, R. E., Catalytic growth of single-walled nanotubes by laser vaporization. *Chemical Physics Letters*, **243**, (1,2), 1995.

APPENDIX-A

Arc Discharge

The carbon arc discharge method, initially used for producing C_{60} fullerenes, is the most common and perhaps easiest way to produce CNTs as it is rather simple to undertake. However, it is a technique that produces a mixture of components and requires separating nanotubes from the soot and the catalytic metals present in the crude product.

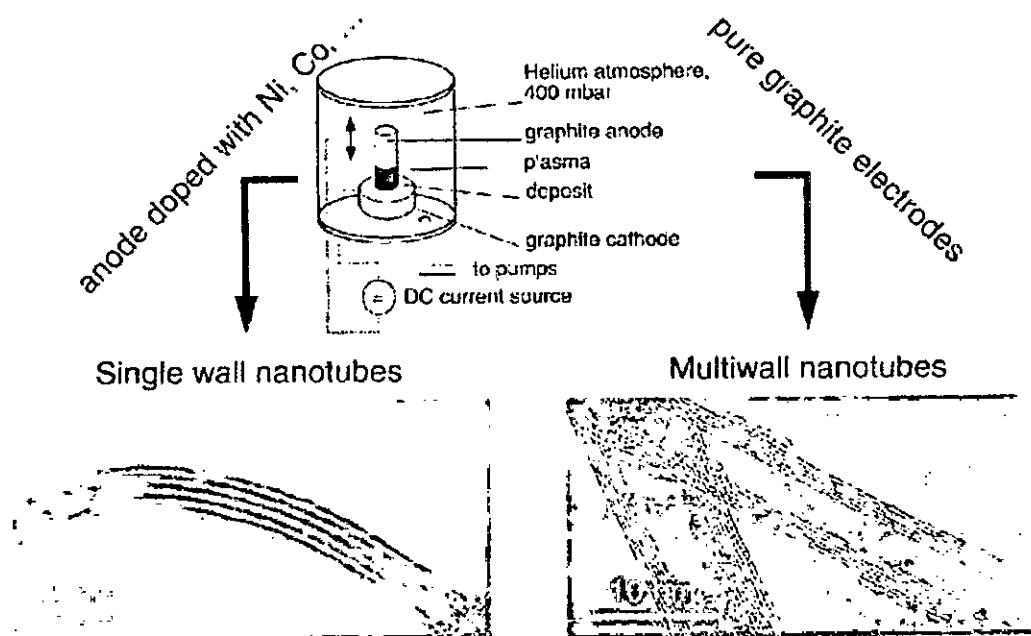


Figure A-1 Experimental set-up of an arc discharge apparatus [63].

This method creates nanotubes through arc-vaporization of two carbon rods placed end to end, separated by approximately 1mm, in an enclosure that is usually filled with inert gas (helium, argon) at low pressure (between 50 and 700 mbar) as shown in the figure A-1. A direct current of 50 to 100 A driven by approximately 20 V creates a high temperature discharge between the two electrodes. The discharge vaporizes one of the carbon rods and forms a small rod shaped deposit on the other rod. Producing

nanotubes in high yield depends on the uniformity of the plasma arc and the temperature of the deposit form on the carbon electrode [63].

Different diameter distributions have been found depending on the mixture of helium and argon. These mixtures have different diffusion coefficients and thermal conductivities. These properties affect the speed with which the carbon and catalyst molecules diffuse and cool, affecting nanotube diameter in the arc process. This implies that single-layer tubules nucleate and grow on metal particles in different sizes depending on the quenching rate in the plasma and it suggests that temperature and carbon and metal catalyst densities affect the diameter distribution of nanotubes. Depending on the exact technique, it is possible to selectively grow SWNTs or MWNTs (see figure A-1[63]). Two distinct methods of synthesis can be performed with the arc discharge apparatus.

If SWNTs are preferable, the anode has to be doped with metal catalyst, such as Fe, Co, Ni, Y or Mo. A lot of elements and mixtures of elements have been tested by various authors [64] and it is noted that the results vary a lot, even though they use the same elements. This is not surprising as experimental conditions differ. The quantity and quality of the nanotubes obtained depend on various parameters such as the metal concentration, inert gas pressure, kind of gas, the current and system geometry. Usually the diameter is in the range of 1.2 to 1.4 nm. A couple of ways to improve the process of arc discharge are stated below.

If both electrodes are graphite, the main product will be MWNTs. But next to MWNTs a lot of side products are formed such as fullerenes, amorphous carbon, and some graphite sheets. Purifying the MWNTs, means loss of structure and disorders the walls. However scientist are developing ways to gain pure MWNTs in a large-scale process without purification. Typical sizes for MWNTs are an inner diameter of 1-3 nm and an outer diameter of approximately 10 nm. Because no catalyst is involved in this process, there is no need for a heavy acidic purification step. This means, the MWNT, can be synthesized with a low amount of defects.

Laser Ablation

In 1995, Smalley's group [65] at Rice University reported the synthesis of CNTs by laser vaporization. The laser vaporization apparatus used by Smalley's group is shown in Figure A-2. A pulsed or continuous laser is used to vaporize a graphite target in an oven at 1200 °C. The main difference between continuous and pulsed laser, is that the pulsed laser demands a much higher light intensity (100 kW/cm² compared with 12 kW/cm²). The oven is filled with helium or argon gas in order to keep the pressure at 500 Torr. A very hot vapor plume forms, then expands and cools rapidly. As the vaporized species cool, small carbon molecules and atoms quickly condense to form larger clusters, possibly including fullerenes. The catalysts also begin to condense, but more slowly at first, and attach to carbon clusters and prevent their closing into cage structures. Catalysts may even open cage structures when they attach to them. From these initial clusters, tubular molecules grow into single-wall carbon nanotubes until the catalyst particles become too large, or until conditions have cooled sufficiently that carbon no longer can diffuse through or over the surface of the catalyst particles. It is also possible that the particles become that much coated with a carbon layer that they cannot absorb more and the nanotube stops growing. The SWNTs formed in this case are bundled together by Van der Waals forces. There are some striking, but not exact similarities, in the comparison of the spectral emission of excited species in laser ablation of a composite graphite target with that of laser-irradiated C₆₀ vapor. This suggests that fullerenes are also produced by laser ablation of catalyst-filled graphite, as is the case when no catalysts are included in the target. However, subsequent laser pulses excite fullerenes to emit C₂ that adsorbs on catalyst particles and feeds SWNT growth. However, there is insufficient evidence to conclude this with certainty.

Laser ablation is almost similar to arc discharge, since the optimum background gas and catalyst mix is the same as in the arc discharge process. This might be due to very similar reaction conditions needed, and the reactions probably occur with the same mechanism.

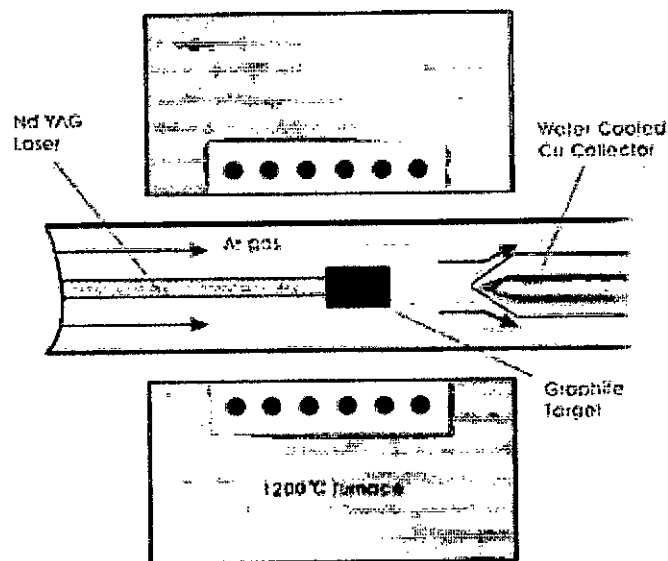


Figure A-2 Schematic drawings of a laser ablation apparatus.

Chemical Vapor Deposition

Chemical vapor deposition (CVD) synthesis is achieved by putting a carbon source in the gas phase and using an energy source, such as plasma or a resistively heated coil, to transfer energy to a gaseous carbon molecule. Commonly used gaseous carbon sources include methane, carbon monoxide and acetylene. The energy source is used to “crack” the molecule into reactive atomic carbon. Then, the carbon diffuses towards the substrate, which is heated and coated with a catalyst (usually a first row transition metal such as Ni, Fe or Co) where it will bind. CNTs will be formed if the proper parameters are maintained. Excellent alignment, as well as positional control on nanometer scale, can be achieved by using CVD. Control over the diameter, as well as the growth rate of the nanotubes can also be maintained. The appropriate metal catalyst can preferentially grow single rather than multi-walled nanotubes.

CVD synthesis is essentially a two-step process consisting of a catalyst preparation step followed by the actual synthesis of the nanotube. The catalyst is generally prepared by sputtering a transition metal onto a substrate and then using either chemical etching or thermal annealing to induce catalyst particle nucleation. Thermal annealing results in cluster formation on the substrate, from which the nanotubes will grow. Ammonia may be used as the etchant. The temperatures for the synthesis of nanotubes by CVD are generally within the 650–900°C range. Typical yields for CVD are approximately 30%.

These are the basic principles of the CVD process. In the last decennia, different techniques for the CNTs synthesis with CVD have been developed, such as plasma enhanced CVD, thermal chemical CVD, alcohol catalytic CVD, vapor phase growth, aero gel-supported CVD and laser assisted CVD.

Purification Techniques

A large problem with nanotube application is next to large-scale synthesis is the purification. In this section, the purification of SWNTs will be discussed. The as-produced SWNT soot contains a lot of impurities. The main impurities in the soot are graphite (wrapped up) sheets, amorphous carbon, metal catalyst and the smaller fullerenes. These impurities will interfere with most of the desired properties of the SWNTs. Also in the fundamental research, it is preferred to obtain SWNTs as pure as possible. In order to understand the measurements better, the SWNT samples also have to be as homogeneous as possible. The common industrial techniques use strong oxidation and acid refluxing techniques, which have an effect on the structure of the tubes.

Here several purification techniques of the SWNT will be discussed. Basically, these techniques can be divided into two mainstreams, structure selective and size selective separations. The first one will separate the SWNTs from the impurities; the second one will give a more homogeneous diameter or size distribution. The techniques that

will be discussed are oxidation, acid treatment, annealing, ultrasonication, micro filtration, ferromagnetic separation, cutting, functionalisation and chromatography techniques.

Oxidation

Oxidative treatment of the SWNTs is a good way to remove carbonaceous impurities or to clear the metal surface. The main disadvantages of oxidation are that not only the impurities are oxidized, but also the SWNTs. Luckily the damage to SWNTs is less than the damage to the impurities. These impurities have relatively more defects or a more open structure. Another reason why impurity oxidation is preferred, is that these impurities are most commonly attached to the metal catalyst, which also acts as oxidizing catalyst. Altogether, the efficiency and the yield of the procedure are highly dependable on a lot of factors, such as metal content, oxidation time, environment, oxidizing agent and temperature.

The fact that metal acts as oxidizing catalyst, the metal content should certainly be taken into consideration, when looking at the oxidizing time. For example, when the temperature is raised above 600°C, SWNTs will also oxidize, even without catalyst. This is the case with thermal, fixed air and pure oxygen oxidations. These can easily oxidize all the components, so the temperature and the time should be in good control.

There are a couple of examples for clearing the metal surface, to prepare the sample for a metal removal step. The first one is (mild) oxidizing in a wet environment with soluble oxidizing agents, such as H_2O_2 and H_2SO_4 . These will only oxidize the defects and will clear the surface of the metal.

Most commonly, the metal catalyst stays intact during these processes, but when oxygen is used in a wet atmosphere, the outer layer of the metal will be oxidised. Then, the density of this surface increases and the surface covering carbon layer ruptures. Not only the carbon impurities are oxidized now, but also the metal is

partially oxidized and exposed. Quite different from the oxidative techniques above is microwave heating. The microwaves will heat up the metal and will catalytically oxidize the carbon attached to the metal.

Acid Treatment

In general the acid treatment will remove the metal catalyst. First of all, the surface of the metal must be exposed by oxidation or sonication. The metal catalyst is then exposed to acid and solvated. The SWNTs remain in suspended form. When using a treatment in HNO_3 , the acid only has an effect on the metal catalyst. It has no effect on the SWNTs and other carbon particles. If a treatment in HCl is used, the acid has also a little effect on the SWNTs and other carbon particles. The mild acid treatment (4 M HCl reflux) is basically the same as the HNO_3 reflux, but here the metal has to be totally exposed to the acid to solvate it.

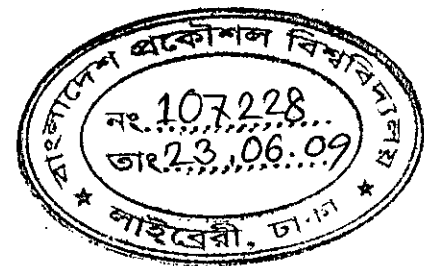
Annealing

Due to high temperatures (873 – 1873 K) the nanotubes will be rearranged and defects will be consumed. The high temperature also causes the graphitic carbon and the short fullerenes to pyrolyse. When using high temperature vacuum treatment⁶¹ (1873 K) the metal will be melted and can also be removed.

Ultrasonication

In this technique particles are separated due to ultrasonic vibrations. Agglomerates of different nano-particles will be forced to vibrate and will become more dispersed. The separation of the particles is highly dependable on the surfactant, solvent and reagent

used. The solvent influences the stability of the dispersed tubes in the system. In poor solvents the SWNTs are more stable if they are still attached to the metal. But in some solvents, such as alcohols, monodispersed particles are relatively stable. When an acid is used, the purity of the SWNTs depends on the exposure time. When the tubes are exposed to the acid for a short time, only the metal solvates, but for a longer exposure time, the tubes will also be chemically cut.



Functionalisation

Functionalisation is based on making SWNTs more soluble than the impurities by attaching other groups to the tubes. Now it is easy to separate them from insoluble impurities, such as metal, with filtration. Another functionalisation technique also leaves the SWNT structure intact and makes them soluble for chromatographic size separation. For recovery of the purified SWNTs, the functional groups can be simply removed by thermal treatment, such as annealing.